A well-defined phosphine free metal-ligand cooperative route for N-alkylation of aromatic amines via activation of renewable alcohols catalyzed by a NNN pincer cobalt(II) complexes

Rahul Saini,[a#] Prashant Kukreti,[a#] Rahul Chauhan,[a] Abhishek Panwar,[b] and Kaushik Ghosh*[a]

[a]Department of Chemistry, Indian Institute of Technology Roorkee, Roorkee-247667, Uttarakhand, India

[b]Department of Chemistry, National Institute of Technology Manipur, Langol-795004, Imphal West, Manipur, India

[#]Authors contributed equally

Table of contents:

1. Experimental

1.1 Materials used

Every reagent and solvent used in this study was purchased from a commercial supplier, such as TCI, SRL, Aldrich, Fisher Scientific, ACROS Organics, and Merck. Reagents and solvents of analytical quality ($CDCl_3$) were used for all tasks and spectroscopic investigations. Catalytic reactions were carried out in an oil bath, and analytical TLC plates (Merck 60 F254 silica gel, 0.25 mm thickness) were employed to measure the reaction progress under ultraviolet light. Column chromatographic separation utilized Merck 60 silica gel with a 60−120 mesh size. NMR spectroscopy was used to identify the catalytic results (^{1}H NMR and ^{13}C NMR). ALPHA II compact FT-IR spectrometer and Shimadzu UV-2600 UV-Vis Spectrophotometer were used to record the IR and UV-Vis spectra, respectively. IR spectra of metal complex and ligand were recorded with the use of KBr pellets (32 scans in cm^{-1}). A Bruker Avance III 500 MHz (AV 500) spectrometer was used to record NMR spectra in deuterated solvents. NMR coupling constants (*J*) are provided in Hertz (Hz), while chemical shift measurements are expressed as δ (ppm) values relative to an internal standard, TMS. Multiplets in the chemical shift are identified by the labels shown as singlet (s), doublet (d), triplet (t), quartet (q), doublet of doublets (dd), doublet of doublets (ddd), doublet of triples (dt), and triplet of doublets (td).

1.2 X-ray crystallography

The X-ray data collection and processing of complex 1 and complex 2 were performed on a Bruker Kappa (D8 QUEST) Apex-IV CMOS diffractometer by using graphite monochromated Mo-Kα radiation (λ = 0.71070 Å) at 293 and 102 K, respectively. The crystal structures were solved by SIR-92 GUI control methods. The Olex[1] software was used to solve the crystal structures and refine them using ShelXT and ShelXL, respectively[2]. The bond lengths and bond angles were computed with the help of MERCURY software. Additionally, ORTEP[3] images were generated using the same MERCURY program. The hydrogen atoms were placed in geometrically determined positions and refined using the riding model. The accompanying supplementary information (SI) files contain pertinent crystallographic parameters.

1.3 Computational methods

Density functional theory (DFT) calculations were performed using Gaussian 09W software. The input files for Gaussian 09 were prepared with Gauss View 5.0.8.[4] The spin-unrestricted B3LYP functional was employed alongside two basis sets: the LanL2DZ basis set for Co and the 6-31+G(d,p) basis set for all other elements. Frequency calculations for the optimized structures were conducted at room temperature (298.15 K). All computations were carried out in toluene using the Integral Equation Formalism Polarizable Continuum Model (IEFPCM) within the self-consistent reaction field (SCRF) approach. Free energy evaluations were also performed at room temperature. The free energy change (ΔG) includes contributions from electronic energy (ΔE), zero-point vibrational energy (ΔZ0), thermal enthalpy (ΔEthermal), and entropy (−TΔS).

2. Characterization of ligand and complexes

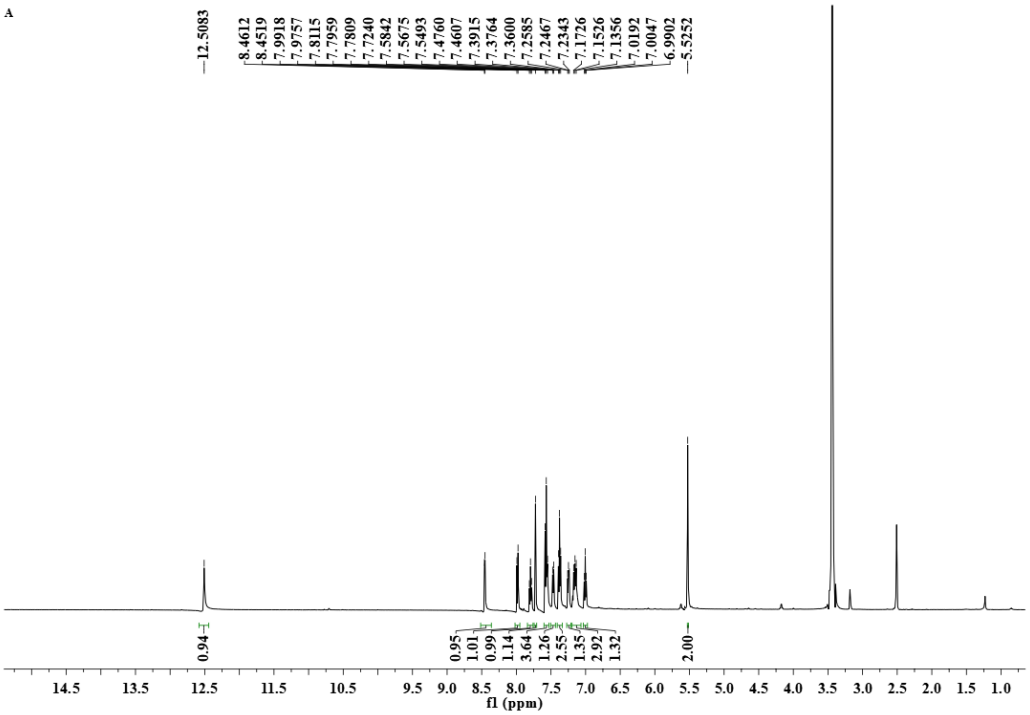

Figure S1. ^{1}H NMR spectrum of Ligand L2 in DMSO-d_6 solvent.

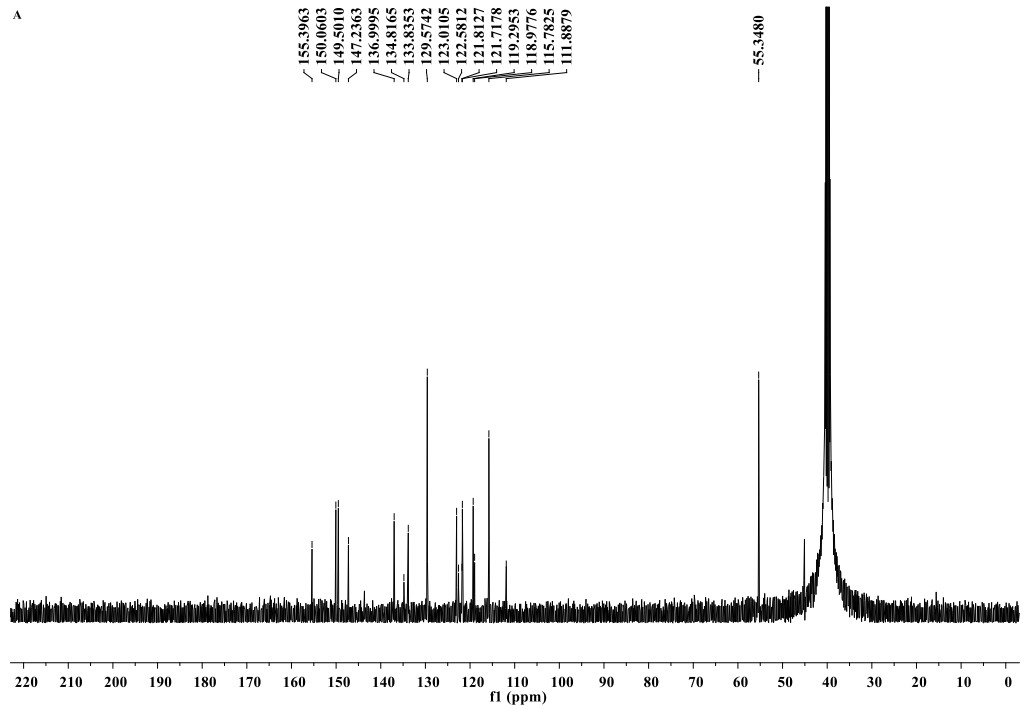

Figure S2. ^{13}C NMR spectrum of Ligand L2 in DMSO-d_6 solvent.

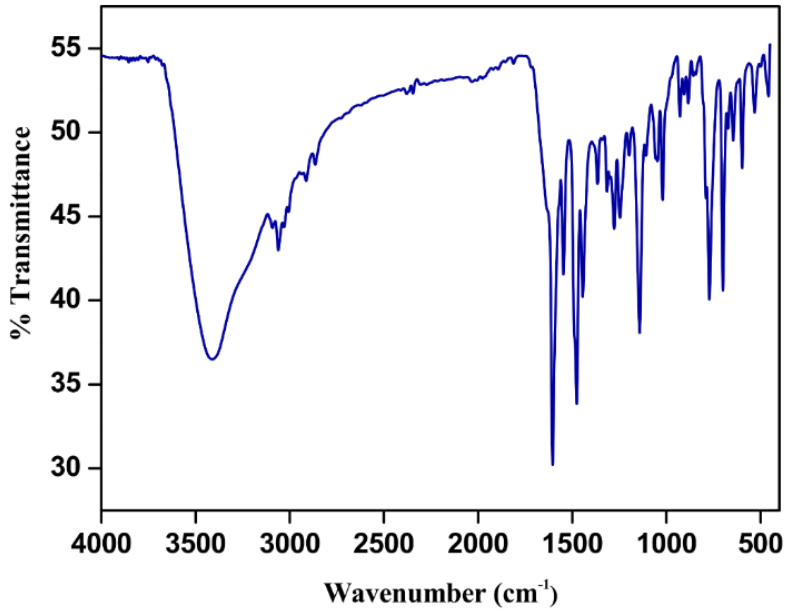

Figure S3. FT-IR spectrum of complex **C1**.

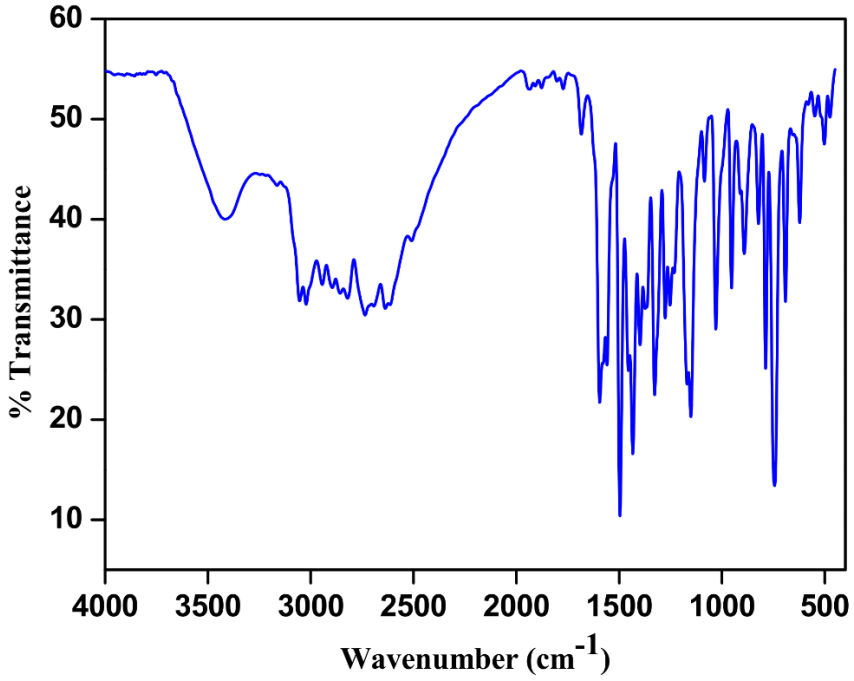

Figure S4. FT-IR spectrum of Ligand L2.

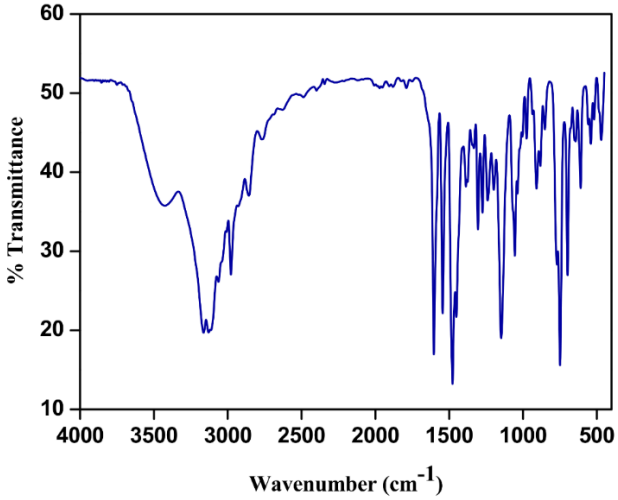

Figure S5. FT-IR spectrum of complex **C2**.

Generally, N-H stretching frequencies generally come in a higher range 3100-3400 cm^{-1}. However, in the IR spectrum of **L2,** we did not find any band in that region. The highest stretching frequency band in the IR spectrum is found at 3055 cm^{-1} which is assigned as N-H stretching. The lower frequency for the N-H bond in the case of **L2** could be possible due to the strong intramolecular hydrogen bonding between the hydrogen atom of N-H with the imine nitrogen atom and pyridine nitrogen in the solid state atom as shown below.

However, in the case of complex **C2** such type of hydrogen bonding is absent due to steric reason, and in the IR spectrum of **C2** shows a band at 3163 cm^{-1} for N-H stretching frequency.

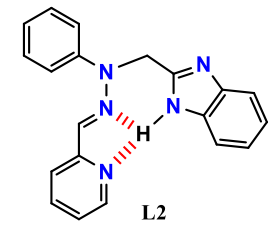

Intramolecular hydrogen bonding

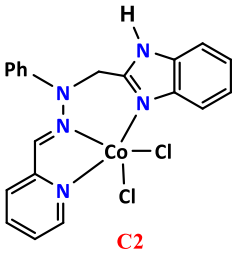

No Intramolecular hydrogen bonding

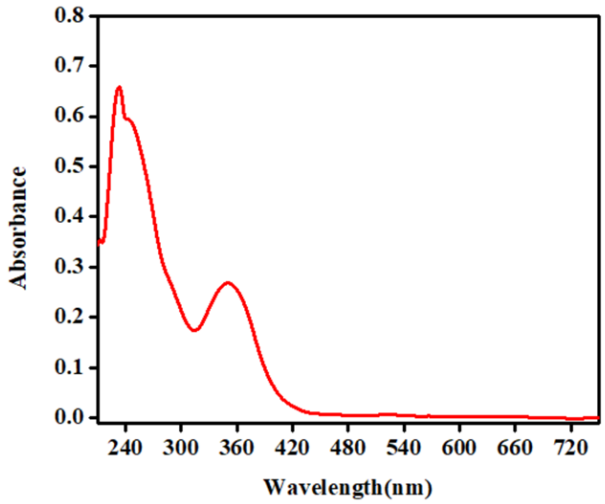

Figure S6. Electronic absorption spectra of complex **C1** in DCM (Concentration 27.90 μM).

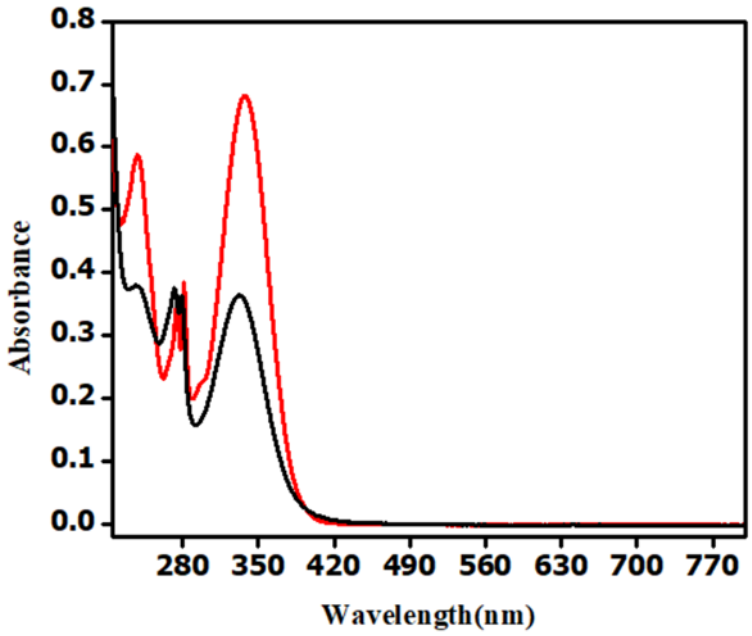

Figure S7. Electronic absorption spectra of ligand (**L2** black line, Concentration 30.54 μM) Complex (**C2** red line, Concentration 32.80 μM) in MeOH.

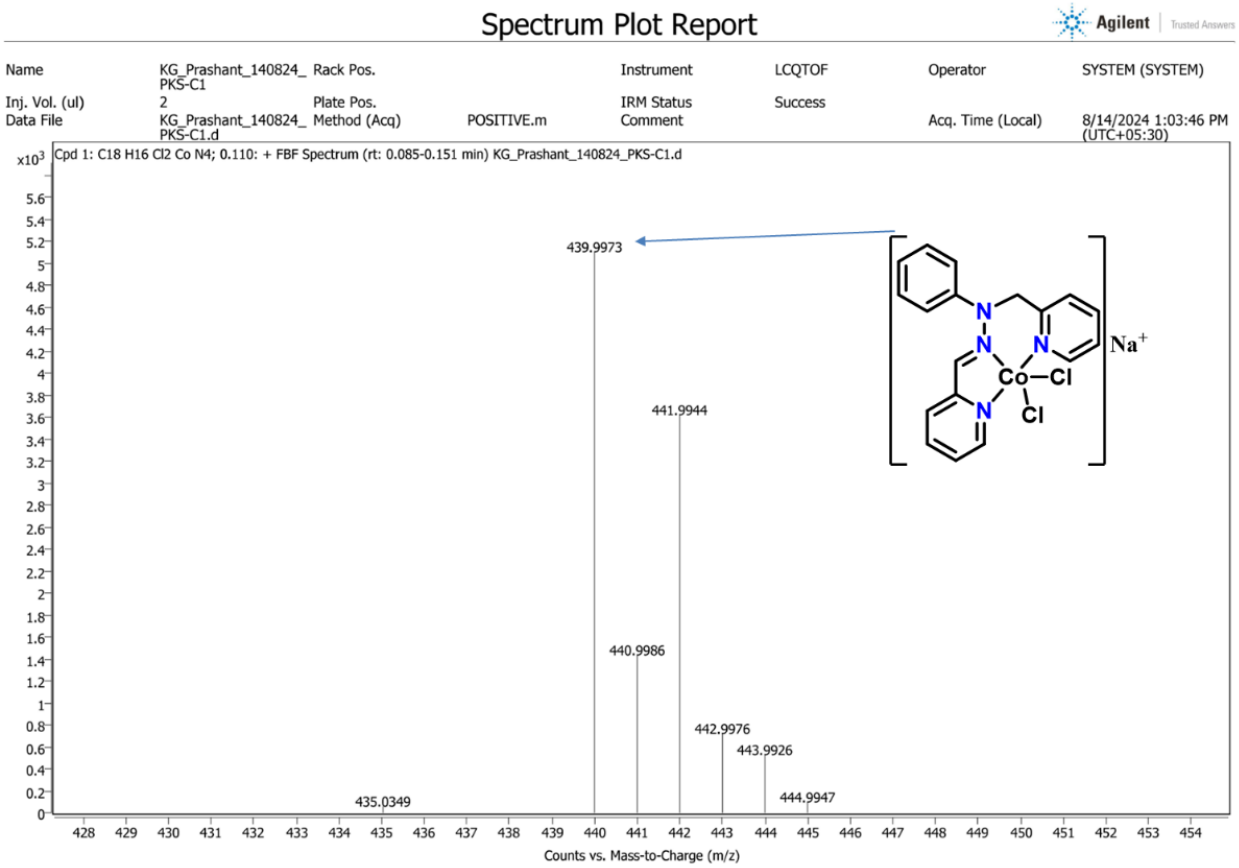

Figure S8 -HRMS spectrum of **C1**

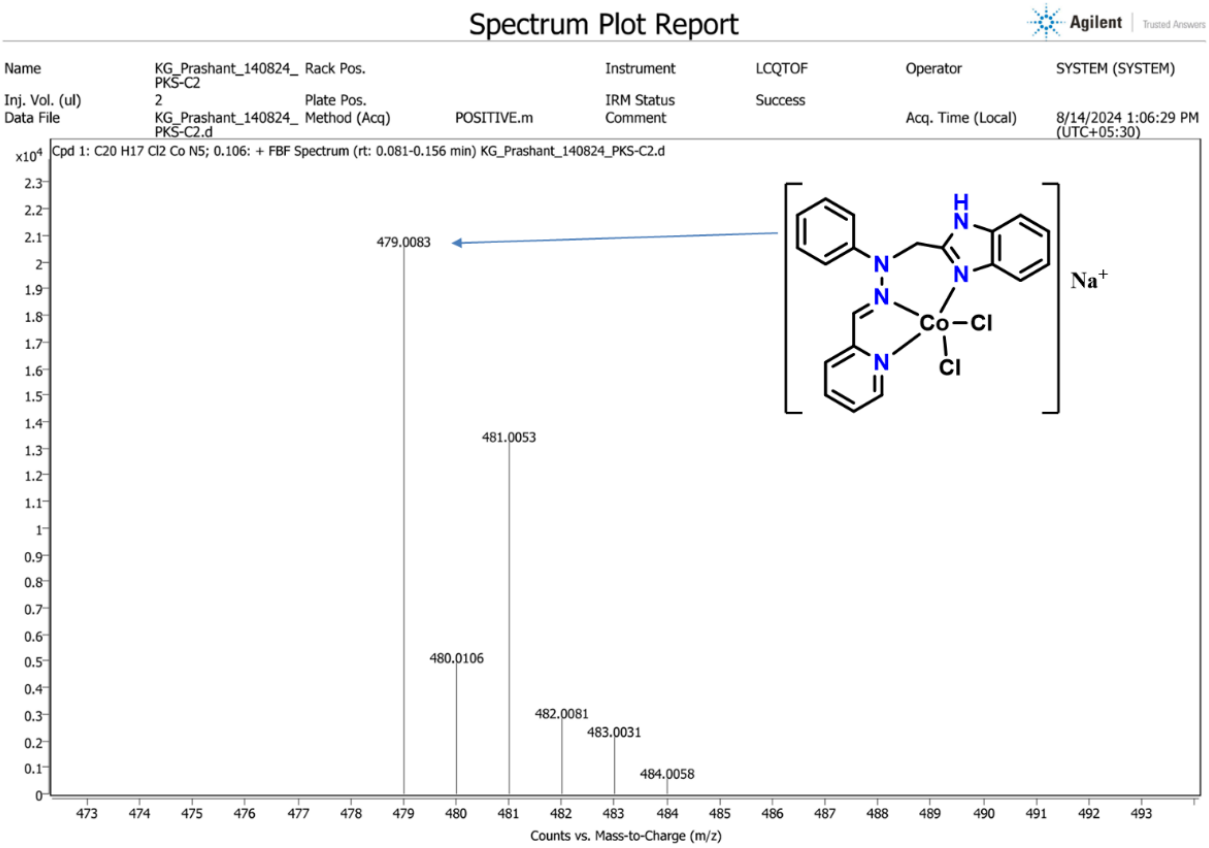

Figure S9 -HRMS spectrum of **C2**

3. Single crystal XRD characterization

3.1 Crystal data collections and refinement parameters

Identification code	C1	C2
Empirical formula	$C_{18}H_{16}Cl_2CoN_4$	$C_{20}H_{17}Cl_2CoN_5$
Formula weight	418.18	457.21
Temperature/K	293(2)	102.00
Crystal system	orthorhombic	monoclinic
Space group	*Pca2₁*	*P2₁/c*
a/Å	12.866(4)	14.7263(6)
b/Å	8.914(2)	13.7199(6)
c/Å	15.975(4)	11.4426(5)
α/°	90	90
β/°	90	109.199(2)
γ/°	90	90
Volume/Å^3	1832.1(8)	2183.32(16)

Z	4	4
ρ_{calc}g/cm^3	1.516	1.391
μ/mm^{-1}	-	1.045
F(000)	852.0	932.0
Crystal size/mm^3	0.31 × 0.25 × 0.2	0.145 × 0.07 × 0.015
Radiation	MoKα (λ = 0.71073)	MoKα (λ = 0.71073)
2Θ range for data collection/°	4.57 to 56.272	4.934 to 50.11
Index ranges	-15 ≤ h ≤ 17, -11 ≤ k ≤ 11, -20 ≤ l ≤ 21	-17 ≤ h ≤ 17, -16 ≤ k ≤ 16, -13 ≤ l ≤ 13
Reflections collected	22037	49192
Independent reflections	4476 [R_{int} = 0.0418, R_{sigma} = 0.0502]	3853 [R_{int} = 0.1082, R_{sigma} = 0.0534]
Data/restraints/parameters	4476/1/226	3853/0/256
Goodness-of-fit on F^2	1.053	1.015
Final R indexes [I>=2σ (I)]	R_1 = 0.0418, wR_2 = 0.1021	R_1 = 0.0406, wR_2 = 0.0847
Final R indexes [all data]	R_1 = 0.0654, wR_2 = 0.1180	R_1 = 0.0663, wR_2 = 0.0962
Largest diff. peak/hole / e Å^{-3}	0.86/-0.57	0.40/-0.43

Table S1 – Crystal data collections and refinement parameters for **C1 and C2.**

3.2 Single crystal structure of C1 = [Co(II)(L1)Cl$_2$]

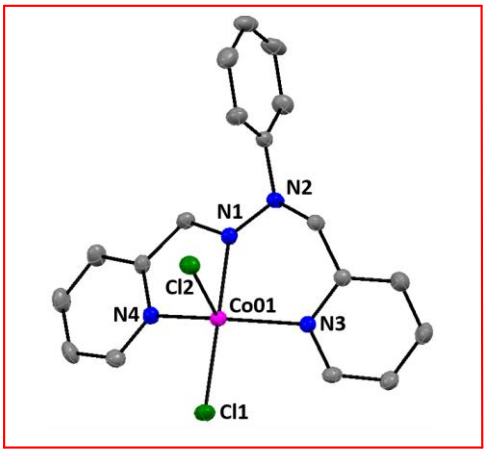

Figure S10 - ORTEP diagram (25% probability level) of **C1** = [Co(II)(L1)Cl$_2$] hydrogen atoms connected to carbon atoms are omitted for clarity.

Atom	Atom	Length/Å	Atom	Atom	Length/Å
Co01	Cl2	2.3291(16)	C3	C4	1.363(10)
Co01	Cl1	2.3109(16)	C3	C2	1.381(10)

Atom	Atom	Length/Å	Atom	Atom	Length/Å
Co01	N3	2.101(5)	C16	C15	1.391(10)
Co01	N4	2.104(5)	C10	C17	1.463(9)
Co01	N1	2.214(4)	C10	C9	1.390(8)
N3	C5	1.351(7)	N1	C17	1.283(7)
N3	C1	1.361(7)	C5	C4	1.380(9)
C11	N2	1.457(7)	C8	C9	1.370(10)
C11	C16	1.389(9)	C8	C7	1.371(10)
C11	C12	1.381(9)	C2	C1	1.376(9)
C18	N2	1.476(7)	C12	C13	1.372(10)
C18	C1	1.485(8)	C15	C14	1.384(12)
N4	C10	1.355(8)	C6	C7	1.386(9)
N4	C6	1.328(8)	C14	C13	1.385(12)
N2	N1	1.373(6)			

Table S2 – Selected bond lengths of **C1** = [Co(II)(L1)Cl_2].

Atom	Atom	Atom	Angle/˚	Atom	Atom	Atom	Angle/˚
Cl1	Co01	Cl2	104.26(6)	C4	C3	C2	118.4(7)
N3	Co01	Cl2	96.42(13)	C11	C16	C15	119.4(7)
N3	Co01	Cl1	115.19(12)	N4	C10	C17	116.0(5)
N3	Co01	N4	130.25(18)	N4	C10	C9	121.8(6)
N3	Co01	N1	82.95(17)	C9	C10	C17	122.1(6)
N4	Co01	Cl2	97.15(14)	N2	N1	Co01	124.1(3)
N4	Co01	Cl1	107.27(15)	C17	N1	Co01	114.3(4)
N4	Co01	N1	75.00(18)	C17	N1	N2	121.2(5)
N1	Co01	Cl2	168.58(13)	N3	C5	C4	123.4(6)
N1	Co01	Cl1	86.19(13)	C9	C8	C7	119.9(6)
C5	N3	Co01	120.3(4)	C3	C4	C5	119.0(6)
C5	N3	C1	117.3(5)	N1	C17	C10	116.4(5)
C1	N3	Co01	122.2(4)	C1	C2	C3	120.8(7)
C16	C11	N2	120.0(5)	C13	C12	C11	120.2(7)
C12	C11	N2	119.2(6)	C14	C15	C16	118.9(7)
C12	C11	C16	120.8(6)	C8	C9	C10	118.5(6)
N2	C18	C1	112.5(5)	N3	C1	C18	116.9(5)
C10	N4	Co01	115.9(4)	N3	C1	C2	121.0(5)
C6	N4	Co01	125.5(4)	C2	C1	C18	122.0(5)
C6	N4	C10	118.6(5)	N4	C6	C7	122.3(6)
C11	N2	C18	115.5(4)	C8	C7	C6	118.9(6)
N1	N2	C11	118.1(4)	C15	C14	C13	121.6(7)
N1	N2	C18	111.8(4)	C12	C13	C14	119.1(7)

Table S3 – Selected bond angles of **C1** = [Co(II)(L1)Cl_2].

3.3 Single crystal structure of C2 = [Co(II)(L2)Cl_2]

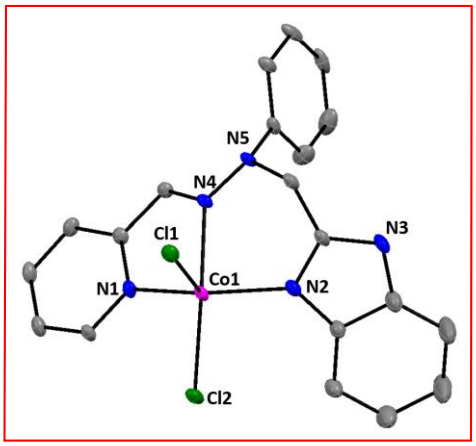

Figure S11 - ORTEP diagram (25% probability level) of **C2** = [Co(II)(L2)Cl_2] hydrogen atoms connected to carbon atoms molecule are omitted for clarity.

Atom	Atom	Length/Å	Atom	Atom	Length/Å
Co1	Cl1	2.3128(9)	C3	C4	1.382(5)
Co1	Cl2	2.3323(9)	C4	C5	1.391(4)
Co1	N1	2.087(3)	C5	C9	1.449(4)
Co1	N2	2.062(3)	C6	C16	1.487(5)
Co1	N4	2.216(3)	C7	C8	1.396(5)
N1	C1	1.345(4)	C7	C17	1.385(6)
N1	C5	1.362(4)	C8	C20	1.391(5)
N2	C6	1.333(4)	C10	C11	1.369(5)
N2	C8	1.397(4)	C10	C15	1.377(5)
N3	C6	1.340(4)	C11	C12	1.395(5)
N3	C7	1.378(5)	C12	C13	1.368(6)
N4	N5	1.371(3)	C13	C14	1.363(6)
N4	C9	1.288(4)	C14	C15	1.393(5)
N5	C10	1.448(4)	C17	C18	1.381(7)
N5	C16	1.470(4)	C18	C19	1.395(7)
C1	C2	1.371(5)	C19	C20	1.371(6)
C2	C3	1.379(5)			

Table S4 – Selected bond lengths of **C2** = [Co(II)(L2)Cl_2]

Atom	Atom	Atom	Angle/˚	Atom	Atom	Atom	Angle/˚
Cl1	Co1	Cl2	102.15(3)	N1	C5	C4	121.7(3)
N1	Co1	Cl1	108.43(8)	N1	C5	C9	115.5(3)
N1	Co1	Cl2	95.85(8)	C4	C5	C9	122.8(3)
N1	Co1	N4	75.12(10)	N2	C6	N3	111.7(3)
N2	Co1	Cl1	113.25(8)	N2	C6	C16	123.7(3)
N2	Co1	Cl2	98.05(8)	N3	C6	C16	124.6(3)
N2	Co1	N1	131.77(10)	N3	C7	C8	105.9(3)

Atom	Atom	Atom	Angle/˚	Atom	Atom	Atom	Angle/˚
N2	Co1	N4	82.15(10)	N3	C7	C17	131.6(4)
N4	Co1	Cl1	89.23(7)	C17	C7	C8	122.4(4)
N4	Co1	Cl2	167.38(7)	C7	C8	N2	108.2(3)
C1	N1	Co1	124.7(2)	C20	C8	N2	131.3(3)
C1	N1	C5	117.9(3)	C20	C8	C7	120.4(4)
C5	N1	Co1	117.2(2)	N4	C9	C5	116.9(3)
C6	N2	Co1	119.3(2)	C11	C10	N5	119.0(3)
C6	N2	C8	106.0(3)	C11	C10	C15	120.8(3)
C8	N2	Co1	134.5(2)	C15	C10	N5	120.3(3)
C6	N3	C7	108.1(3)	C10	C11	C12	118.5(4)
N5	N4	Co1	125.04(19)	C13	C12	C11	121.3(4)
C9	N4	Co1	114.8(2)	C14	C13	C12	119.6(3)
C9	N4	N5	119.7(3)	C13	C14	C15	120.2(4)
N4	N5	C10	118.0(2)	C10	C15	C14	119.6(4)
N4	N5	C16	111.7(2)	N5	C16	C6	112.8(3)
C10	N5	C16	116.7(3)	C18	C17	C7	116.4(5)
N1	C1	C2	122.9(3)	C17	C18	C19	121.6(5)
C1	C2	C3	119.4(3)	C20	C19	C18	121.9(4)
C2	C3	C4	119.0(3)	C19	C20	C8	117.3(4)
C3	C4	C5	119.1(3)				

Table S5 – Selected bond angles of **C2** = $[Co(II)(L2)Cl_2]$

4. Spin density digrams for C1 and C2

In the computational study of Co (II) complexes using Gaussian, we employed spin-unrestricted Density Functional Theory (DFT) calculations to represent the electronic structure of complexes with unpaired electrons accurately. In this method, electrons are treated with either alpha (spin-up) or beta (spin-down) orientations, allowing for independent occupancy of molecular orbitals by electrons with different spins. This approach is essential for accurately describing the magnetic properties and electronic distribution in systems where electron spins are not completely paired, as is common in transition metal complexes. For better understanding, we have included detailed spin density diagrams of complex C1 and C2 in the revised manuscript that illustrate the electronic distributions across the orbitals, these distributions enhancing the clarity of our electronic structure discussion." From our computational study, these Cobalt(II) complexes are best described as S=3/2 having quartet spin multiplicity, which defines these complexes as high spin. Moreover, these findings were also validated by our experimental data, which suggest these complexes are high spin, making them best suited for S=3/2.

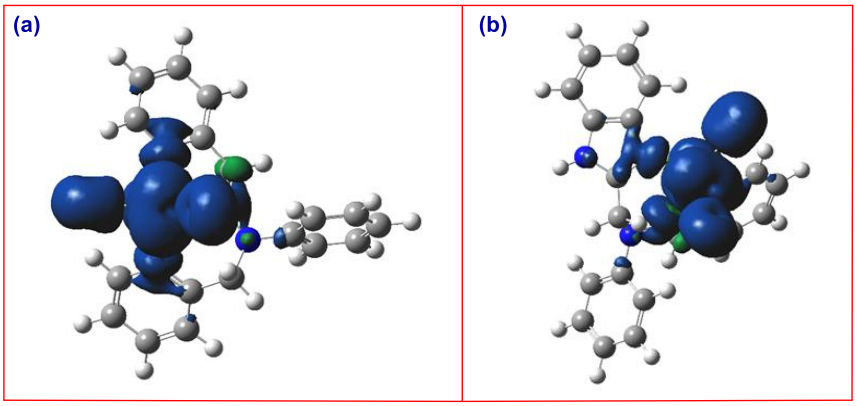

Figure 12. Spin density plot of **C1** (a) and **C2** (b)

5. Magnetic moment calculation and determination of the number of unpaired electrons in the complex (Evans Method)

A 500 μL solution of complexes (**C1** or **C2**) containing HMDS (internal standard) in DMSO-d_6 was taken in a Wilmad screw-cap NMR tube. HMDS in DMSO-d_6 was taken in Wilmad coaxial insert stem, and the tube was carefully inserted inside the screw-cap NMR tube. ^{1}H NMR spectra of complexes was recorded in a Jeol 500 MHz NMR instrument at 25 °C. Paramagnetic susceptibility of the complexes was determined using the following equation: $\chi_P = \chi_0 + 3000\Delta\nu/4\pi\nu_0 cM$ Here, χ_0 = diamagnetic susceptibility, $\Delta\nu$ = shift of frequency of the methyl protons of HMDS in Hz, ν_0 = frequency of the NMR instrument used during the measurement, c = concentration of the complexes and M = molecular weight. Effective magnetic moment (μeff) of the KRS-1 was determined using the following equation: $\mu_{eff} = (3k_B\chi_P T/NA\beta^2)^{1/2} = (8 \times \chi_P \times T)^{1/2}$ Where kB = Boltzmann's constant, T = Temperature, NA = Avogadro's number, β = Bohr magneton. The ratio of 3kB /NA$\beta^2 \approx 8$. Molar paramagnetic susceptibility was estimated from the χ_P value and molecular weight of the complexes.

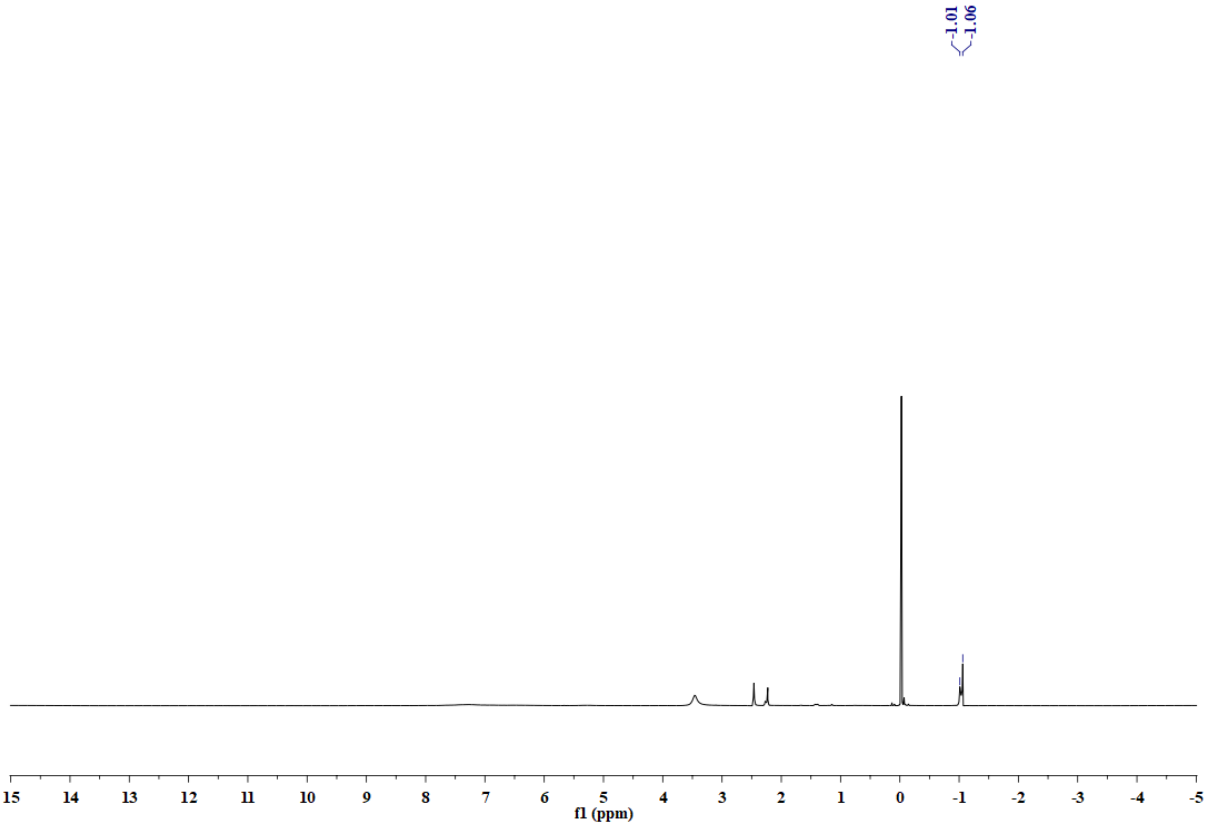

Figure S13: The shift of methyl protons of HMDS was observed (0.05 ppm) for **C1** (2.39×10^{-3} M) in DMSO-d_6 at 25 °C. This shift value provides a magnetic moment value (μ_{eff}) of 3.54 BM.

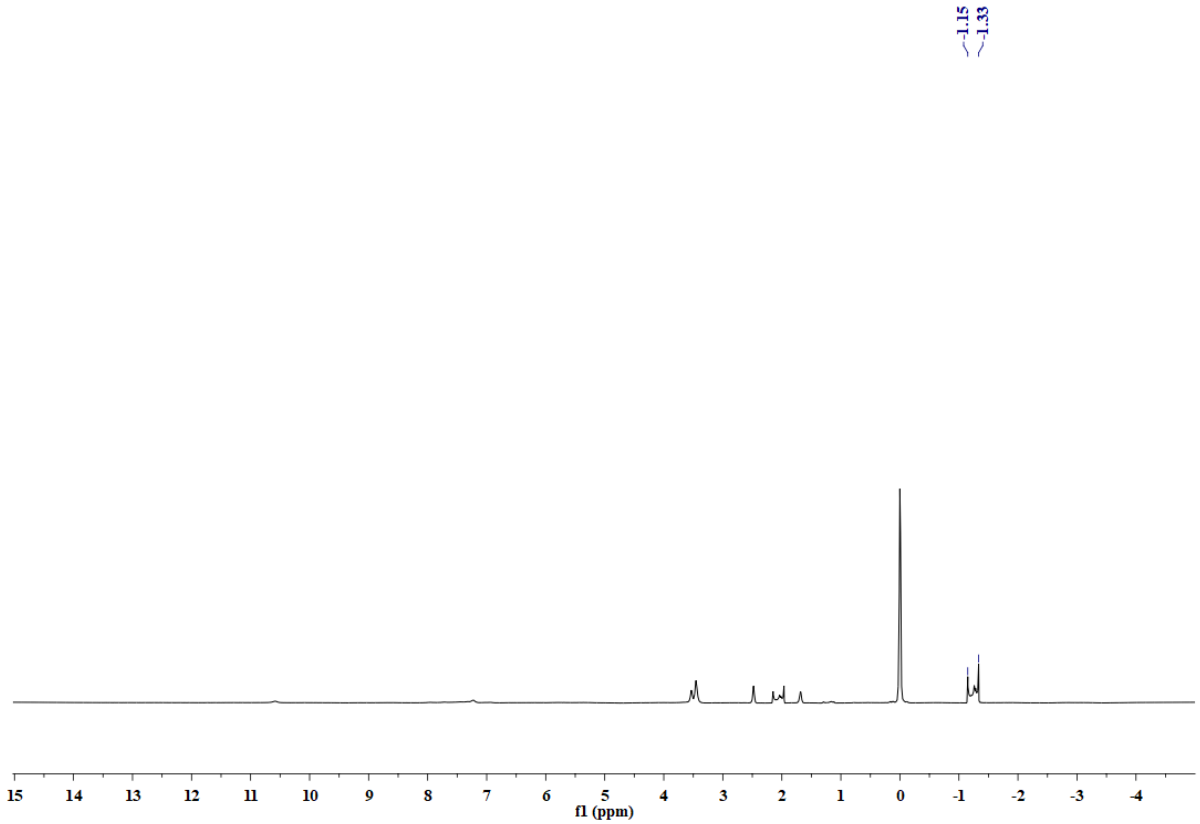

Figure S14: The shift of methyl protons of HMDS was observed (0.18 ppm) for **C2** (7.87×10^{-3} M) in DMSO-d_6 at 25 °C. This shift value provides a magnetic moment value (μ_{eff}) of 3.7 BM.

6. Cyclic voltammetry studies of the complexes (C1 and C2)

Electrochemical nature of all the complexes **C1** and **C2** was investigated in DMF at 10^{-3} M concentration, using a three-electrode assembly containing glassy carbon working electrode, platinum auxiliary electrode and Ag/AgCl reference electrode at room temperature. $TBAPF_6$ (0.1 M) was used as supporting- electrolyte and the ferrocenium-ferrocene redox couple was used as a standard for calibration. A voltammogram of complex **C1** recorded in the range -1.75 V to 1.5 V, at the scan rate of 100 mV/s is shown in Figure below.

The cyclic voltammogram of **C1** reveals two oxidation peaks centered at -0.14 V and +1.24 V. The first one is associated with the irreversible Co(II) / Co(III) oxidation while the second one is attributed to the oxidation of ligand L coordinated to the metal center. **C1** shows two reduction peaks centered at -0.94 V for Co(III) / Co(II) redox process and at -1.35 V is assigned for reduction of ligand. In the cyclic voltammogram of **C2** reveals two oxidation peaks centered at -0.05 V and +1.36 mV. The first one is associated with the irreversible Co(II) / Co(III) oxidation and the second one is attributed to the oxidation of ligand L coordinated to metal center. **C2** shows two reduction peaks centered at -0.88 V for Co(III) / Co(II) redox process and at -1.35 V is assigned for reduction of ligand.

S. No	Complex	E_{pa} (V)	E_{pc} (V)	ΔE_p	$E_{1/2}$
1	**C1**	-0.14	-0.94	0.80	-0.54
2	**C2**	-0.05	-0.88	0.83	-0.465

Data from cyclic voltametric measurements; $E_{1/2}$ is calculated as average of anodic (E_{pa}) and cathodic (E_{pc}) peak potentials; $E_{1/2} = (E_{pa} + E_{pc})/2$ and $\Delta E_p = E_{pa} - E_{pc}$.

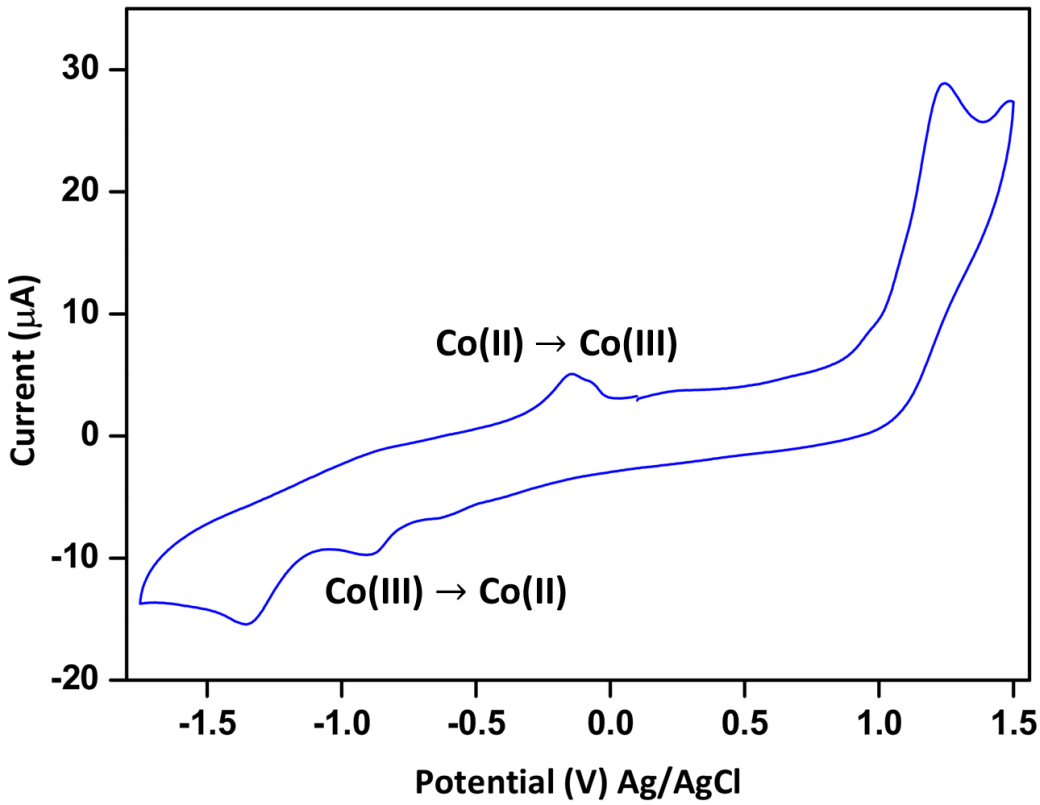

Figure S15- Cyclic voltammogram of complex **C1**

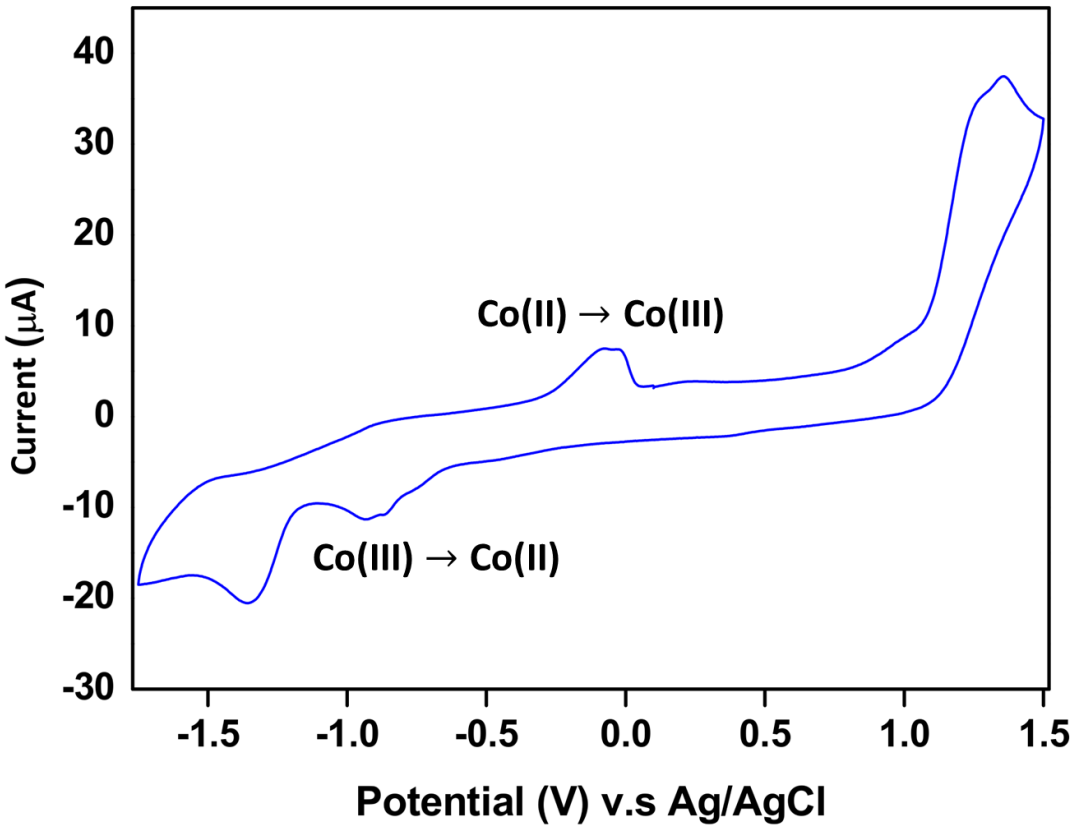

Figure S16- Cyclic voltammogram of complex **C2**

The anodic potentials of **C1** (-0.14 V) and **C2** (-0.05 V) vs. Ag/AgCl in cyclic voltammetry indicate differences in electron density at the Co(II) center. The more negative potential for **C1** suggests a higher electron density, stabilizing Co(II) and making oxidation to Co(III) less favorable. In contrast, the less negative potential for **C2** implies lower electron density, facilitating the Co(II) → Co(III) transition. These observations highlight the influence of ligand effects on the redox behavior of the cobalt center. The more positive oxidation potential (closer to zero) indicates that the Co(II) center in this complex is less easily oxidized to Co(III). This suggests that the electron density on the Co(II) center is lower in the **C2**.

Complex	Anodic Potential (V vs. Ag/AgCl)	Electron Density on Co(II) Center
C1 (more negative potential)	-0.14 V	Higher electron density on Co(II) (more easily oxidized)
C2 (less negative potential)	-0.05 V	Lower electron density on Co(II) (less easily oxidized)

Cyclic voltammetry reveals that **C2** has a more electron-deficient metal center than **C1**, indicating greater π-acidity of ligand L2 over L1. The electron deficiency in **C2** enhances its catalytic efficiency, as it facilitates the binding of the π-donor alkoxide anion during the catalytic cycle, promoting key reaction intermediates.

7. Optimization of reaction conditions

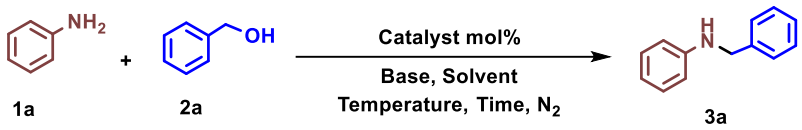

1a + 2a → 3a

Entry	Catalyst Mol%	Base	Temperature	Time (hours)	Solvent	Yield (%)
1	L1 or L2 (2mol%)	^{t}BuOK 0.5eq	110	12	Toluene	NR
2	$CoCl_2.6H_2O$ (2mol%)	^{t}BuOK 0.5eq	110	12	Toluene	NR
3	C1 (2mol%)	^{t}BuOK 0.5eq	110	12	Toluene	66
4	C2 (2mol%)	^{t}BuOK 0.5eq	110	12	Toluene	88
5	C2 (2mol%)	No base	110	12	Toluene	NR
6	C2 (2mol%)	KOH 0.5eq	110	12	Toluene	65
7	C2 (2mol%)	NaOH 0.5eq	110	12	Toluene	56
8	C2 (2mol%)	Na_2CO_3 0.5eq	110	12	Toluene	24
9	C2 (2mol%)	K_2CO_3 0.5eq	110	12	Toluene	27
10	C2 (2mol%)	Cs_2CO_3 0.5eq	110	12	Toluene	35
11	C2 (2mol%)	$NaHCO_3$ 0.5eq	110	12	Toluene	NR
12	C2 (2mol%)	^{t}BuOK 0.5eq	110	12	Xylene	77
13	C2 (2mol%)	^{t}BuOK 0.5eq	110	12	Benzene	69
14	C2 (2mol%)	^{t}BuOK 0.5eq	110	12	DMF	NR
15	C2 (2mol%)	^{t}BuOK 0.5eq	110	12	DMSO	NR
16	C2 (2mol%)	^{t}BuOK 0.5eq	110	12	1,4-dioxane	38
17	C2 (2mol%)	^{t}BuOK 0.5eq	110	12	t-amyl alcohol	23
18	C2 (2mol%)	^{t}BuOK 0.5eq	110	12	BuOH	32
19	C2 (2mol%)	^{t}BuOK 0.5eq	110	12	^{i}PrOH	25

20	C2 (2mol%)	^{t}BuOK 0.1eq	110	12	Toluene	NR
21	C2 (2mol%)	^{t}BuOK 0.2eq	110	12	Toluene	37
22	C2 (2mol%)	^{t}BuOK 0.3eq	110	12	Toluene	55
23	C2 (2mol%)	^{t}BuOK 0.4eq	110	12	Toluene	76
24	C2 (2mol%)	^{t}BuOK 0.6eq	110	12	Toluene	88
25	C2 (2mol%)	^{t}BuOK 0.7eq	110	12	Toluene	88
26	C2 (0.5mol%)	^{t}BuOK 0.5eq	110	12	Toluene	12
27	C2 (1mol%)	^{t}BuOK 0.5eq	110	12	Toluene	36
28	C2 (1.5mol%)	^{t}BuOK 0.5eq	110	12	Toluene	48
29	C2 (2.5mol%)	^{t}BuOK 0.5eq	110	12	Toluene	88
30	C2 (2mol%)	^{t}BuOK 0.5eq	110	9	Toluene	64
31	C2 (2mol%)	^{t}BuOK 0.5eq	110	10	Toluene	72
32	C2 (2mol%)	^{t}BuOK 0.5eq	110	11	Toluene	83
33	C2 (2mol%)	^{t}BuOK 0.5eq	110	13	Toluene	88
34	C2 (2mol%)	^{t}BuOK 0.5eq	80	13	Toluene	56
35	C2 (2mol%)	^{t}BuOK 0.5eq	90	12	Toluene	63
36	C2 (2mol%)	^{t}BuOK 0.5eq	100	12	Toluene	74
37	C2 (2mol%)	^{t}BuOK 0.5eq	120	12	Toluene	88

Table S6: Optimization of reaction conditions for N-alkylation of amine. **Reaction conditions and stoichiometry:** aniline(1a) (1.0 mmol), benzyl alcohol (2a) (1.0 mmol), temperature: 90-110 °C; base: 0.1-0.7 equivalent and time 9-13 h. Isolated yields after column chromatography.

8. Characterization of intermediates and side product (H_2) by GC-MS

8.1 Detection of H_2 via styrene reduction in presence of 10% Pd-C

In a round bottom 20 ml flask Benzyl alcohol (2.0 mmol) ^{t}BuOK (0.5 equivalent) and catalyst (**C2**, 2 mol%) were taken in 8 ml toluene. This round bottom flask then connected to another round bottom flask having styrene (2.0 mmol) with 10% Pd-C in 10 ml THF by a U-shaped glass tube under nitrogen atmosphere. First round bottom flask heated at 110 °C and second one is stirred at room temperature for next 12 hours. The H_2 liberated from first round bottom flask reached to second round bottom flask through U-shaped tube. In presence of Pd-C reduction of styrene to ethylbenzene by H_2 was detected by GC-MS confirms the formation of H_2 during catalytic cycle.

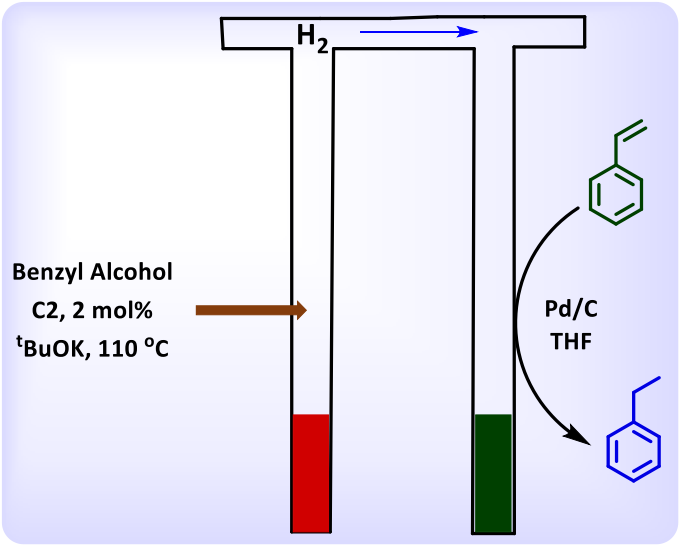

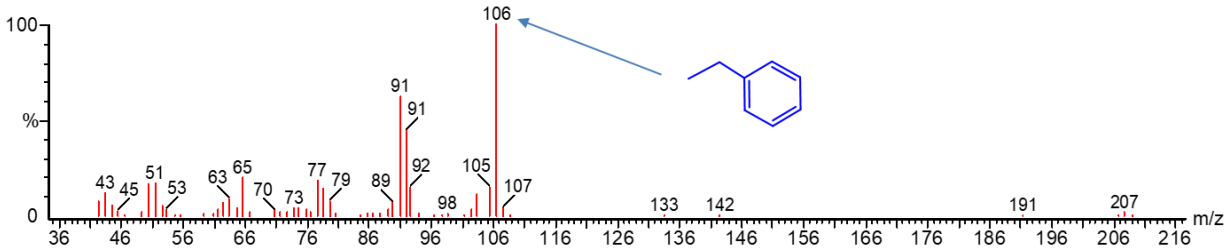

Figure S17- GC–MS spectrum of Styrene and ethyl benzene

8.2 Detection of imine intermediate during catalytic cycle

In a 10 ml catalytic tube Aniline (1.0 mmol), 4-methoxy benzyl alcohol (1.0 mmol) ^{t}BuOK (0.5 equivalent) and catalyst (**C2**, 2 mol%) were taken in 2 ml toluene. Now reaction tube is heated at 110 °C for next 4 hours and then crude reaction mixture is analyzed through GC-MS. In-situ formed imine derivative is characterized at *m/z* = 211.

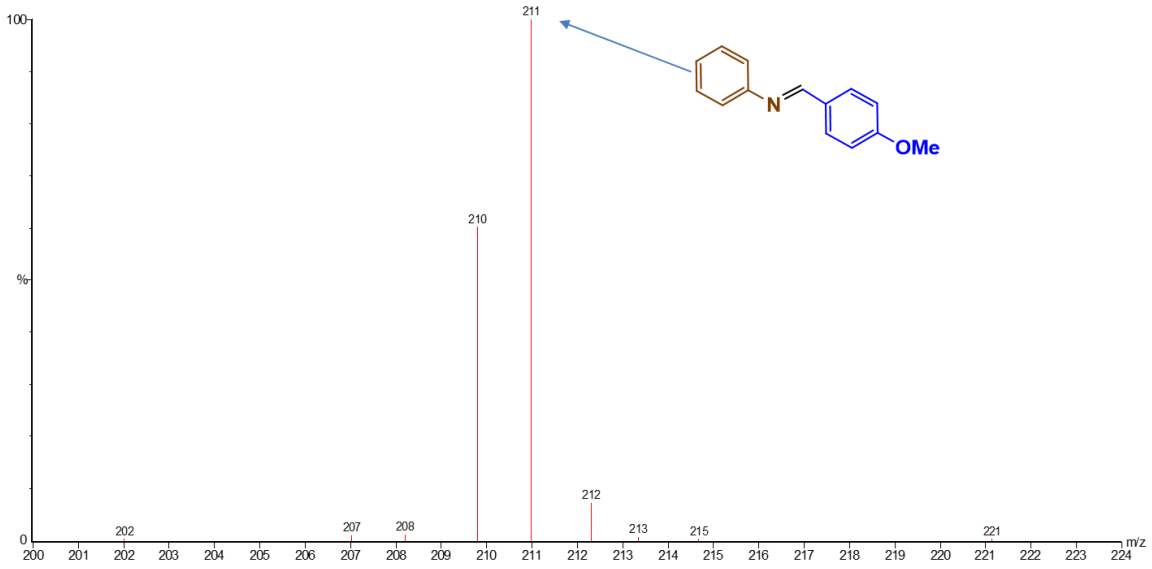

Figure S18- GC–MS spectrum of imine intermediate during catalytic cycle

8.3 Detection of Co(II) intermediates during catalysis

In a 10 ml pressure tube Aniline (1.0 mmol), benzyl alcohol (1.0 mmol), ^{t}BuOK (0.5 equivalent), **C2** (2 mol%) was taken in 2 ml dry toluene. The pressure tube was then heated at 110 °C for next 4 hours. Cool the reaction mixture at room temperature and Reaction mixture was analyzed by HRMS study. All the cobalt-hydride and cobalt-alkoxy intermediate formed by the reaction of catalysts **C2** was detected by HRMS.

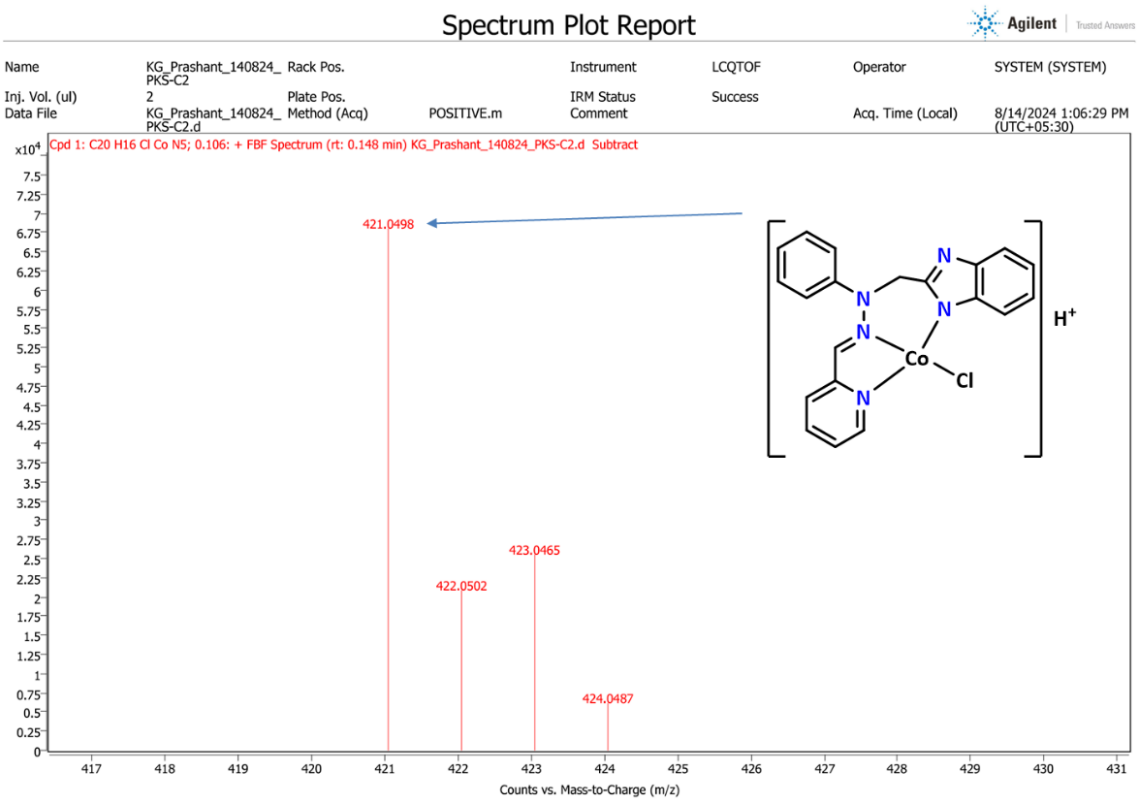

Figure S19- HRMS spectrum **C2A**

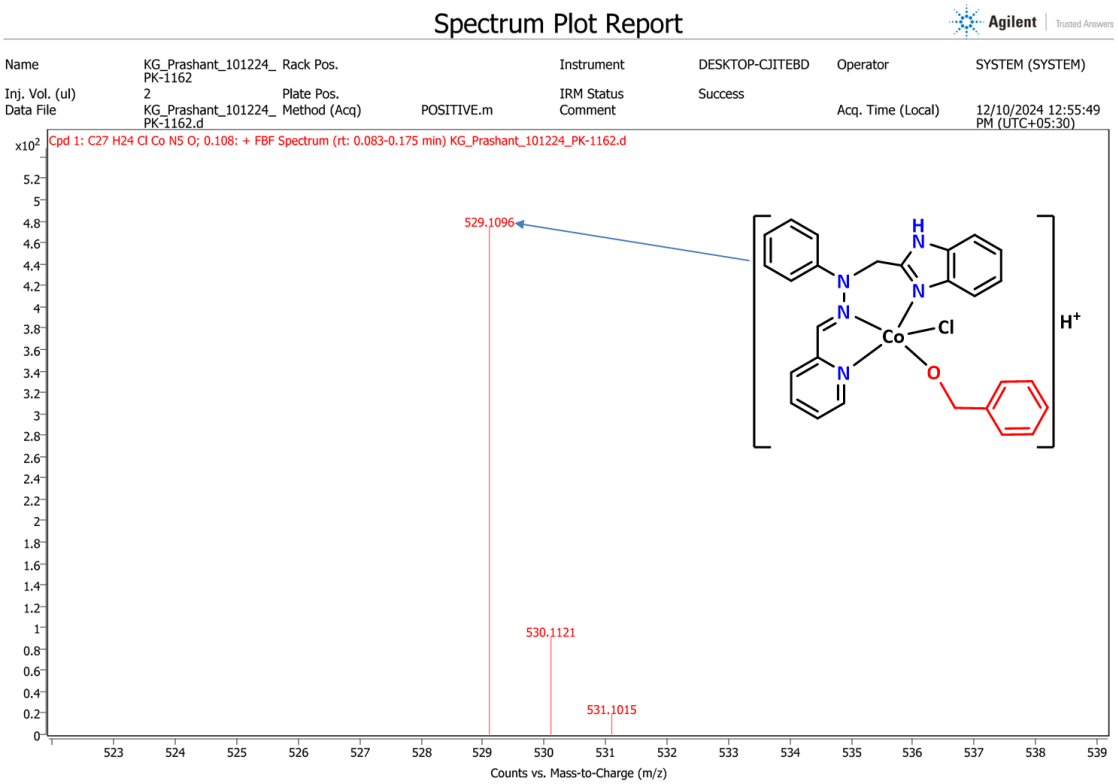

Figure S20- HRMS spectrum **C2B**

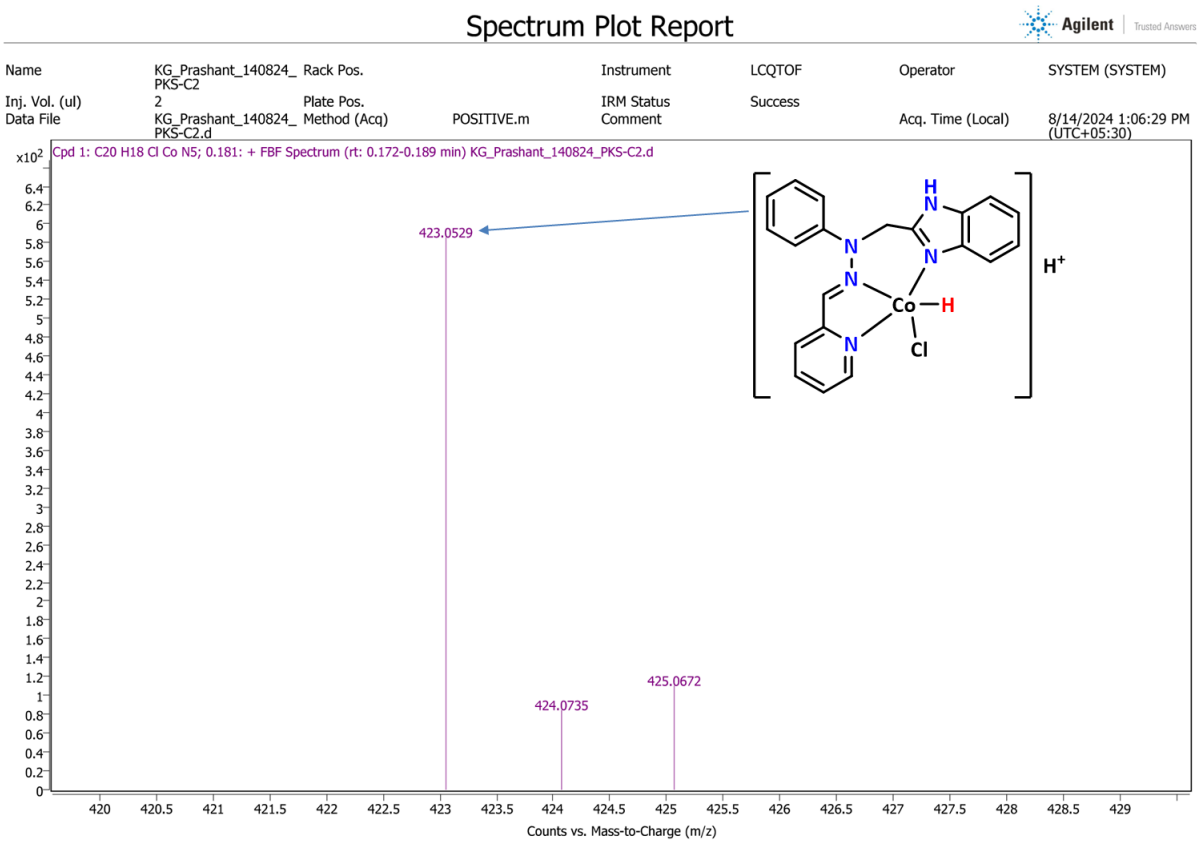

Figure S21- HRMS spectrum **C2C**

9. ^{1}H and ^{13}C NMR characterization of N-alkylated products

N-benzylaniline (3a):

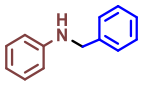

^{1}H NMR (500 MHz, $CDCl_3$) δ 7.38 – 7.32 (m, 4H), 7.27 (t, J = 7.0 Hz, 1H), 7.17 (dd, J = 8.4, 7.4 Hz, 2H), 6.72 (t, J = 7.3 Hz, 1H), 6.63 (d, J = 7.7 Hz, 2H), 4.31 (s, 2H), 4.00 (s, 1H). ^{13}C NMR (126 MHz, $CDCl_3$) δ 148.23 (s), 139.52 (s), 129.34 (s), 128.71 (s), 127.58 (s), 127.30 (s), 117.63 (s), 112.92 (s), 48.37 (s).

N-(4-methoxybenzyl)aniline (3b):

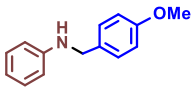

^{1}H NMR (500 MHz, $CDCl_3$) δ 7.28 (d, J = 8.6 Hz, 2H), 7.18 – 7.15 (m, 2H), 6.87 (d, J = 8.6 Hz, 2H), 6.71 (t, J = 7.3 Hz, 1H), 6.63 (d, J = 7.7 Hz, 2H), 4.24 (s, 2H), 3.93 (s, 1H), 3.79 (s, 3H). ^{13}C NMR (126 MHz, $CDCl_3$) δ 158.89 (s), 148.25 (s), 131.45 (s), 129.29 (s), 128.84 (s), 117.53 (s), 115.00 (s), 114.06 (s), 112.87 (s), 55.33 (s), 47.82 (s).

N-(2-methoxybenzyl)aniline (3c):

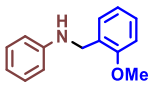

^{1}H NMR (500 MHz, $CDCl_3$) δ 7.32 – 7.28 (m, 1H), 7.25 – 7.18 (m, 2H), 6.99 (dd, J = 13.7, 4.9 Hz, 2H), 6.86 (dd, J = 8.2, 2.4 Hz, 1H), 6.76 (t, J = 7.3 Hz, 1H), 6.68 (dd, J = 8.5, 0.9 Hz, 2H), 4.35 (s, 2H), 4.08 (s, 1H), 3.84 (s, 3H). ^{13}C NMR (126 MHz, $CDCl_3$) δ 159.95 (s), 148.16 (s), 141.20 (s), 129.68 (s), 129.28 (s), 119.76 (s), 117.63 (s), 113.05(s),112.90 (s), 112.68(s), 55.23 (s), 48.36 (s).

N-(2,4-dimethoxybenzyl)aniline (3d):

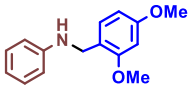

^{1}H NMR (500 MHz, $CDCl_3$) δ 7.25 – 7.18 (m, 3H), 6.75 – 6.67 (m, 3H), 6.51 (d, J = 2.3 Hz, 1H), 6.47 (dd, J = 8.3, 2.4 Hz, 1H), 4.29 (s, 2H), 4.08 (s, 1H), 3.87 (s, 3H), 3.83 (s, 3H). ^{13}C NMR (126 MHz, $CDCl_3$) δ 160.22 (s), 158.45 (s), 148.52 (s), 129.71 (s), 129.17 (s), 119.78 (s), 117.29 (s), 113.11 (s), 103.88 (s), 98.63 (s), 55.40(s), 55.37(s), 43.17 (s).

N-benzyl-4-methylaniline (3e):

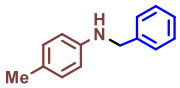

^{1}H NMR (500 MHz, $CDCl_3$) δ 7.41 – 7.29 (m, 5H), 7.01 (d, J = 8.1 Hz, 2H), 6.63 (d, J = 8.4 Hz, 2H), 4.35 (s, 2H), 3.33 (s, 1H), 2.27 (s, 3H); ^{13}C NMR (126 MHz, $CDCl_3$) δ 145.08 (s), 139.11 (s), 129.76 (s), 128.60 (s), 127.72 (s), 127.51 (s), 127.27 (s), 113.71 (s), 49.11 (s), 20.42 (s).

N-(4-methoxybenzyl)-4-methylaniline (3f):

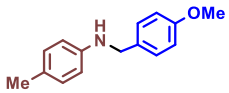

^{1}H NMR (500 MHz, $CDCl_3$) δ 7.40 – 7.25 (m, 3H), 7.02 (d, J = 8.9 Hz, 2H), 6.91 (d, J = 8.9 Hz, 2H), 6.60 (d, J = 8.7 Hz, 2H), 4.26 (s, 2H), 3.83 (s, 3H), 2.27 (s, 3H). ^{13}C NMR (126 MHz, $CDCl_3$) δ 158.80 (s), 145.98 (s), 131.65 (s), 129.72 (s), 128.78 (s), 126.70 (s), 113.99 (s), 113.01 (s), 55.30 (s), 48.14 (s), 20.39 (s).

4-methyl-N-(4-methylbenzyl)aniline (3g):

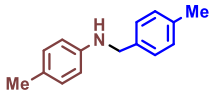

^{1}H NMR (500 MHz, $CDCl_3$) δ 7.36 (d, J = 7.9 Hz, 2H), 7.26 (d, J = 7.8 Hz, 2H), 7.10 (d, J = 8.1 Hz, 2H), 6.66 (d, J = 8.4 Hz, 2H), 4.35 (s, 2H), 3.93 (s, 1H), 2.45 (s, 3H), 2.35 (s, 3H); ^{13}C NMR (126 MHz, $CDCl_3$) δ 146.11 (s), 136.84, 136.71 (s), 129.83 (s), 129.37 (s), 127.60 (s), 126.71 (s), 115.00 (s), 113.09 (s), 48.48 (s), 21.20 (s), 20.50 (s).

N-(4-fluorobenzyl)-4-methylaniline (3h):

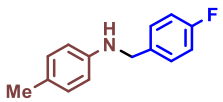

^{1}H NMR (500 MHz, $CDCl_3$) δ 7.36 (dd, J = 8.5, 5.4 Hz, 2H), 7.04 (dd, J = 19.5, 8.4 Hz, 4H), 6.58 (d, J = 8.4 Hz, 2H), 4.31 (s, 2H), 3.92 (s, 1H), 2.27 (s, 3H); ^{13}C NMR (126 MHz, $CDCl_3$) δ 145.69 (s), 135.34 (s), 129.77 (s), 128.97 (d, J = 8.2 Hz), 126.95 (s), 115.39 (d, J = 21.5 Hz), 113.03 (s), 47.94 (s), 20.39 (s).

N-(4-chlorobenzyl)-4-methylaniline (3i):

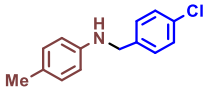

^{1}H NMR (500 MHz, $CDCl_3$) δ 7.34 (s, 4H), 7.02 (d, J = 8.1 Hz, 2H), 6.57 (d, J = 8.4 Hz, 2H), 4.32 (s, 2H), 3.97 (s, 1H), 2.28 (s, 3H); ^{13}C NMR (126 MHz, $CDCl_3$) δ 145.59 (s), 138.25 (s), 132.79 (s), 129.79 (s), 128.72 (s), 127.02 (s), 114.98 (s), 113.05 (s), 47.94 (s), 20.30 (s).

N-(3-methoxybenzyl)-4-methylaniline (3j):

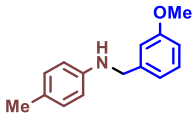

^{1}H NMR (500 MHz, $CDCl_3$) δ 7.36 (d, J = 7.9 Hz, 2H), 7.26 (d, J = 7.8 Hz, 2H), 7.10 (d, J = 8.1 Hz, 2H), 6.66 (d, J = 8.4 Hz, 2H), 4.35 (s, 2H), 3.92 (s, 1H), 2.45 (s, 3H), 2.35 (s, 3H). ^{13}C NMR (126 MHz, $CDCl_3$) δ 129.74(s), 129.61 (s), 119.75 (s), 113.03 (s), 112.62 (s), 55.22 (s), 48.69 (s), 20.39 (s).

N-(furan-2-ylmethyl)-4-methylaniline (3k):

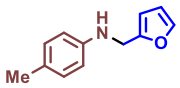

^{1}H NMR (500 MHz, $CDCl_3$) δ 7.41 (s, 1H), 7.06 (d, J = 8.2 Hz, 2H), 6.66 (d, J = 8.3 Hz, 2H), 6.37 (s, 1H), 6.28 (s, 1H), 4.34 (s, 2H), 3.94 (s, 1H), 2.30 (s, 3H). ^{13}C NMR (126 MHz, $CDCl_3$) δ 153.02 (s), 145.41 (s), 141.90 (s), 129.77 (s), 127.32 (s), 113.42 (s), 110.37 (s), 106.94 (s), 41.83 (s), 20.47 (s).

N-benzyl-4-methoxyaniline (3l):

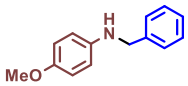

^{1}H NMR (500 MHz, $CDCl_3$) δ 7.47 – 7.34 (m, 5H), 7.30 (dd, J = 13.2, 6.1 Hz, 1H), 6.84 – 6.80 (m, 2H), 6.67 – 6.63 (m, 2H), 4.32 (s, 2H), 3.78 (s, 3H). ^{13}C NMR (126 MHz, $CDCl_3$) δ 152.24 (s), 142.50 (s), 139.73 (s), 128.61 (s), 127.57 (s), 127.19 (s), 115.00 (s), 114.15 (s), 55.84 (s), 49.28 (s).

N-benzyl-2-methoxyaniline (3m):

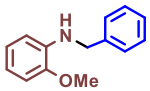

^{1}H NMR (500 MHz, $CDCl_3$) δ 7.43 – 7.35 (m, 4H), 7.30 (d, J = 7.2 Hz, 1H), 6.88 – 6.81 (m, 2H), 6.71 (td, J = 7.8, 1.5 Hz, 1H), 6.63 (dd, J = 7.8, 1.4 Hz, 1H), 4.65 (s, 1H), 4.38 (s, 2H), 3.88 (s, 3H); ^{13}C NMR (126 MHz, $CDCl_3$) δ 146.82 (s), 139.61 (s), 138.18 (s), 128.57 (s), 127.51 (s), 127.11 (s), 121.30 (s), 116.63 (s), 110.10 (s), 109.45 (s), 55.43 (s), 48.06 (s).

N-benzyl-2,3-dimethylaniline (3n):

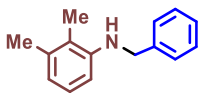

^{1}H NMR (500 MHz, $CDCl_3$) δ 7.44 – 7.36 (m, 4H), 7.32 (d, J = 7.1 Hz, 1H), 7.03 (t, J = 7.8 Hz, 1H), 6.64 (d, J = 7.5 Hz, 1H), 6.55 (d, J = 8.1 Hz, 1H), 4.39 (s, 2H), 3.90 (s, 1H), 2.32 (s, 3H), 2.11 (s, 3H); ^{13}C NMR (126

MHz, $CDCl_3$) δ 146.06 (s), 139.66 (s), 136.55 (s), 128.65 (s), 127.57 (s), 127.21 (s), 126.22 (s), 120.27 (s), 119.56 (s), 115.00 (s), 108.25 (s), 48.64 (s), 23.23 (s), 20.72 (s).

N-benzyl-3,5-dimethoxyaniline (3o):

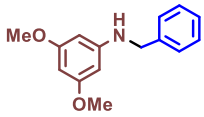

^{1}H NMR (500 MHz, $CDCl_3$) δ 7.45 – 7.36 (m, 5H), 7.31 (d, J = 7.2 Hz, 1H), 6.53 (dd, J = 18.1, 5.6 Hz, 2H), 6.42 (dd, J = 8.5, 2.6 Hz, 1H), 4.35 (s, 2H), 3.87 (s, 3H), 3.79 (s, 3H). ^{13}C NMR (126 MHz, $CDCl_3$) δ 152.02 (s), 147.93 (s), 139.89 (s), 132.62 (s), 128.55 (s), 127.56 (s), 127.07 (s), 115.00 (s), 110.40 (s), 103.84 (s), 99.27 (s), 55.82 (s), 55.49 (s), 48.85 (s).

N-benzyl-4-chloroaniline (3p):

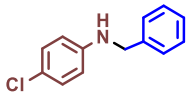

^{1}H NMR (500 MHz, $CDCl_3$) δ 7.40 (d, *J* = 4.5 Hz, 4H), 7.34 (dd, *J* = 8.8, 4.6 Hz, 1H), 7.16 (d, *J* = 8.9 Hz, 2H), 6.59 (d, *J* = 8.9 Hz, 2H), 4.35 (s, 2H), 4.10 (s, 1H); ^{13}C NMR (126 MHz, $CDCl_3$) δ 146.71 (s), 139.00 (s), 129.11 (s), 128.74 (s), 127.45 (s), 127.41 (s), 122.15 (s), 113.98 (s), 48.39 (s).

N-benzyl-4-bromoaniline (3q):

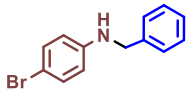

^{1}H NMR (500 MHz, $CDCl_3$) δ 7.38 (d, *J* = 4.4 Hz, 4H), 7.32 (dt, *J* = 8.8, 4.3 Hz, 1H), 7.29 – 7.26 (m, 2H), 6.54 (d, *J* = 8.9 Hz, 2H), 4.33 (s, 2H), 4.10 (s, 1H). ^{13}C NMR (126 MHz, $CDCl_3$) δ 147.03 (s), 138.85 (s), 131.94 (s), 128.72 (s), 127.41 (s), 127.39, 114.44 (s), 109.49(s), 48.26 (s).

N-benzyl-4-nitroaniline (3r):

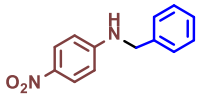

^{1}H NMR (500 MHz, $CDCl_3$) δ 8.11 (d, J = 9.5 Hz, 2H), 7.37 (ddd, J = 15.4, 13.2, 7.7 Hz, 4H), 6.60 (d, J = 9.5 Hz, 2H), 4.87 (d, J = 44.2 Hz, 2H), 4.46 (d, J = 6.1 Hz, 2H). ^{13}C NMR (126 MHz, $CDCl_3$) δ 138.20 (s), 137.36 (s), 128.98 (s), 127.90 (s), 127.37 (s), 126.42 (s), 115.00 (s), 111.36 (s), 47.68 (s).

2-(benzylamino)benzaldehyde (3s):

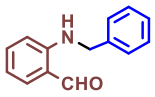

^{1}H NMR (500 MHz, $CDCl_3$) δ 9.89 (s, 1H), 8.78 (s, 1H), 7.53 (d, *J* = 7.2 Hz, 1H), 7.42 – 7.24 (m, 6H), 6.74 (t, *J* = 7.4 Hz, 1H), 6.67 (d, *J* = 8.5 Hz, 1H), 4.52 (d, *J* = 5.8 Hz, 2H). ^{13}C NMR (126 MHz, $CDCl_3$) δ 194.14 (s), 150.58 (s), 138.28 (s), 136.68 (s), 135.85 (s), 128.75 (s), 127.30 (s), 127.00 (s), 118.68 (s), 115.30 (s), 111.35 (s), 46.60 (s).

N-benzylnaphthalen-1-amine (3t):

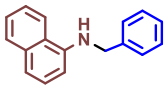

^{1}H NMR (500 MHz, $CDCl_3$) δ 7.88 (d, J = 8.1 Hz, 2H), 7.53 – 7.33 (m, 9H), 6.69 (d, J = 7.4 Hz, 1H), 4.73 (s, 1H), 4.53 (d, J = 22.6 Hz, 2H). ^{13}C NMR (126 MHz, $CDCl_3$) δ 143.29 (s), 139.18 (s), 134.36 (s), 128.80 (s), 128.68(s), 128.12 (s), 127.80 (s), 127.47 (s), 126.70 (s), 125.83 (s), 124.82 (s), 119.99 (s), 117.69 (s), 104.81 (s), 48.65 (s).

N-(4-methoxybenzyl)naphthalen-1-amine (3u):

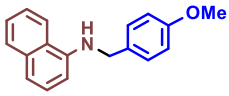

^{1}H NMR (500 MHz, $CDCl_3$) δ 7.84 (d, J = 8.3 Hz, 2H), 7.52 – 7.36 (m, 5H), 7.32 – 7.28 (m, 1H), 6.99 – 6.93 (m, 2H), 6.69 (d, J = 7.4 Hz, 1H), 4.66 (s, 1H), 4.46 (s, 2H), 3.86 (s, 3H). ^{13}C NMR (126 MHz, $CDCl_3$) δ 159.04 (s), 143.31 (s), 134.31 (s), 131.10 (s), 129.11 (s), 128.71 (s), 126.66 (s), 125.77 (s), 124.75 (s), 123.39 (s), 119.94 (s), 117.59 (s), 114.15 (s), 104.69 (s), 55.36 (s), 48.14 (s).

N-benzylpyridin-2-amine (3v):

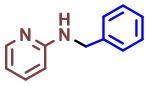

^{1}H NMR (500 MHz, $CDCl_3$) δ 8.11 (d, J = 6.1 Hz, 1H), 7.44 – 7.34 (m, 5H), 7.31 (d, J = 7.0 Hz, 1H), 6.63 – 6.59 (m, 1H), 6.39 (d, J = 8.4 Hz, 1H), 5.22 (s, 1H), 4.53 (d, J = 5.5 Hz, 2H). ^{13}C NMR (126 MHz, $CDCl_3$) δ 158.77 (s), 148.20 (s), 139.29 (s), 137.49 (s), 128.65 (s), 127.43 (s), 127.23 (s), 113.10 (s), 106.79 (s), 46.33 (s).

N-(4-methoxybenzyl)pyridin-2-amine (3w):

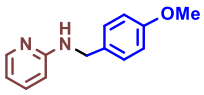

^{1}H NMR (500 MHz, $CDCl_3$) δ 8.12 (dd, J = 5.0, 1.0 Hz, 1H), 7.45 – 7.40 (m, 1H), 7.31 (d, J = 8.7 Hz, 2H), 6.92 – 6.88 (m, 2H), 6.61 (ddd, J = 7.1, 5.1, 0.7 Hz, 1H), 6.39 (d, J = 8.4 Hz, 1H), 4.89 (s, 1H), 4.45 (d, J = 5.6 Hz, 2H), 3.82 (s, 3H). ^{13}C NMR (126 MHz, $CDCl_3$) δ 158.87 (s), 158.63 (s), 148.16 (s), 137.49 (s), 131.13 (s), 128.72 (s), 114.04 (s), 113.09 (s), 106.82 (s), 55.30 (s), 45.84 (s).

N-benzyl-3-methylpyridin-2-amine (3x):

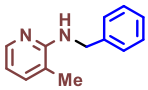

^{1}H NMR (500 MHz, $CDCl_3$) δ 8.08 (d, J = 4.1 Hz, 1H), 7.43 – 7.36 (m, 4H), 7.33 – 7.28 (m, 2H), 6.59 (dd, J = 7.0, 5.1 Hz, 1H), 4.72 (d, J = 5.0 Hz, 2H), 4.38 (s, 1H), 2.12 (s, 3H). ^{13}C NMR (126 MHz, $CDCl_3$) δ 156.66 (s), 145.52 (s), 139.99 (s), 136.89 (s), 135.23 (s), 128.62 (s), 127.90 (s), 127.21 (s), 125.04 (s), 116.53 (s), 112.93 (s), 45.87 (s), 23.44 (s).

N-(4-methoxybenzyl)-6-methylpyridin-2-amine (3y):

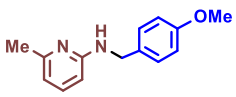

^{1}H NMR (500 MHz, $CDCl_3$) δ 7.40 – 7.27 (m, 6H), 6.49 (d, J = 7.3 Hz, 1H), 6.19 (d, J = 8.3 Hz, 1H), 4.94 (s, 1H), 4.48 (d, J = 5.9 Hz, 2H), 2.41 (s, 3H). ^{13}C NMR (126 MHz, $CDCl_3$) δ 158.36 (s), 157.04 (s), 139.20 (s), 137.98 (s), 128.61 (s), 127.35 (s), 127.20 (s), 112.58 (s), 102.86 (s), 46.60 (s), 24.34 (s).

5-bromo-N-(4-methoxybenzyl)pyridin-2-amine (3z):

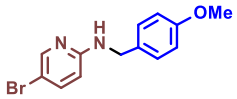

^{1}H NMR (500 MHz, $CDCl_3$) δ 8.13 (d, J = 2.3 Hz, 1H), 7.48 (dd, J = 8.8, 2.4 Hz, 1H), 7.37 (d, J = 4.7 Hz, 4H), 7.34 – 7.29 (m, 1H), 6.31 (d, J = 8.8 Hz, 1H), 5.03 (s, 1H), 4.50 (d, J = 5.8 Hz, 2H). ^{13}C NMR (126 MHz, $CDCl_3$) δ 157.17 (s), 148.76 (s), 139.80 (s), 138.68 (s), 128.73 (s), 127.43 (s), 127.39 (s), 115.00 (s), 108.30 (s), 107.30 (s), 46.37 (s).

(E)-2-(phenyldiazenyl)-N-(pyridin-2-ylmethyl)aniline (3aa):

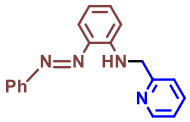

^{1}H NMR (500 MHz, $CDCl_3$) δ 9.57 (s, 1H), 8.69 (d, *J* = 4.6 Hz, 1H), 7.93 (d, *J* = 8.0 Hz, 3H), 7.68 (t, *J* = 7.7 Hz, 1H), 7.53 (t, *J* = 7.5 Hz, 2H), 7.44 (t, *J* = 7.3 Hz, 1H), 7.37 (d, *J* = 7.8 Hz, 1H), 7.28 (t, *J* = 7.7 Hz, 1H), 7.26 – 7.22 (m, 1H), 6.85 (t, *J* = 7.5 Hz, 1H), 6.77 (d, *J* = 8.4 Hz, 1H), 4.71 (d, *J* = 5.3 Hz, 2H). ^{13}C NMR (126 MHz, $CDCl_3$) δ 158.06 (s), 152.85 (s), 149.35 (s), 143.01 (s), 136.79(s), 136.73(s), 132.72 (s), 130.69 (s), 129.78 (s), 129.09 (s), 122.24(s), 122.12(s), 121.23 (s), 116.23 (s), 112.24 (s), 48.48 (s).

N1,N2-dibenzylbenzene-1,2-diamine (3ab):

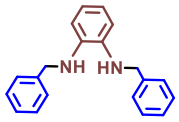

^{1}H NMR (500 MHz, $CDCl_3$) δ 7.49 – 7.40 (m, 8H), 7.36 (t, J = 6.3 Hz, 2H), 6.84 (ddd, J = 38.5, 5.2, 2.9 Hz, 4H), 4.39 (s, 4H), 3.73 (s, 2H). ^{13}C NMR (126 MHz, $CDCl_3$) δ 139.50 (s), 137.22 (s), 128.68 (s), 127.90 (s), 127.33 (s), 119.51 (s), 112.06 (s), 48.86 (s).

N1,N2-dibenzyl-4-methylbenzene-1,2-diamine (3ac):

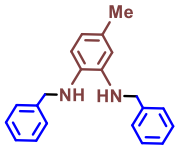

^{1}H NMR (500 MHz, $CDCl_3$) δ 7.54 – 7.31 (m, 10H), 6.73 (d, *J* = 7.9 Hz, 1H), 6.70 – 6.57 (m, 2H), 4.39 (s, 2H), 4.37 (s, 2H), 3.70 (s, 2H), 2.34 (s, 3H). ^{13}C NMR (126 MHz, $CDCl_3$) δ 139.52 (s), 137.72 (s), 129.55 (s), 129.35 (s), 128.67 (s), 128.63 (s), 127.98 (s), 127.94 (s), 127.59 (s), 127.31 (s), 127.29 (s), 119.41 (s), 115.00 (s), 112.96 (s), 49.29 (s), 48.84 (s), 21.20 (s).

N1,N4-dibenzylbenzene-1,4-diamine (3ad):

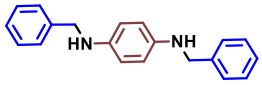

^{1}H NMR (500 MHz, $CDCl_3$) δ 7.39 (dd, J = 13.3, 7.2 Hz, 8H), 7.31 (d, J = 7.1 Hz, 2H), 6.69 – 6.65 (m, 4H), 4.36 (s, 4H), 4.06 (s, 2H). ^{13}C NMR (126 MHz, $CDCl_3$) δ 129.27 (s), 128.64 (s), 127.52 (s), 127.23 (s), 117.58 (s), 112.85 (s), 48.35 (s).

10. ^{1}H and ^{13}C NMR spectrum of N-alkylated products

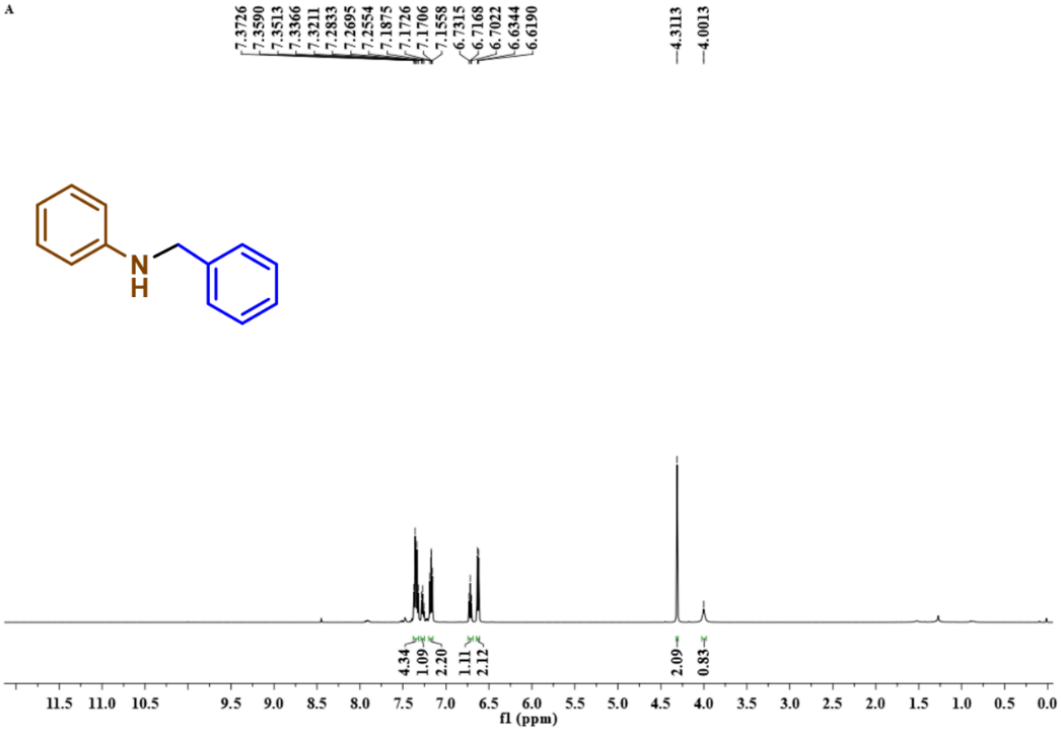

Figure S22: ^{1}H NMR spectrum of 3a in $CDCl_3$ at 500 MHz.

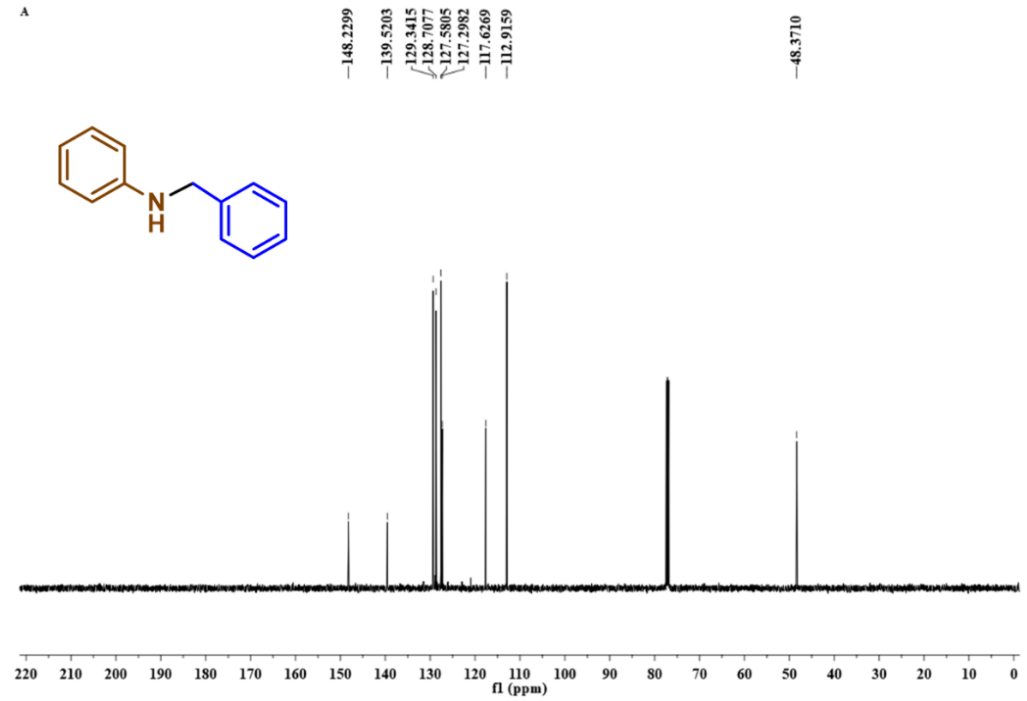

Figure S23: ^{13}C NMR spectrum of 3a in $CDCl_3$ at 126 MHz.

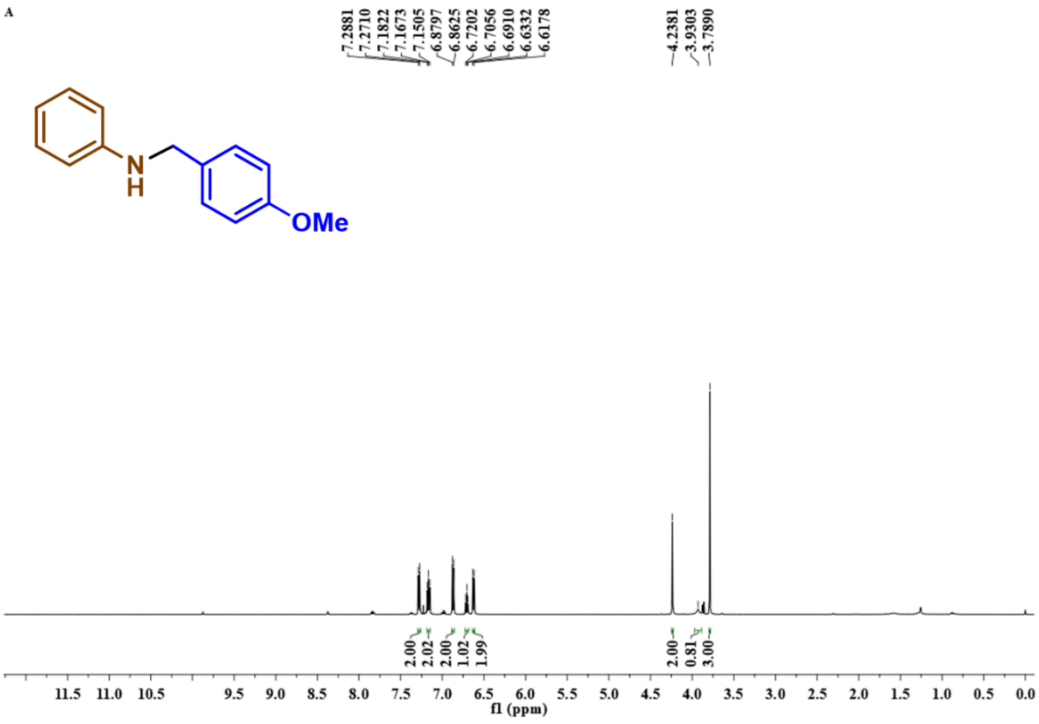

Figure S24: ^{1}H NMR spectrum of 3b in $CDCl_3$ at 500 MHz.

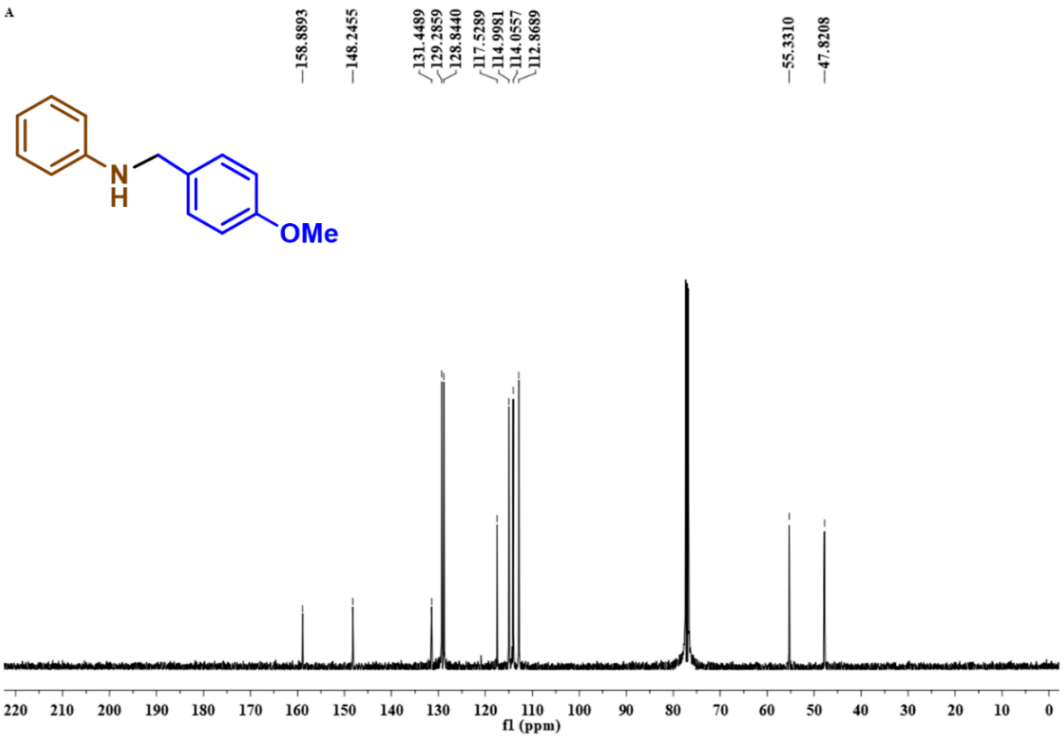

Figure S25: ^{13}C NMR spectrum of 3b in $CDCl_3$ at 126 MHz.

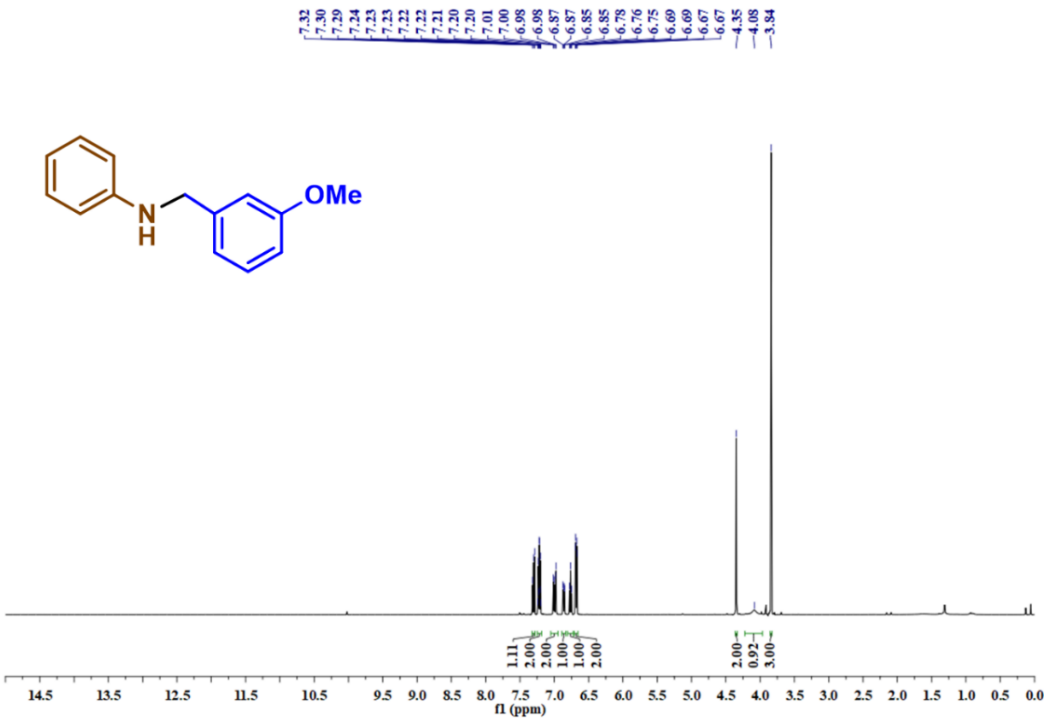

Figure S26: ^{1}H NMR spectrum of 3c in $CDCl_3$ at 500 MHz.

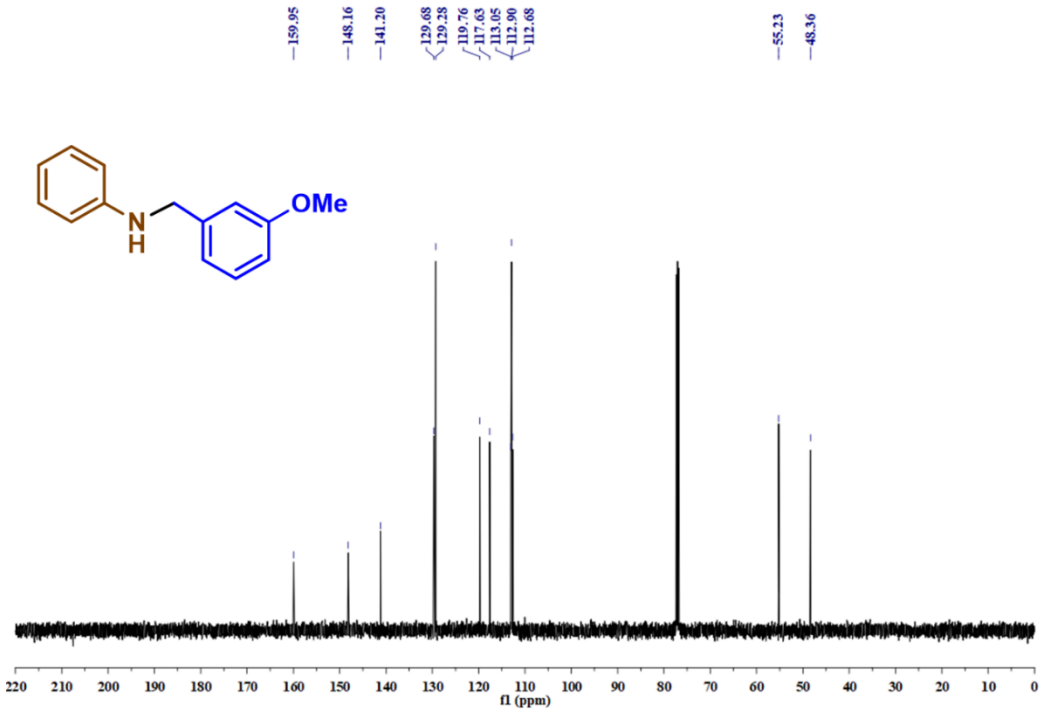

Figure S27: ^{13}C NMR spectrum of 3c in $CDCl_3$ at 126 MHz.

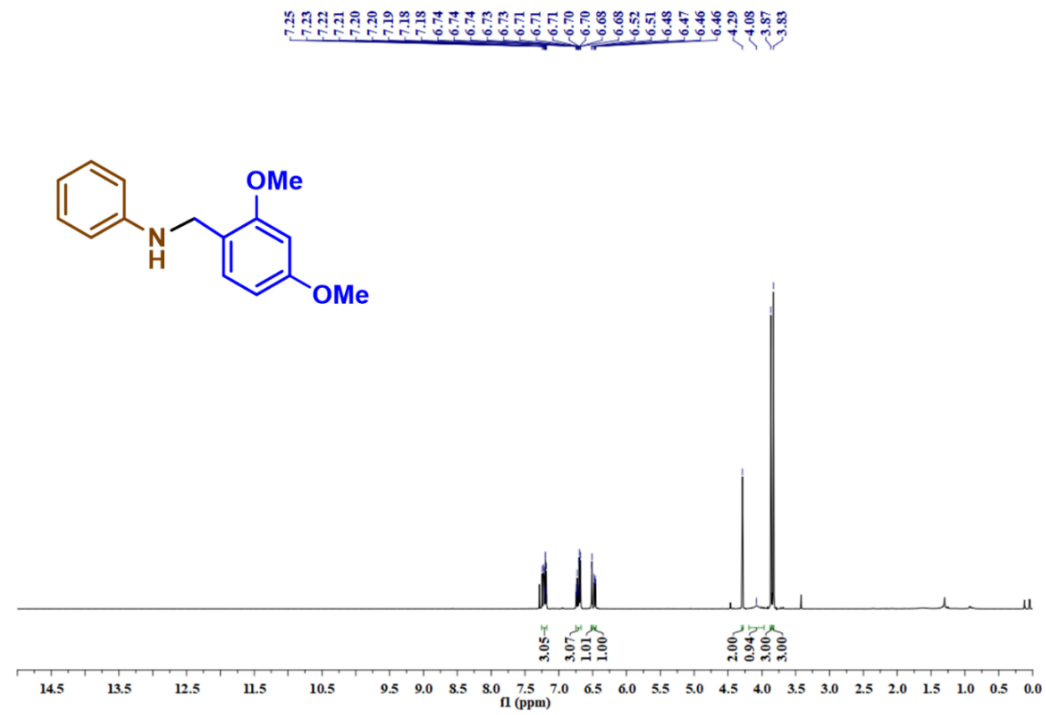

Figure S28: ^{1}H NMR spectrum of 3d in $CDCl_3$ at 500 MHz.

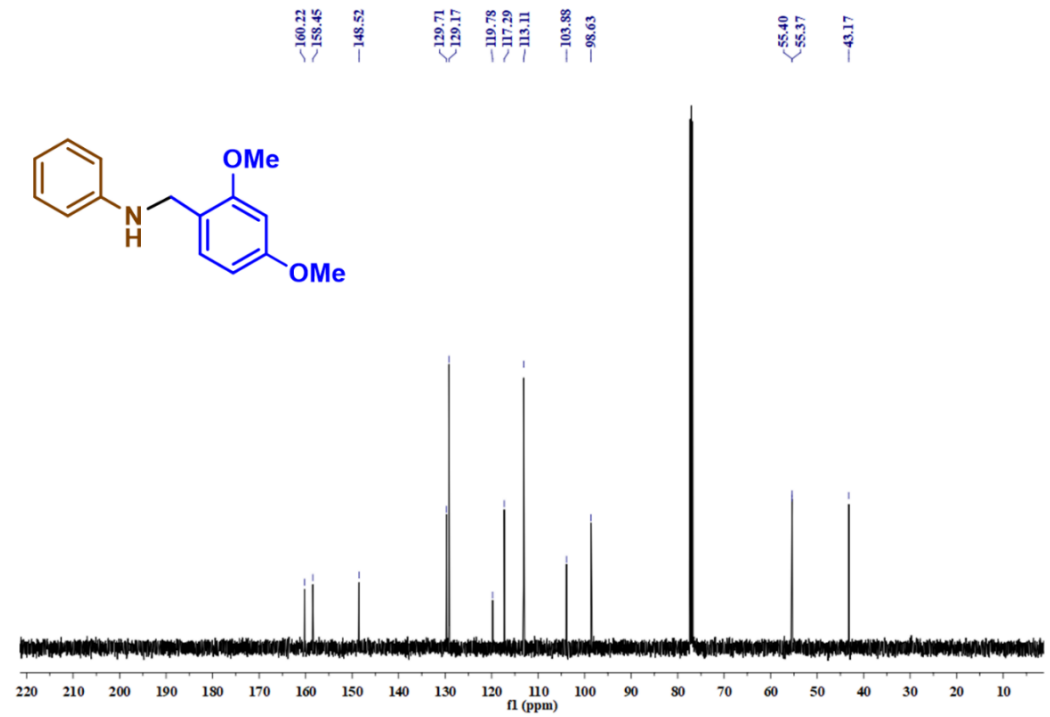

Figure S29: ^{13}C NMR spectrum of 3d in $CDCl_3$ at 126 MHz.

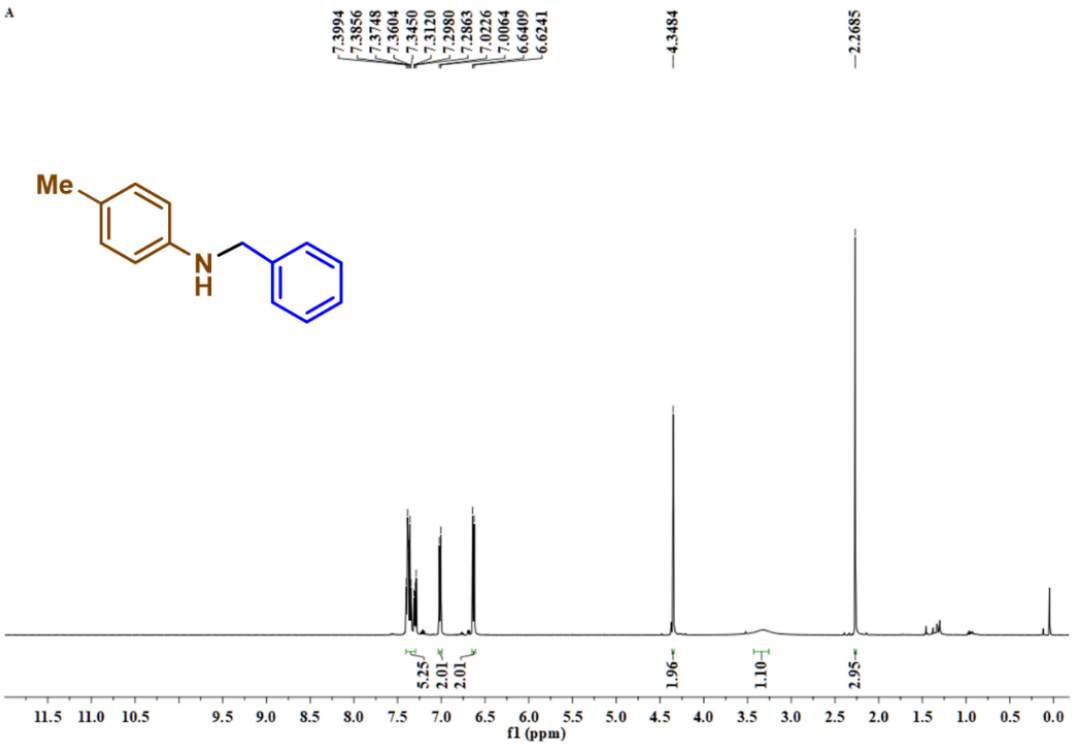

Figure S30: ^{1}H NMR spectrum of 3e in $CDCl_3$ at 500 MHz.

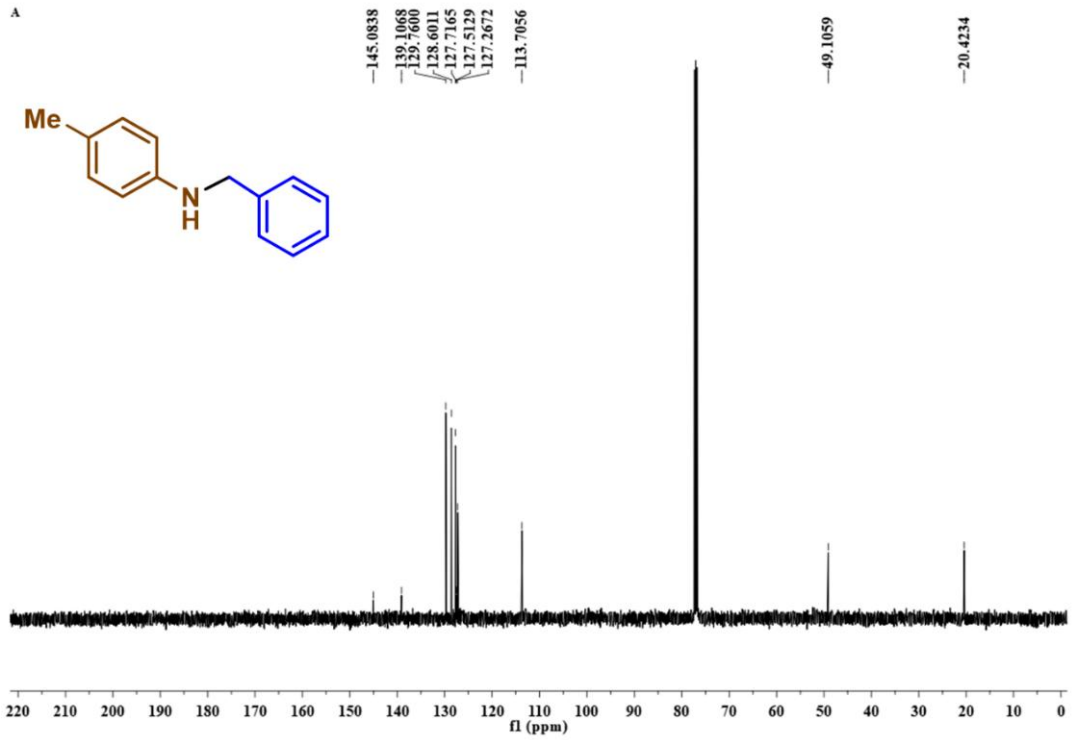

Figure S31: ^{13}C NMR spectrum of 3e in $CDCl_3$ at 126 MHz.

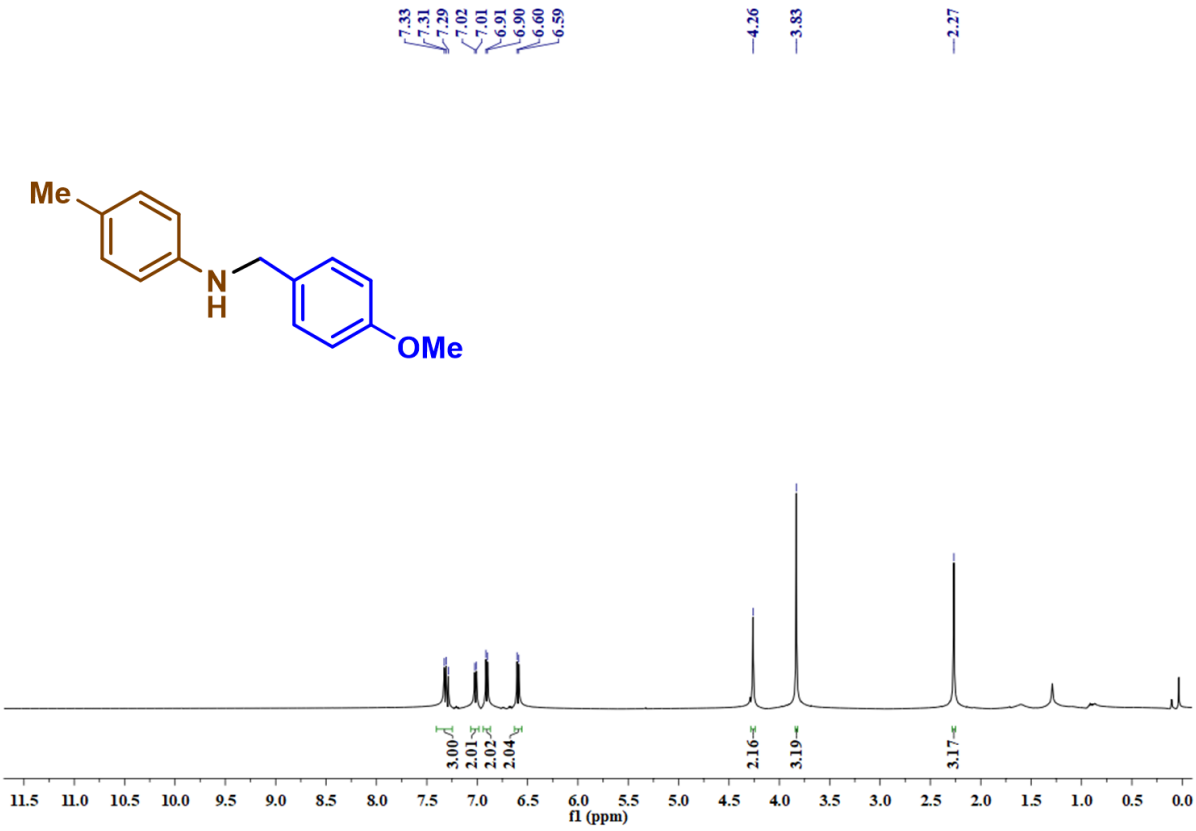

Figure S32: ^{1}H NMR spectrum of 3f in $CDCl_3$ at 500 MHz.

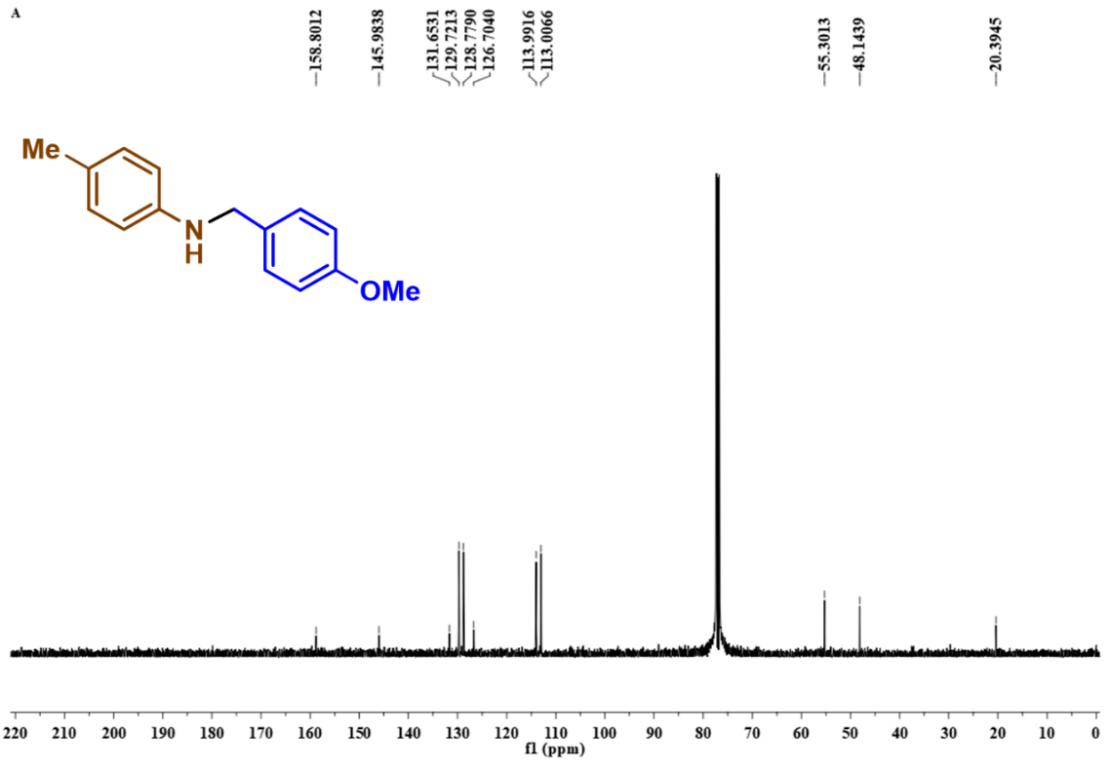

Figure S33: ^{13}C NMR spectrum of 3f in $CDCl_3$ at 126 MHz.

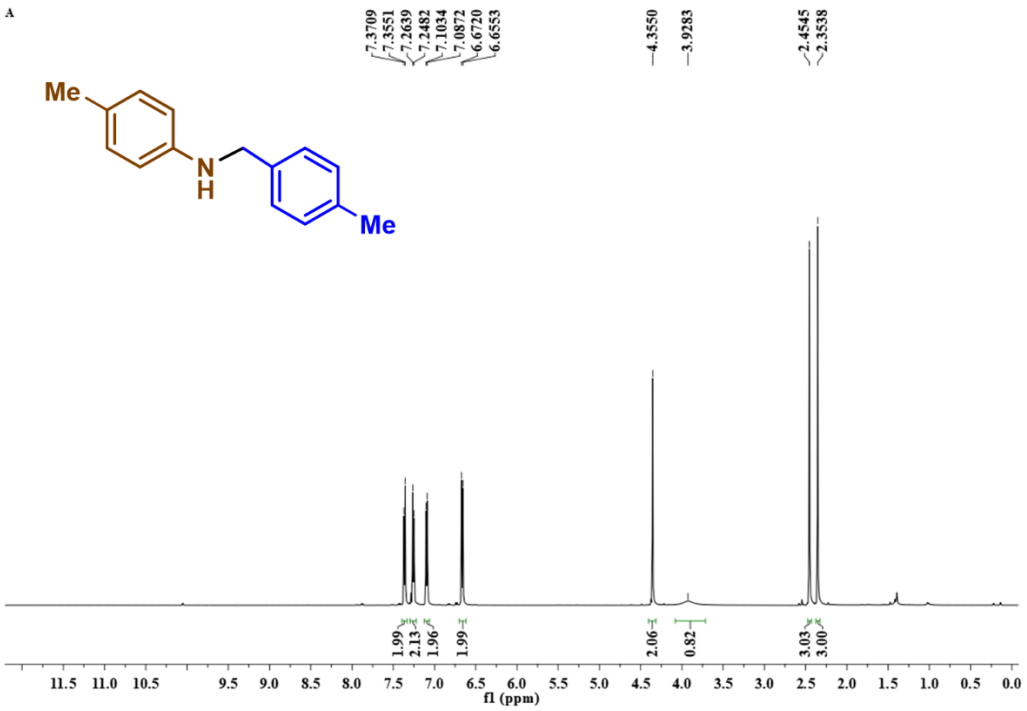

Figure S34: ^{1}H NMR spectrum of 3g in $CDCl_3$ at 500 MHz.

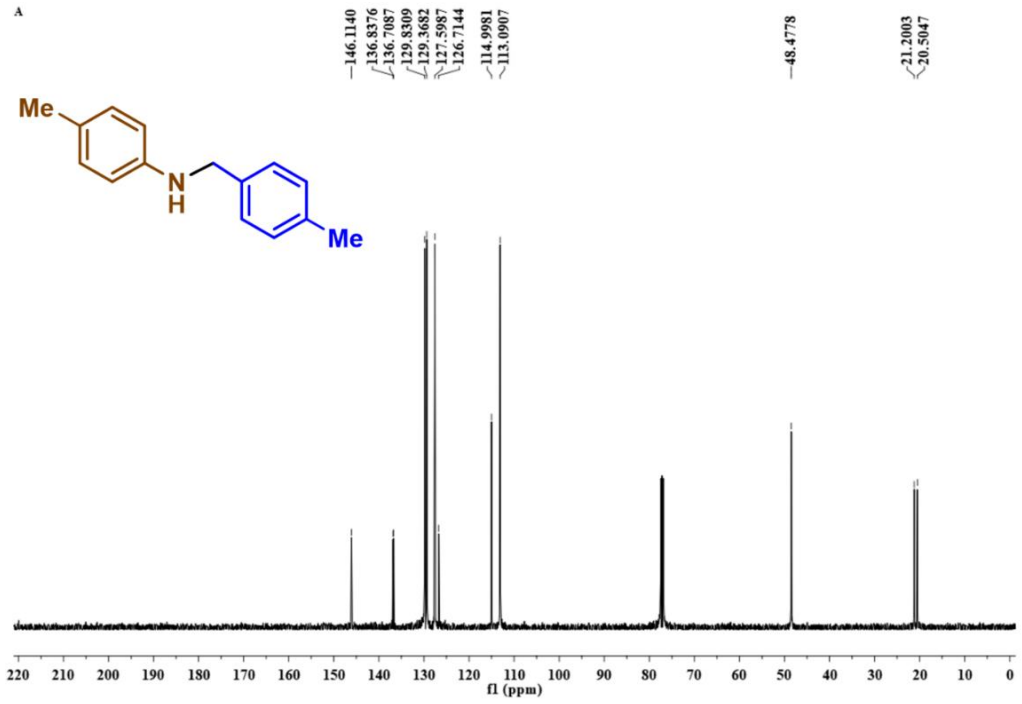

Figure S35: ^{13}C NMR spectrum of 3g in $CDCl_3$ at 126 MHz.

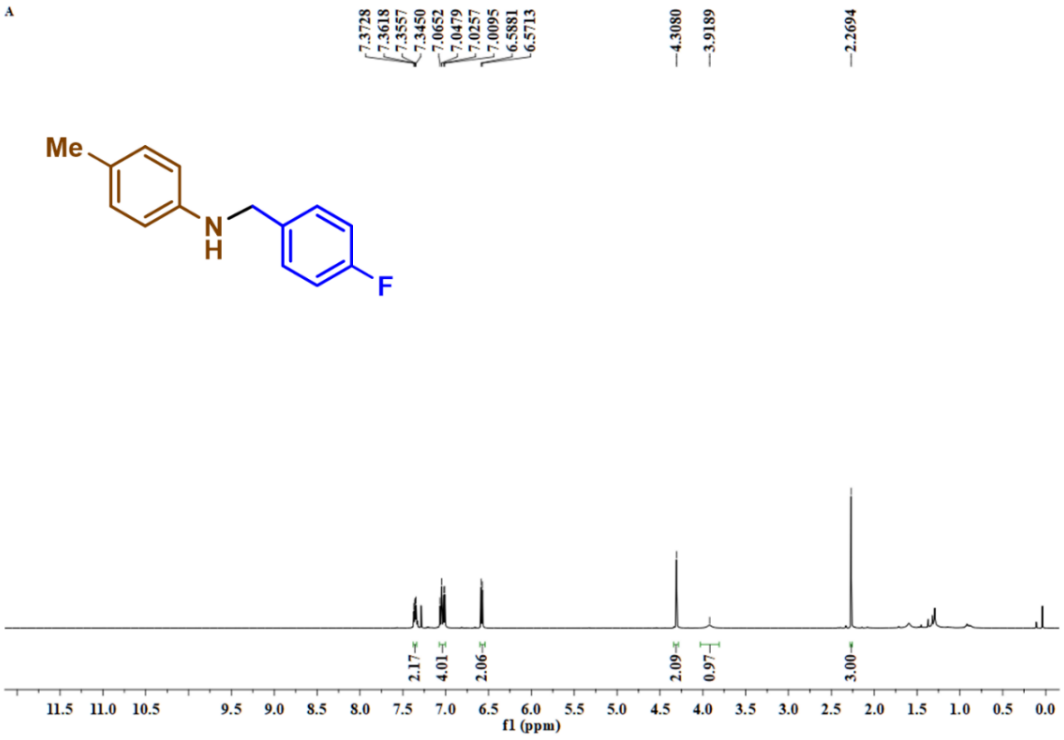

Figure S36: ^{1}H NMR spectrum of 3h in $CDCl_3$ at 500 MHz.

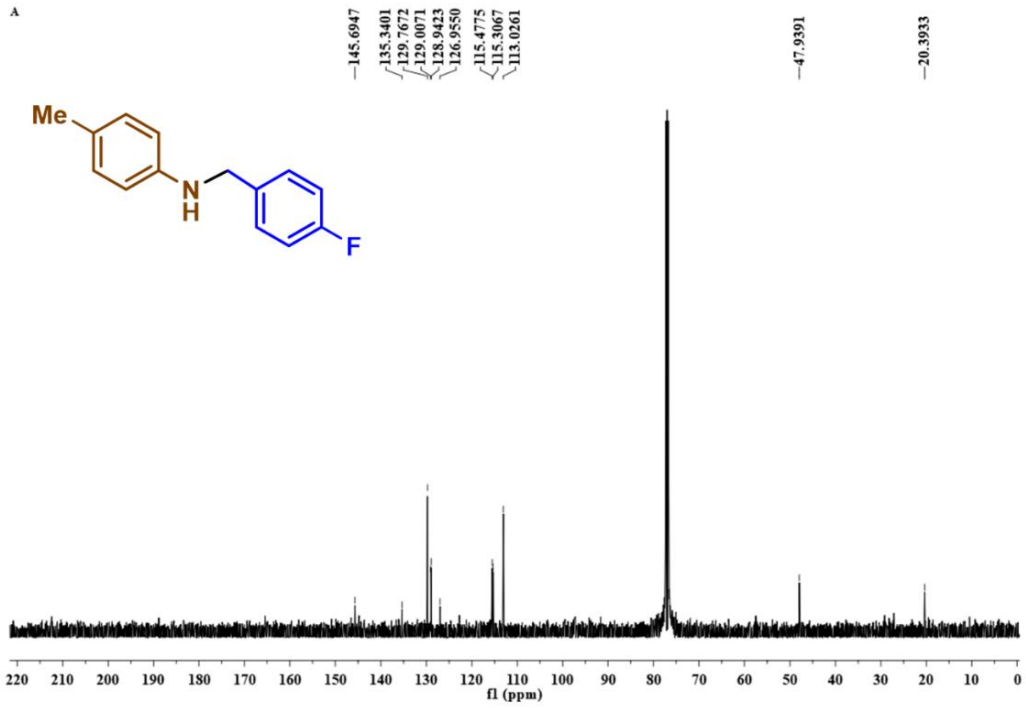

Figure S37: ^{13}C NMR spectrum of 3h in $CDCl_3$ at 126 MHz.

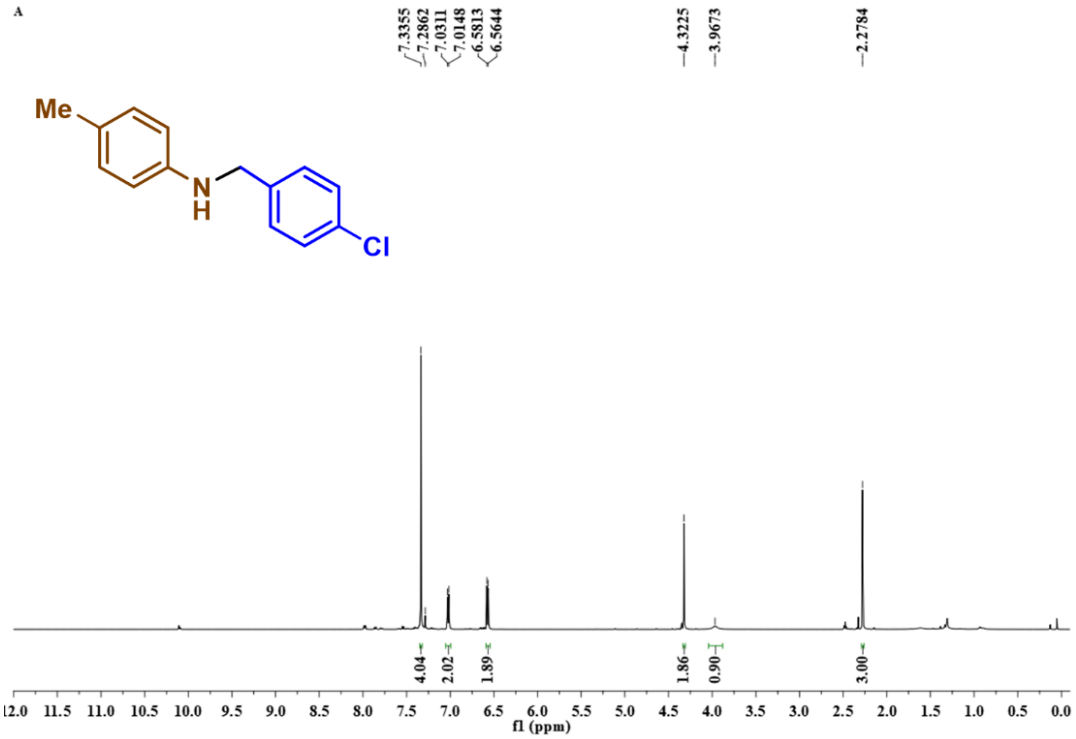

Figure S38: ^{1}H NMR spectrum of 3i in $CDCl_3$ at 500 MHz.

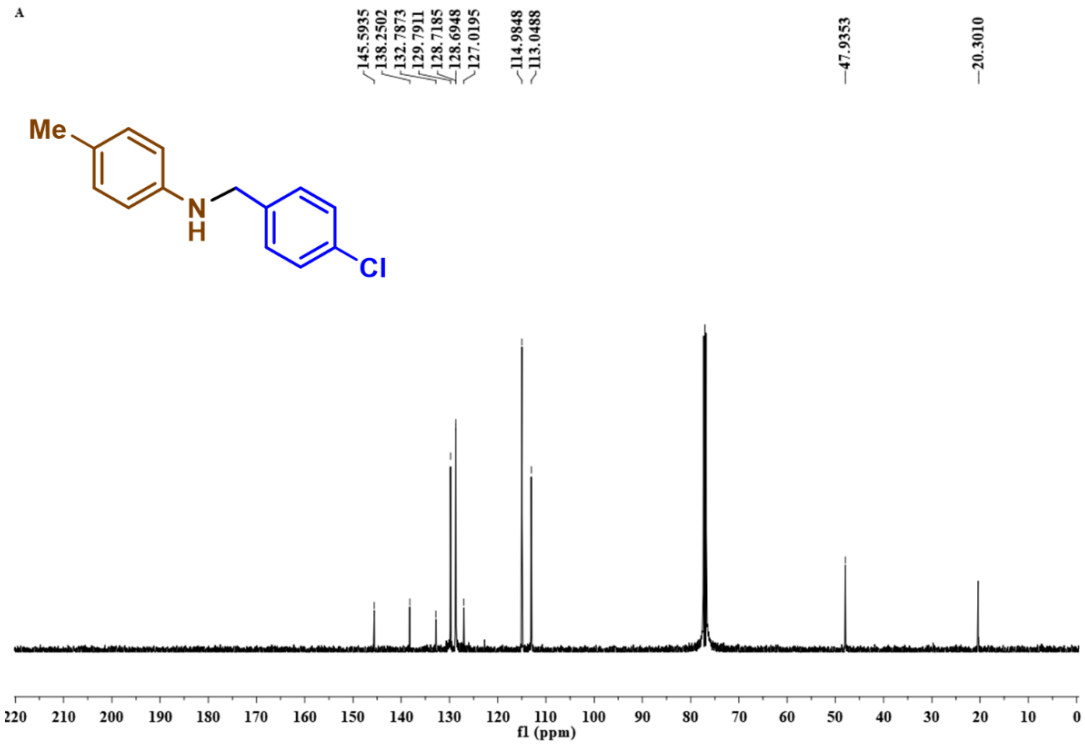

Figure S39: ^{13}C NMR spectrum of 3i in $CDCl_3$ at 126 MHz.

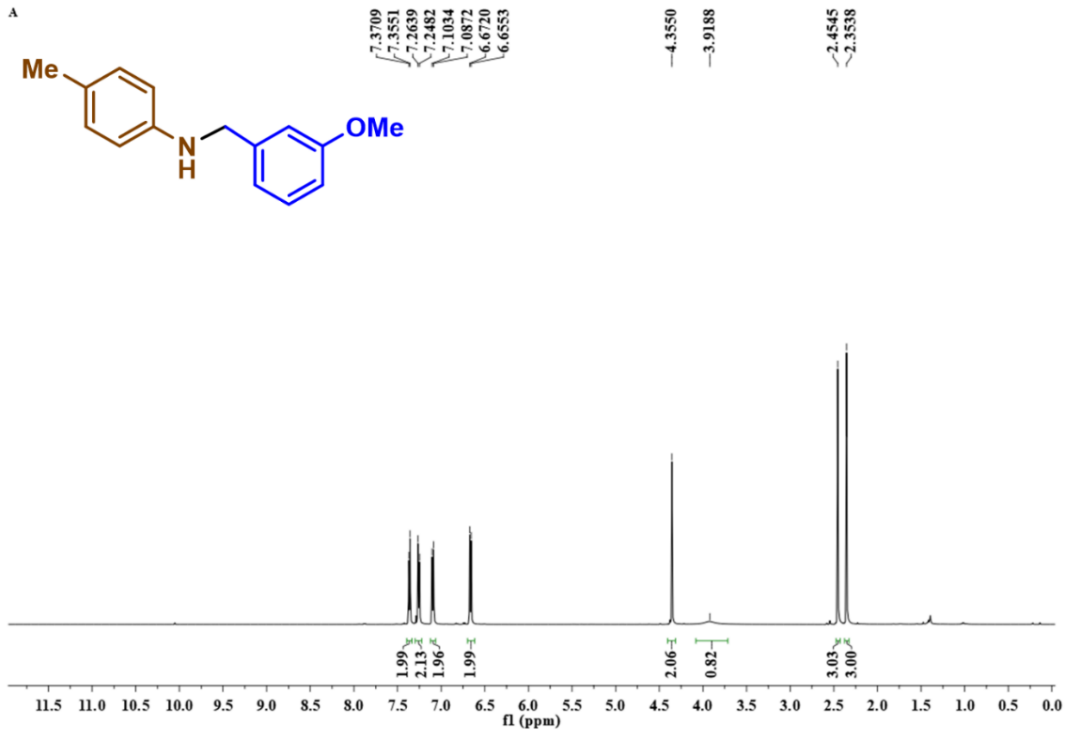

Figure S40: ^{1}H NMR spectrum of 3j in $CDCl_3$ at 500 MHz.

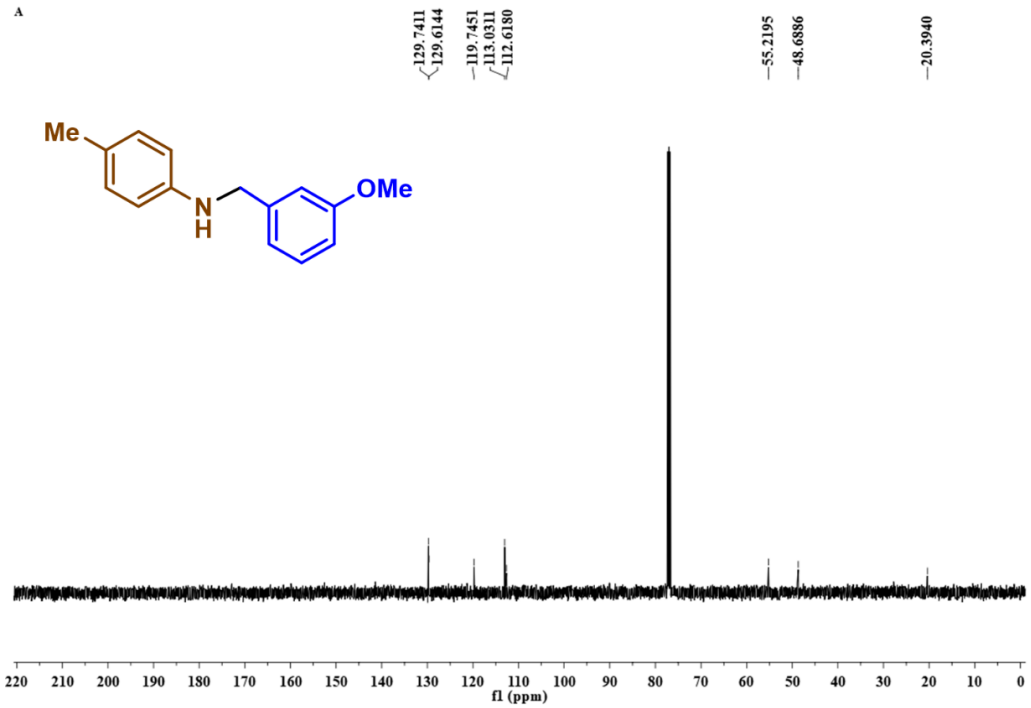

Figure S41: ^{13}C NMR spectrum of 3j in $CDCl_3$ at 126 MHz.

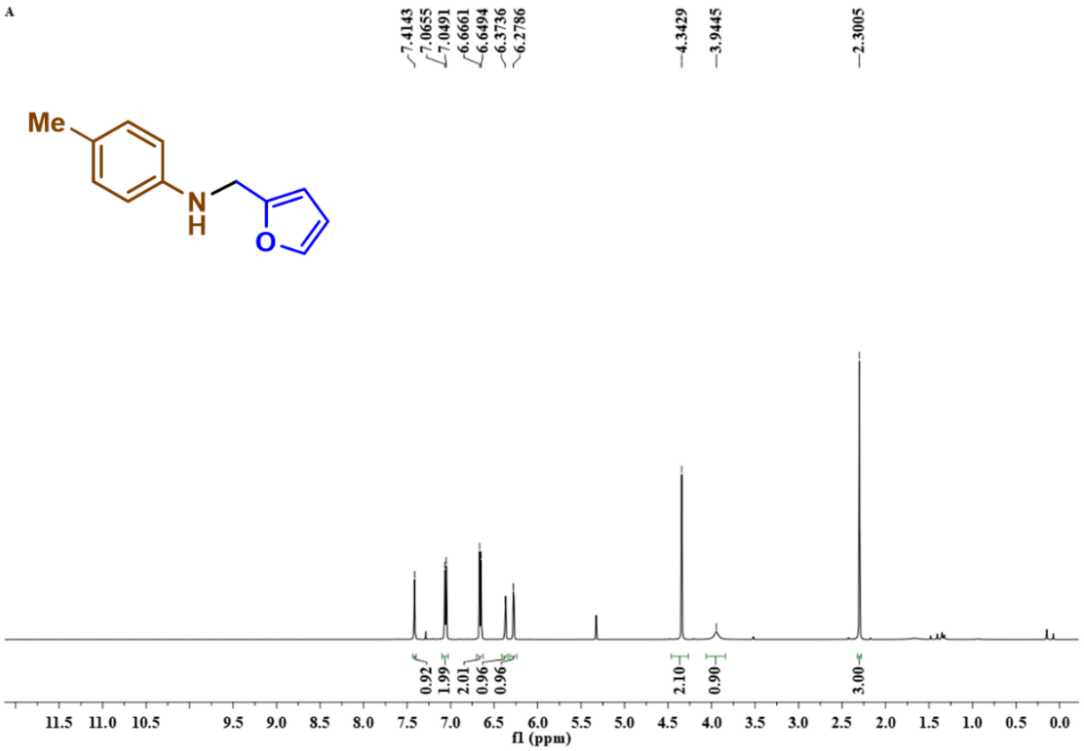

Figure S42: ^{1}H NMR spectrum of 3k in $CDCl_3$ at 500 MHz.

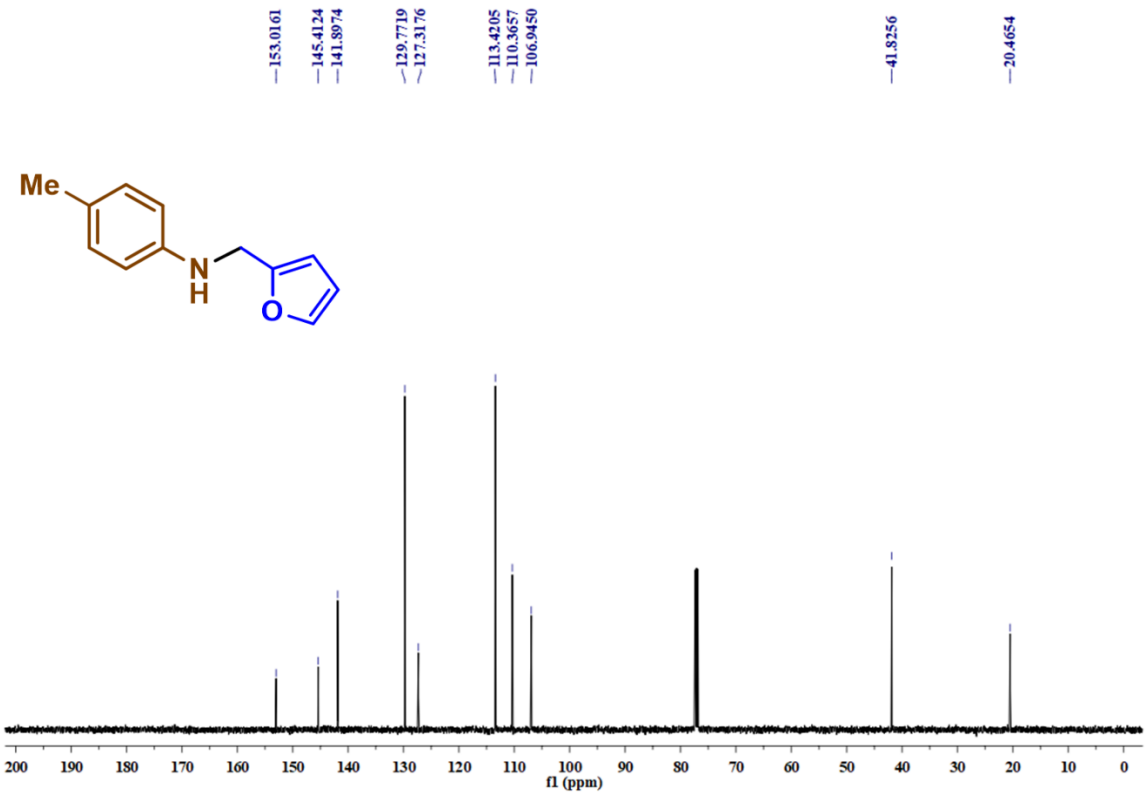

Figure S43: ^{13}C NMR spectrum of 3k in $CDCl_3$ at 126 MHz.

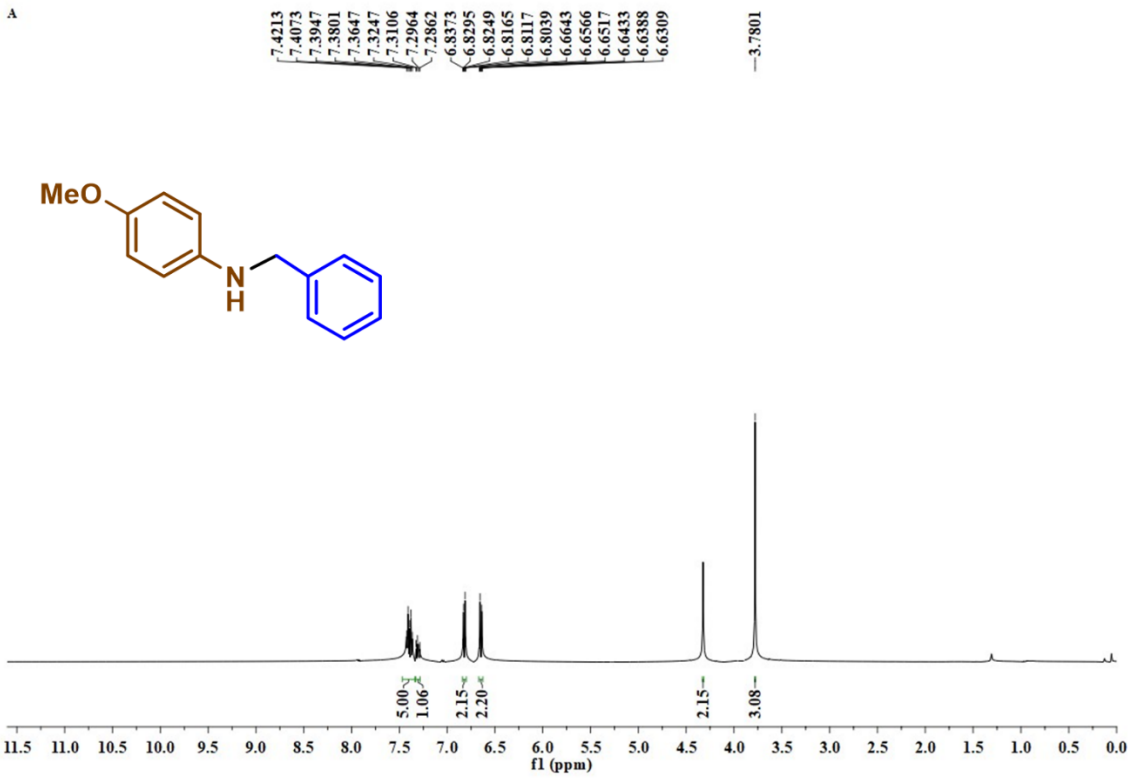

Figure S44: ^{1}H NMR spectrum of 3l in $CDCl_3$ at 500 MHz.

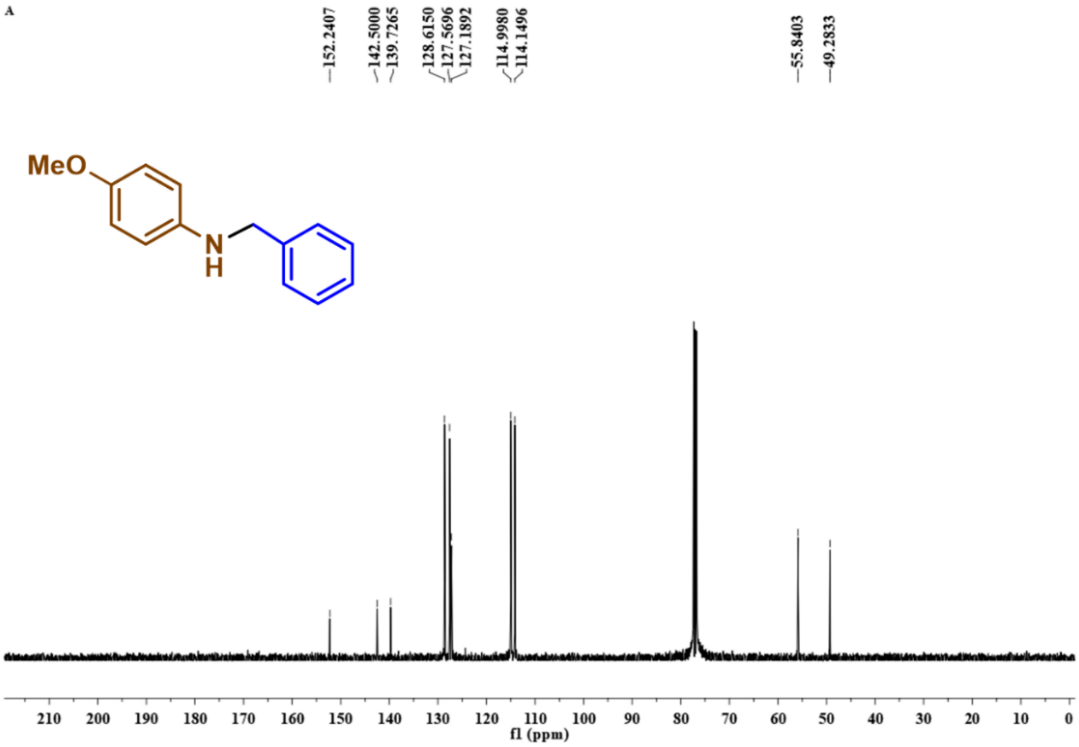

Figure S45: ^{13}C NMR spectrum of 3l in $CDCl_3$ at 126 MHz.

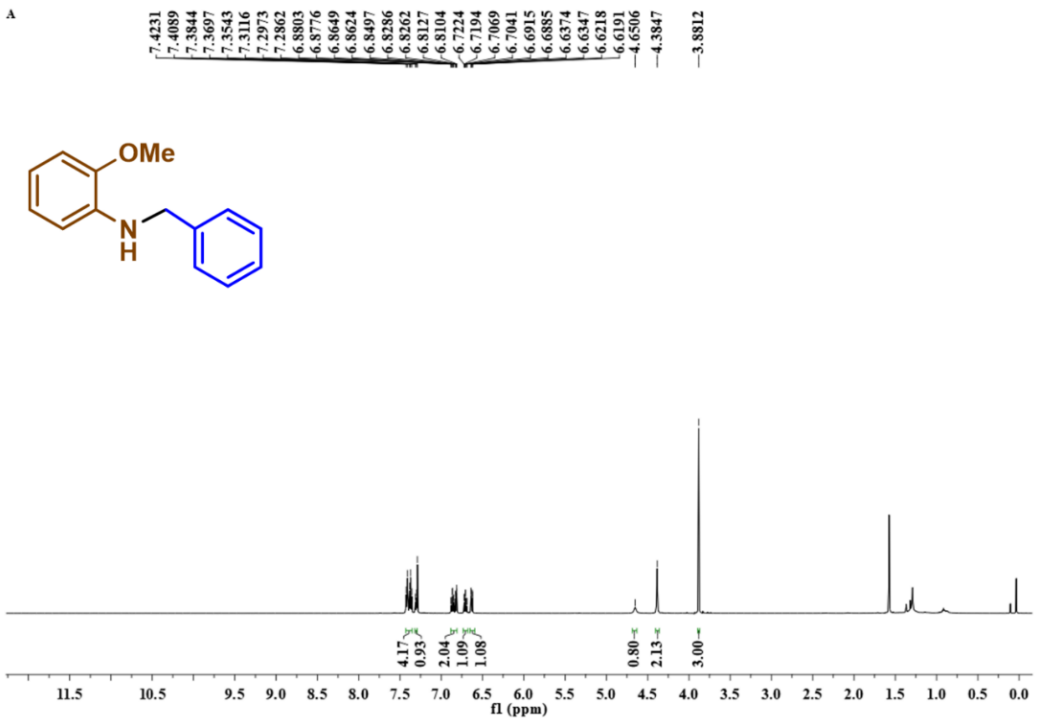

Figure S46: ^{1}H NMR spectrum of 3m in $CDCl_3$ at 500 MHz.

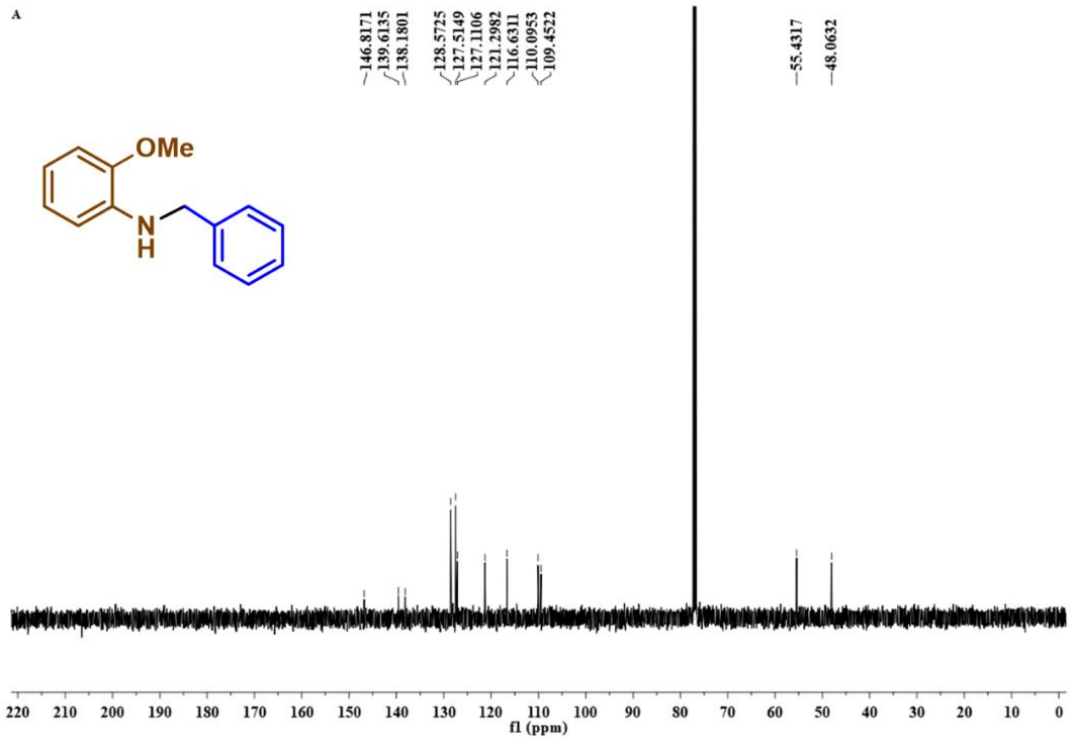

Figure S47: ^{13}C NMR spectrum of 3m in $CDCl_3$ at 126 MHz.

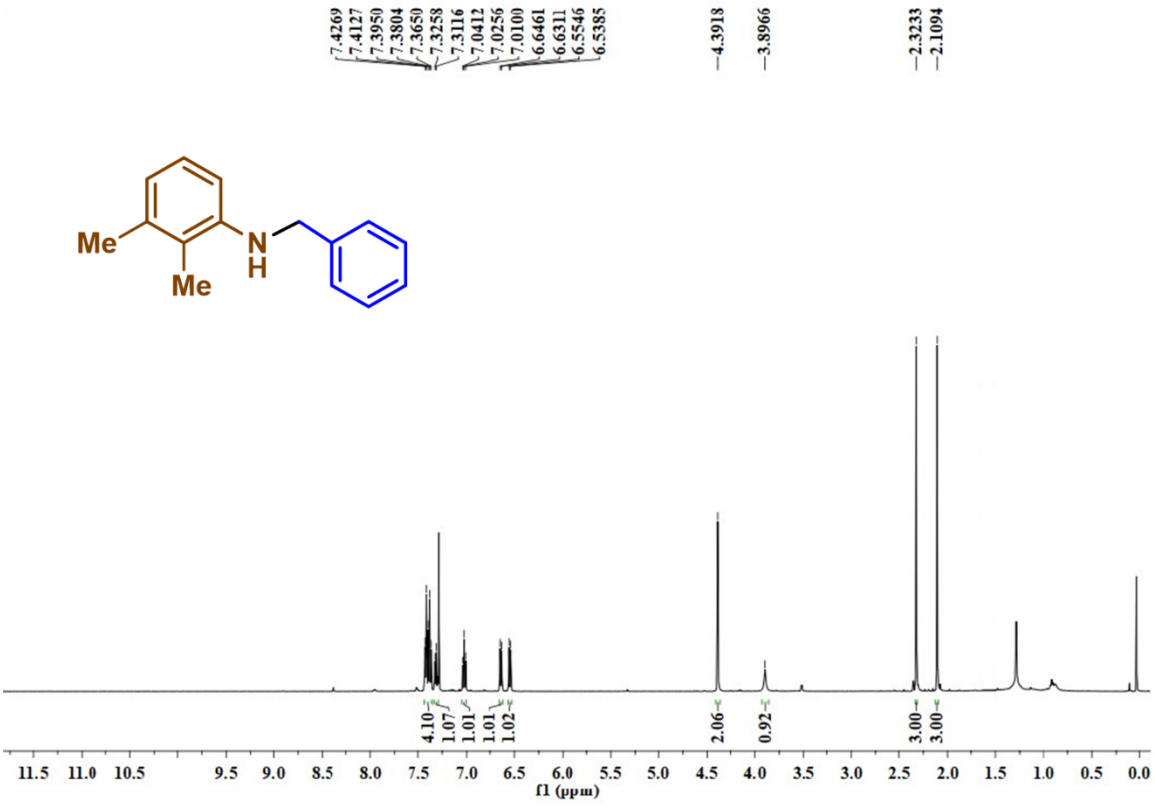

Figure S48: ^{1}H NMR spectrum of 3n in $CDCl_3$ at 500 MHz.

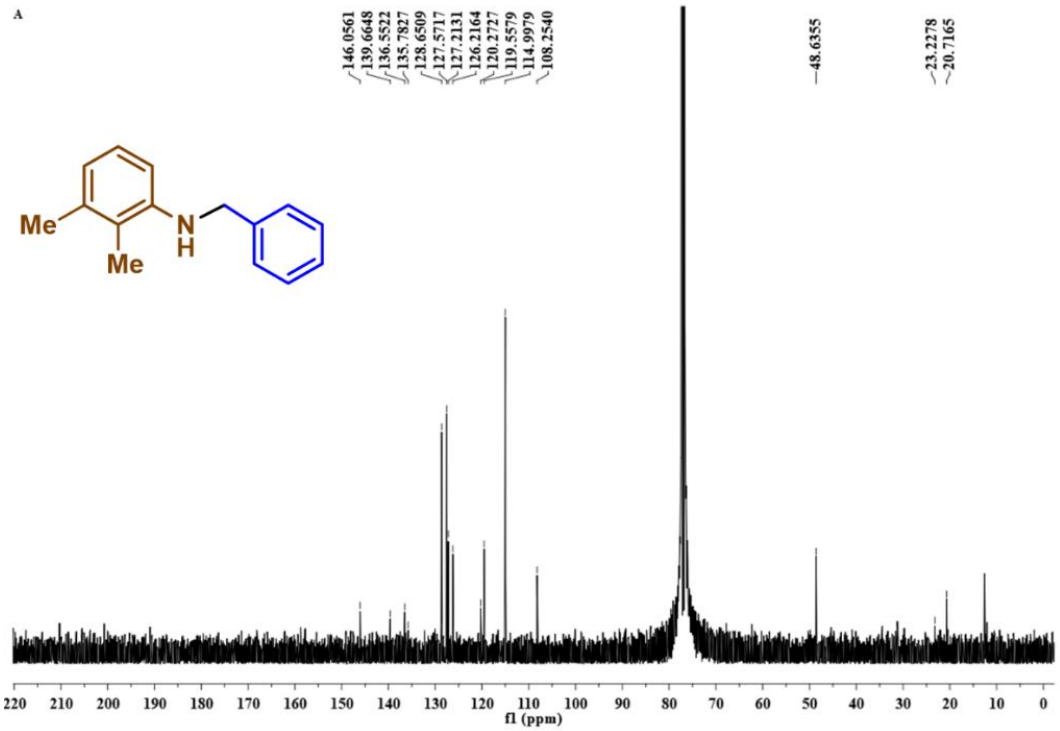

Figure S49: ^{13}C NMR spectrum of 3n in $CDCl_3$ at 126 MHz.

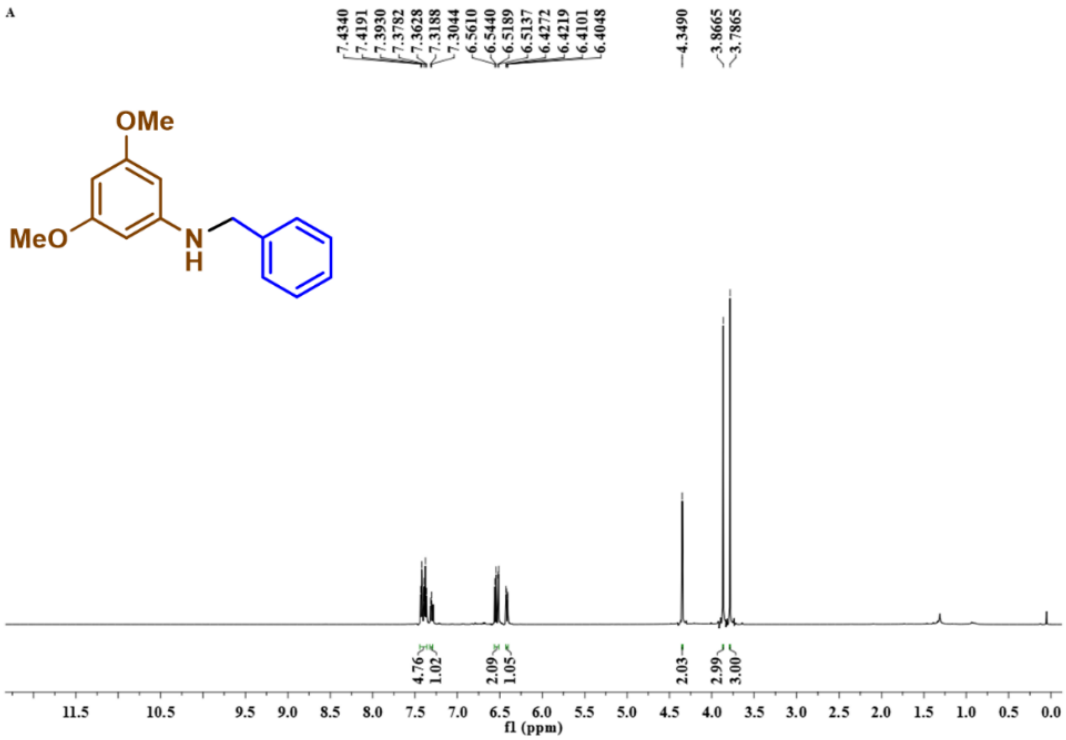

Figure S50: ^{1}H NMR spectrum of 3o in $CDCl_3$ at 500 MHz.

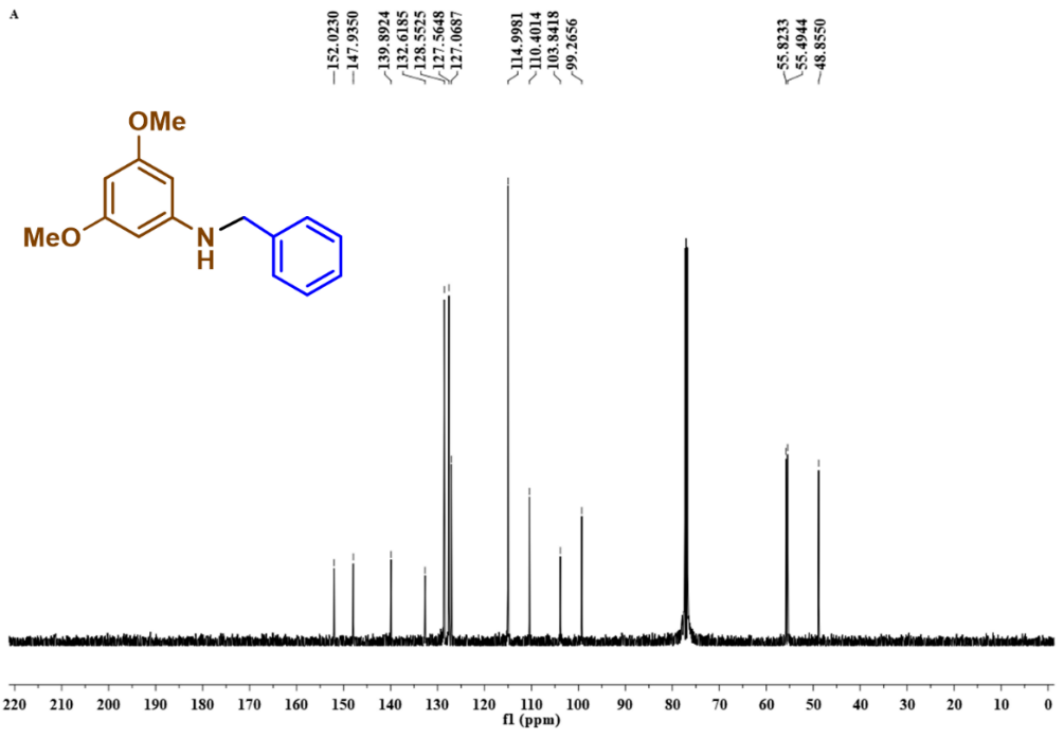

Figure S51: ^{13}C NMR spectrum of 3o in $CDCl_3$ at 126 MHz.

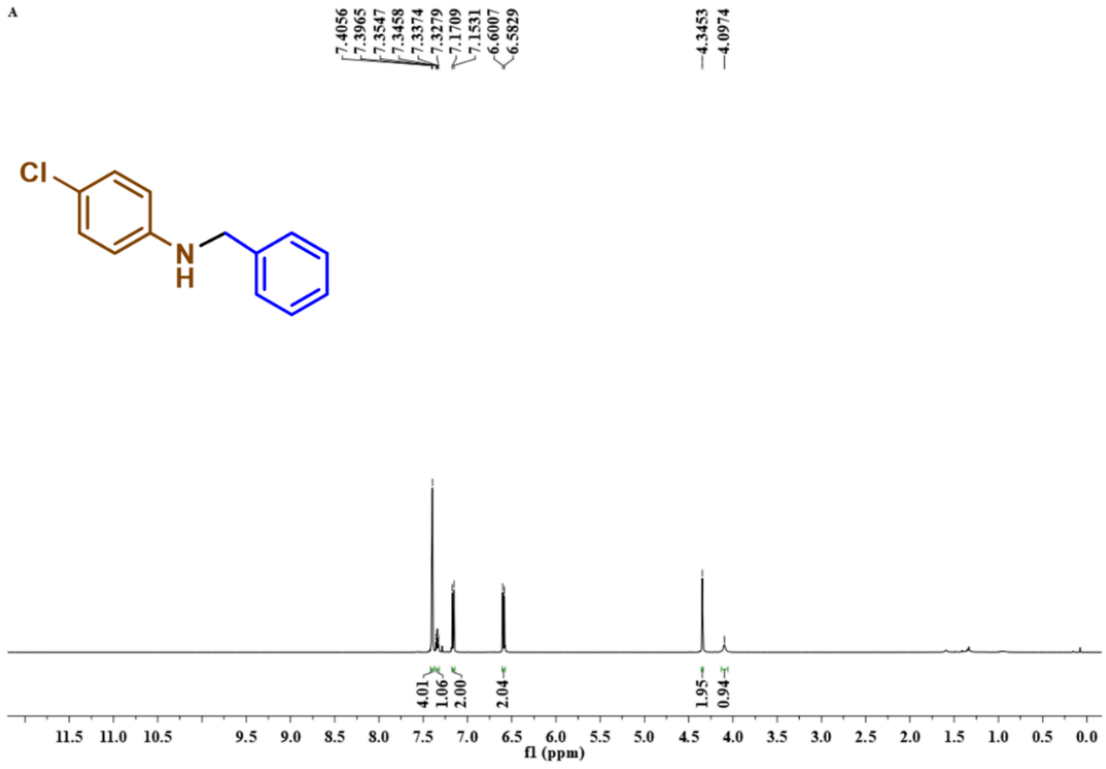

Figure S52: ^{1}H NMR spectrum of 3p in $CDCl_3$ at 500 MHz.

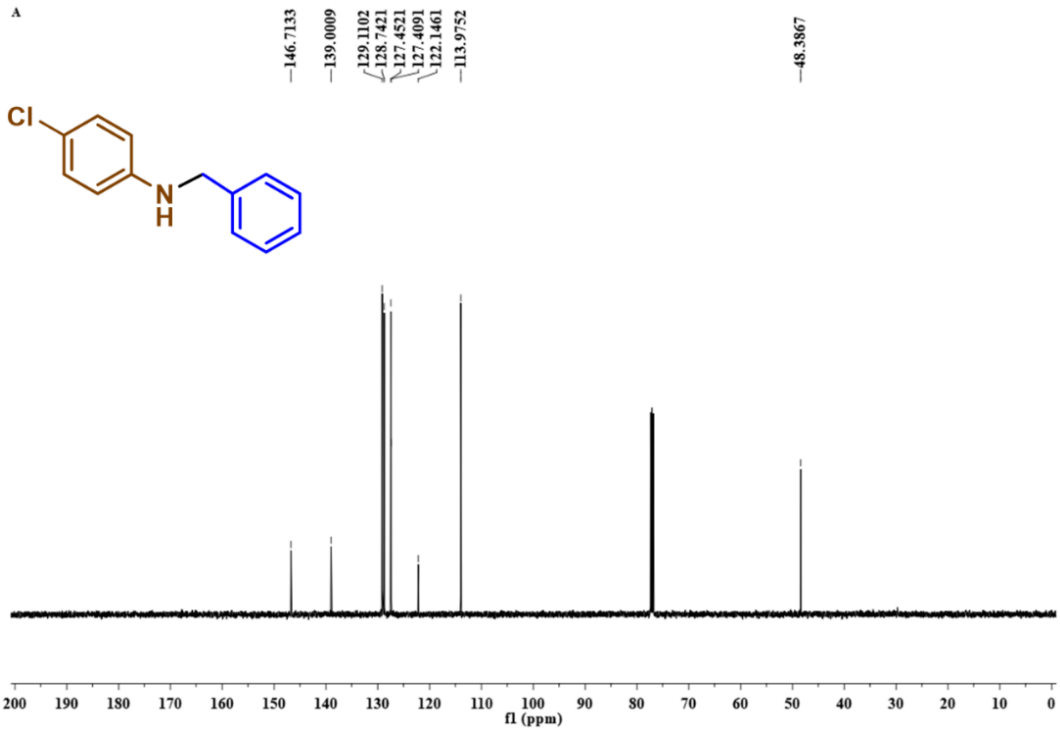

Figure S53: ^{13}C NMR spectrum of 3p in $CDCl_3$ at 126 MHz.

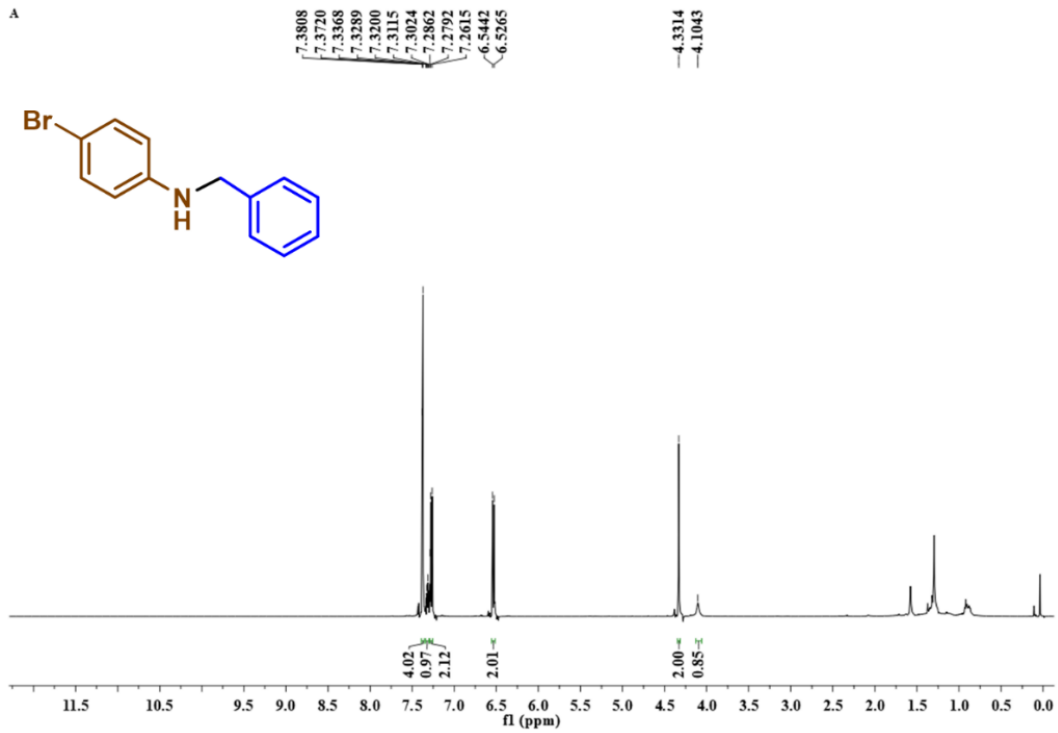

Figure S54: ^{1}H NMR spectrum of 3q in $CDCl_3$ at 500 MHz.

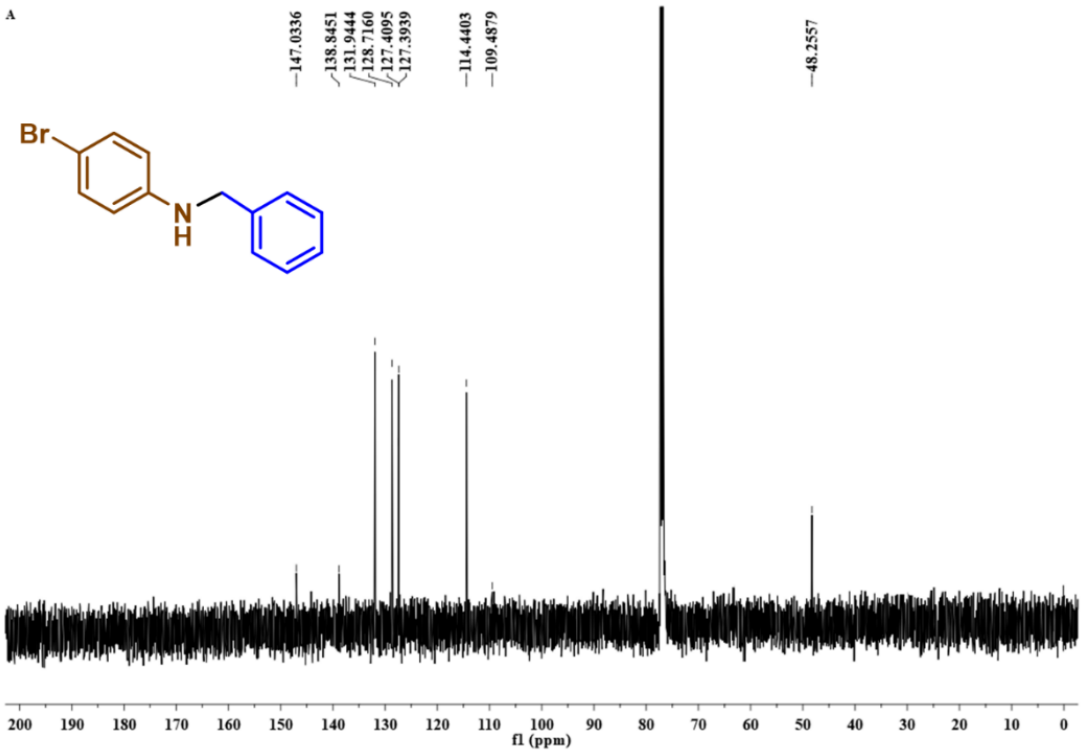

Figure S55: ^{13}C NMR spectrum of 3q in $CDCl_3$ at 126 MHz.

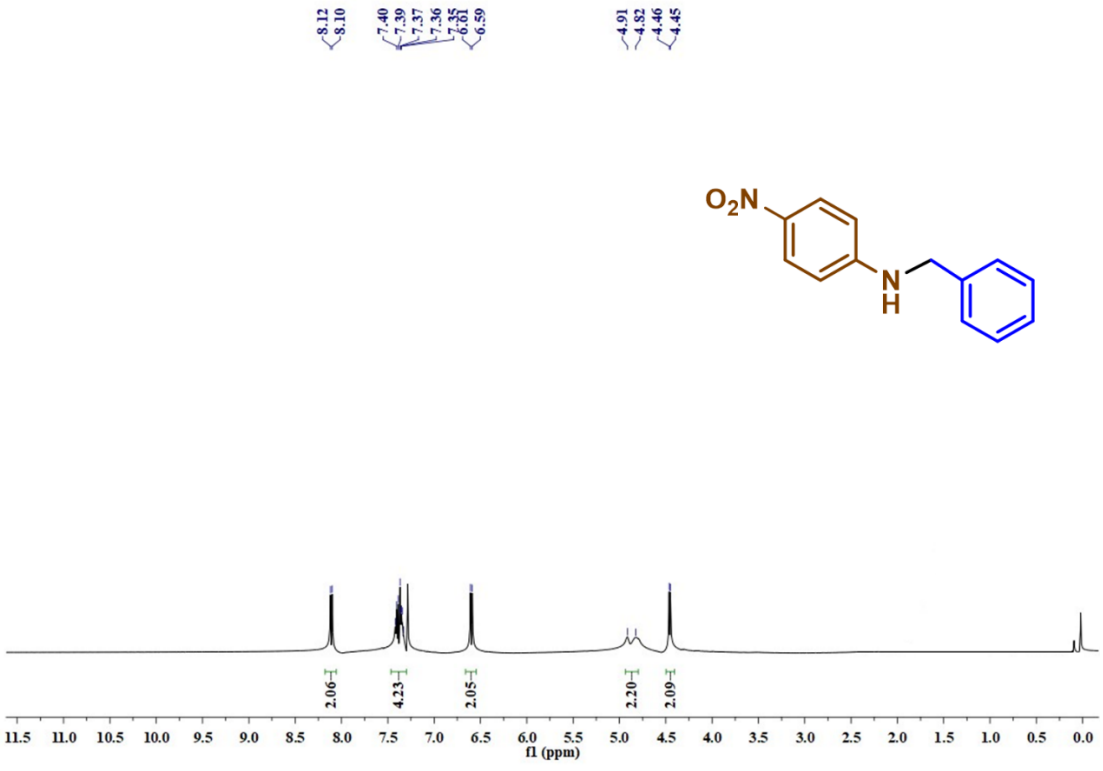

Figure S56: ^{1}H NMR spectrum of 3r in $CDCl_3$ at 500 MHz.

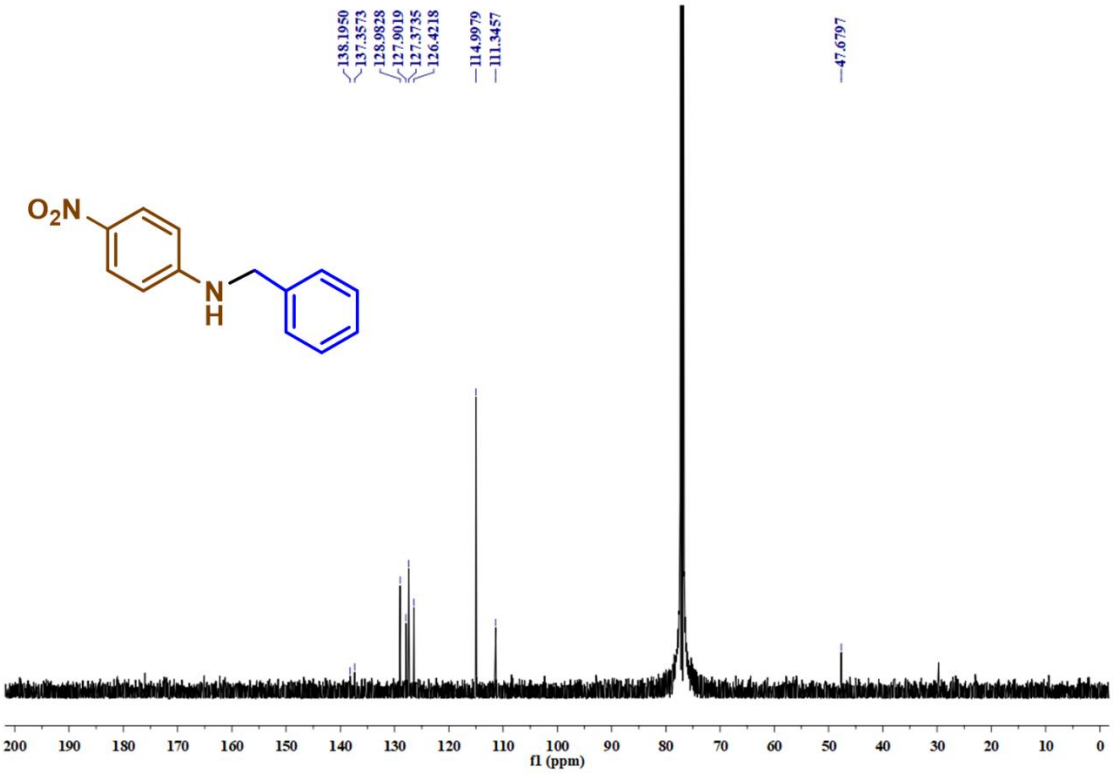

Figure S57: ^{13}C NMR spectrum of 3r in $CDCl_3$ at 126 MHz.

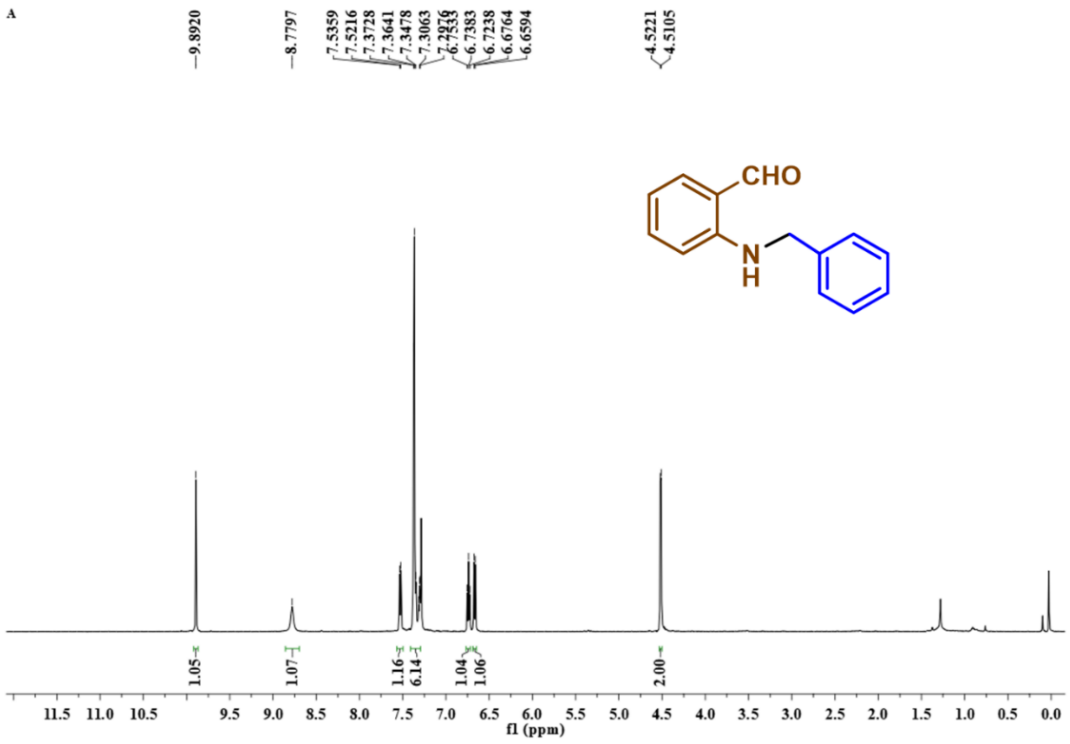

Figure S58: ^{1}H NMR spectrum of 3s in $CDCl_3$ at 500 MHz.

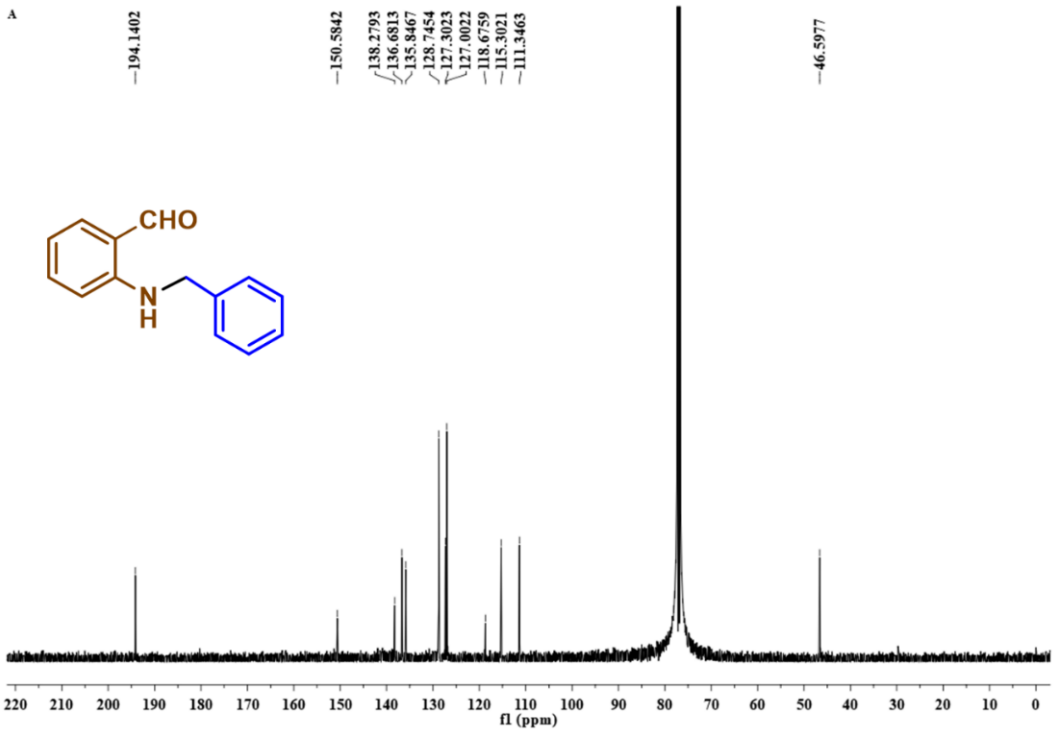

Figure S59: ^{13}C NMR spectrum of 3s in $CDCl_3$ at 126 MHz.

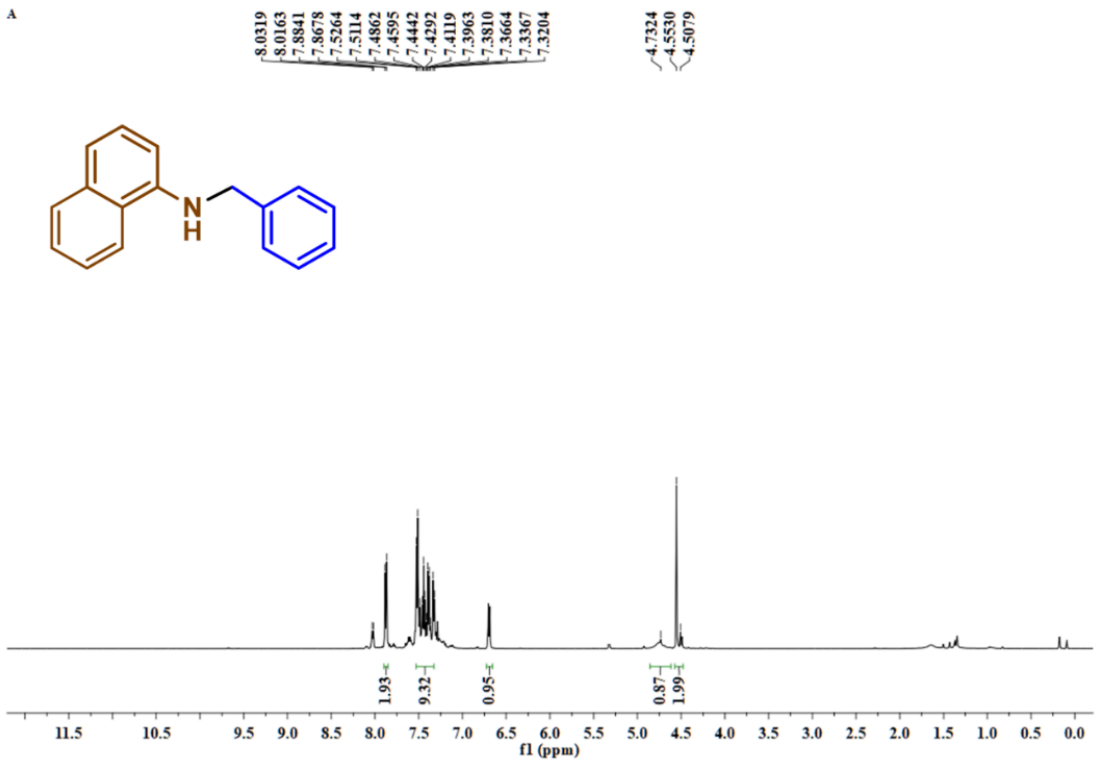

Figure S60: ^{1}H NMR spectrum of 3t in $CDCl_3$ at 500 MHz.

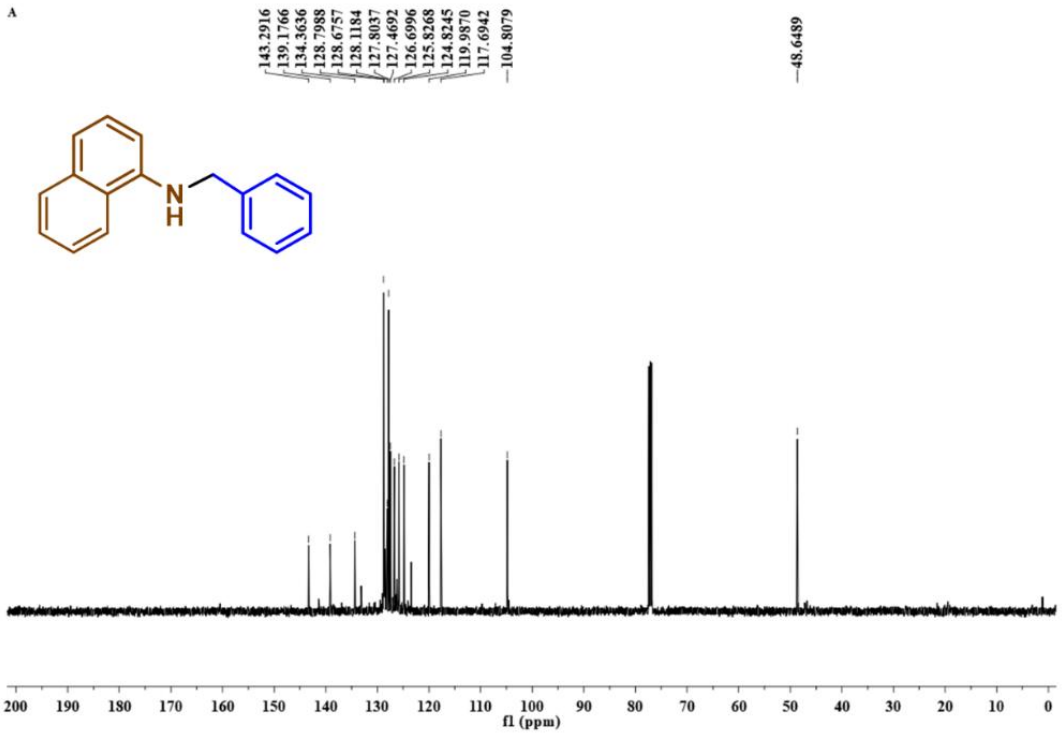

Figure S61: ^{13}C NMR spectrum of 3t in $CDCl_3$ at 126 MHz.

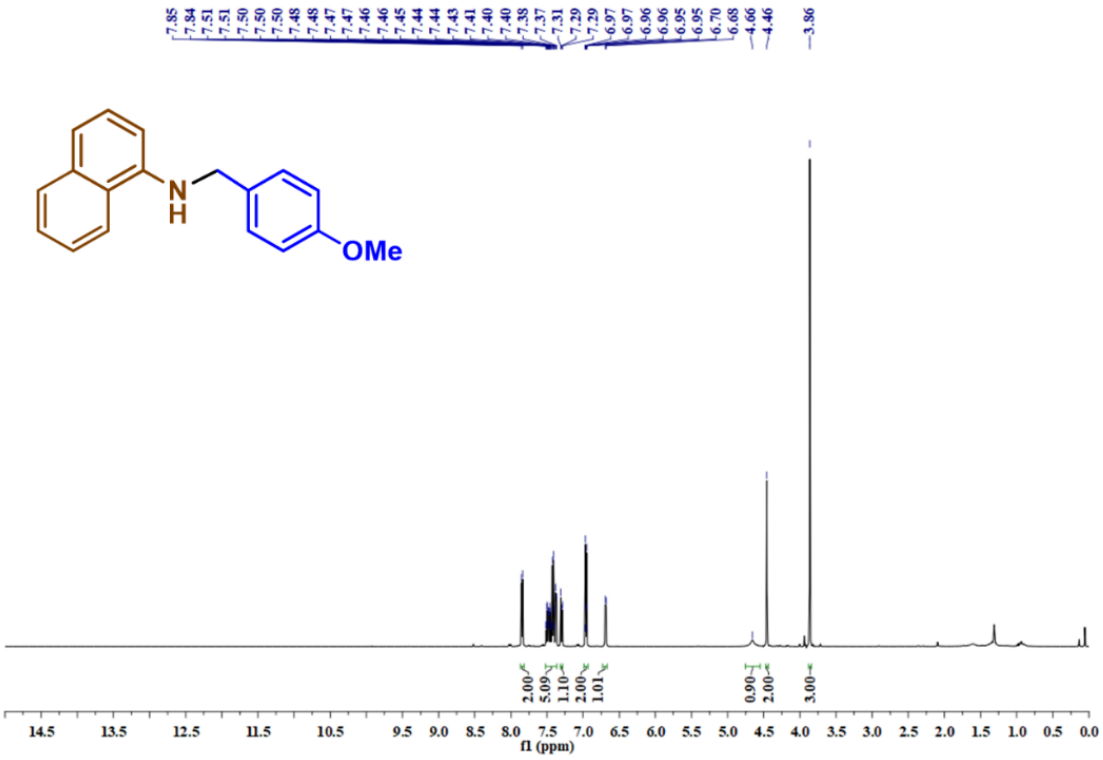

Figure S62: ^{1}H NMR spectrum of 3u in $CDCl_3$ at 500 MHz.

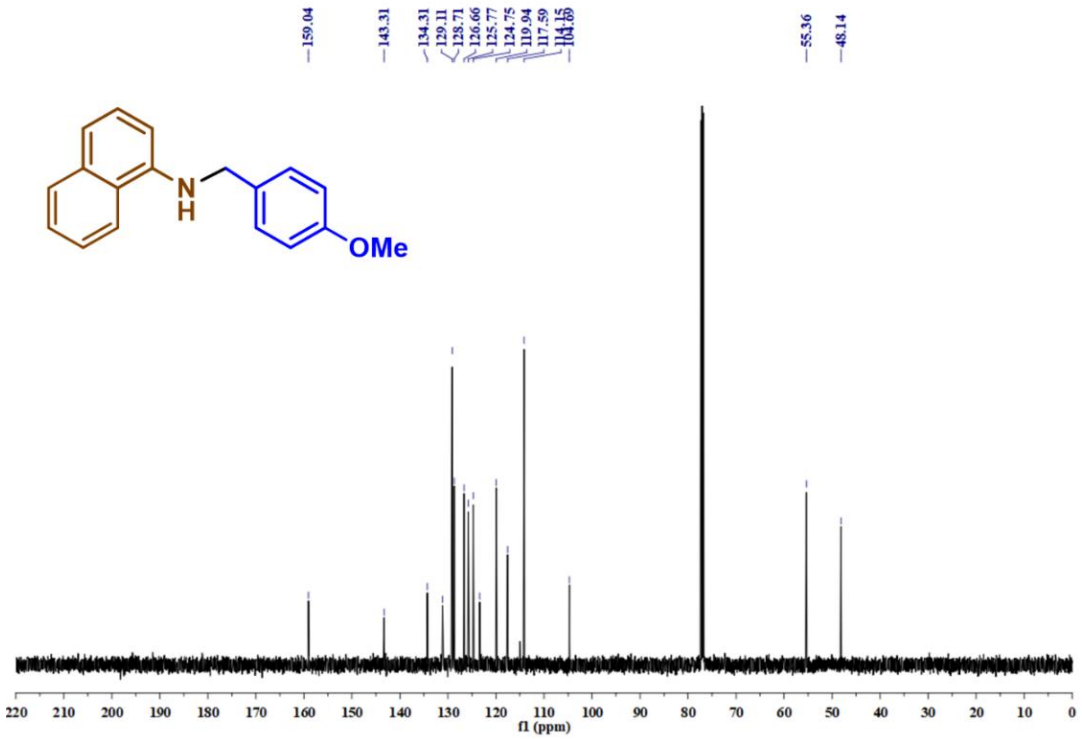

Figure S63: ^{13}C NMR spectrum of 3u in $CDCl_3$ at 126 MHz.

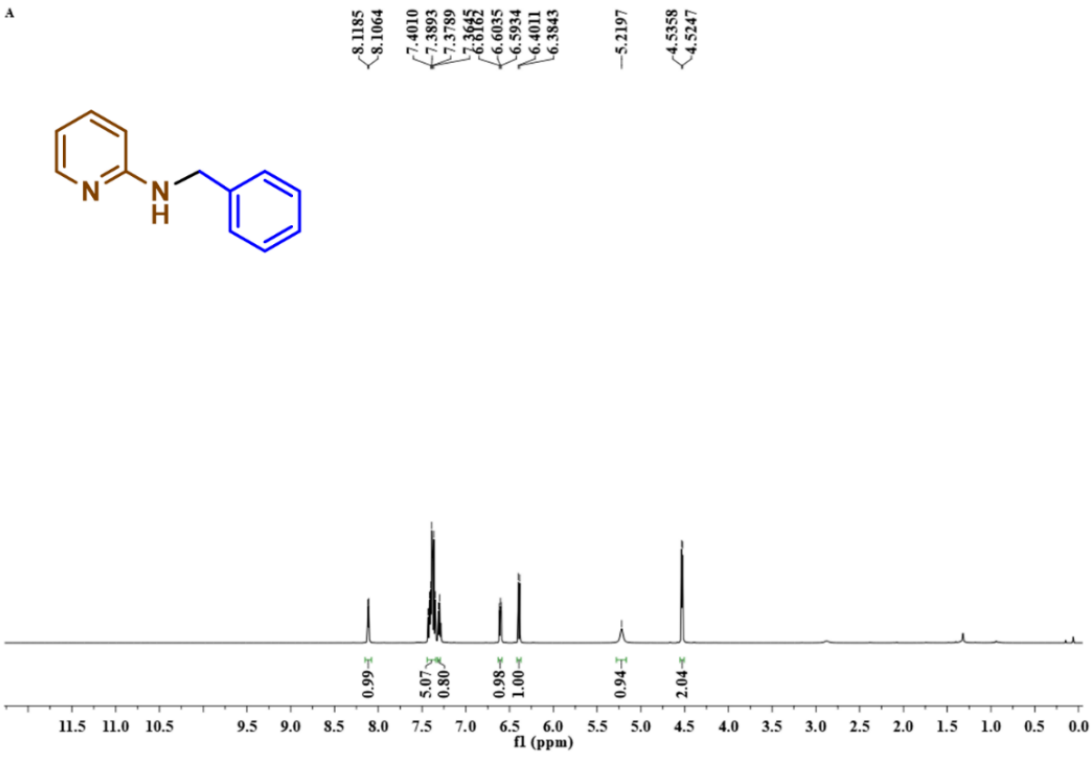

Figure S64: ^{1}H NMR spectrum of 3v in $CDCl_3$ at 500 MHz.

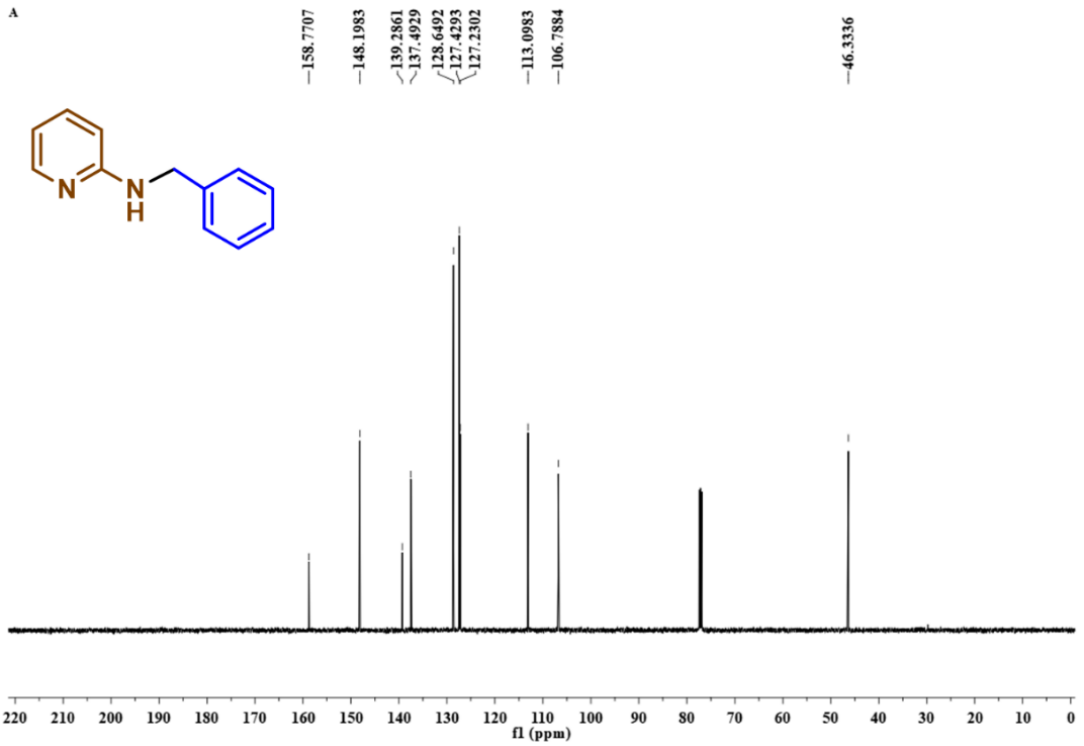

Figure S65: ^{13}C NMR spectrum of 3v in $CDCl_3$ at 126 MHz.

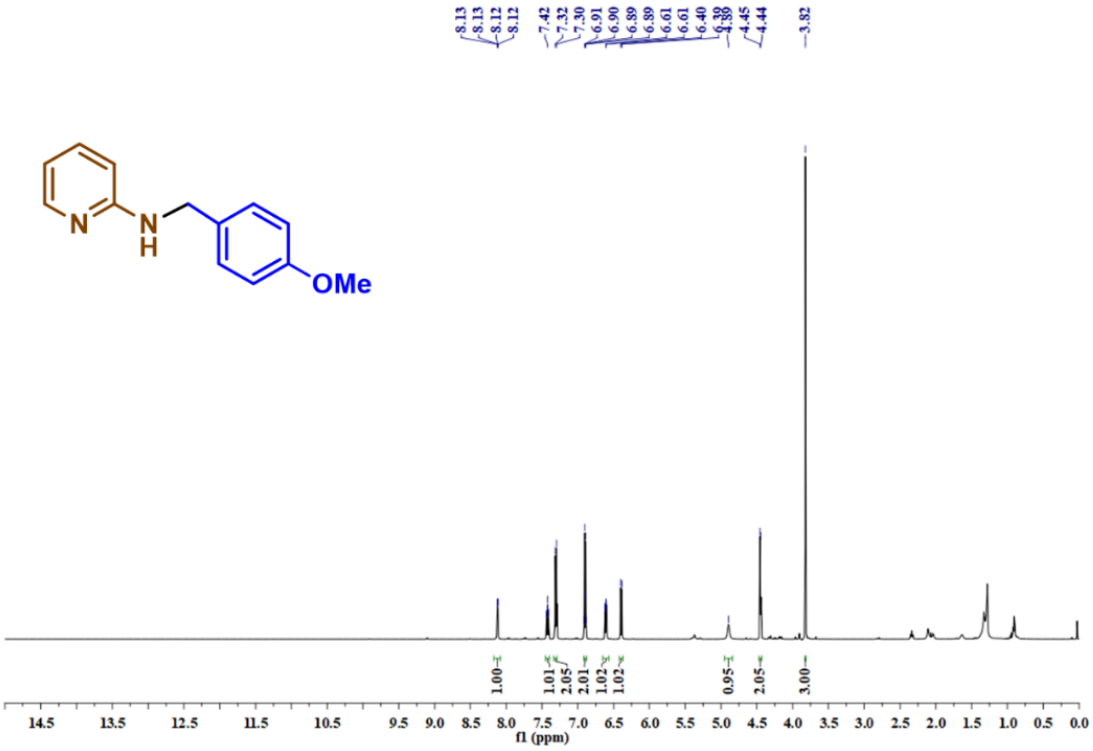

Figure S66: ^{1}H NMR spectrum of 3w in $CDCl_3$ at 500 MHz.

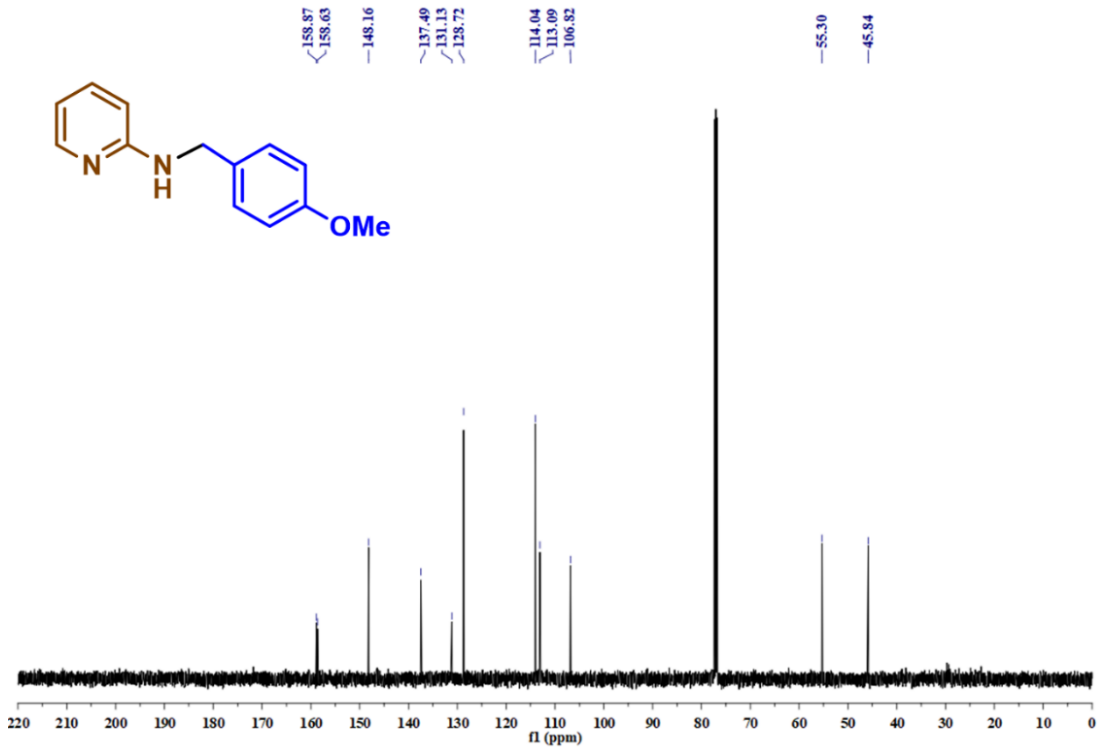

Figure S67: ^{13}C NMR spectrum of 3w in $CDCl_3$ at 126 MHz.

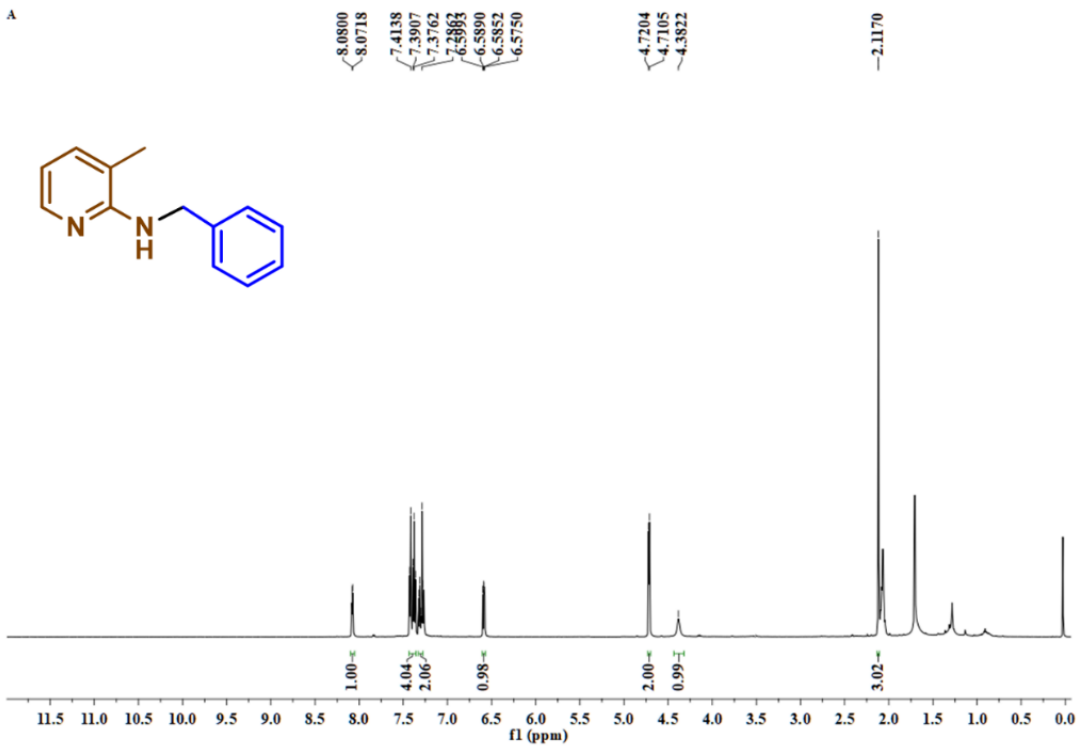

Figure S68: ^{1}H NMR spectrum of 3x in $CDCl_3$ at 500 MHz.

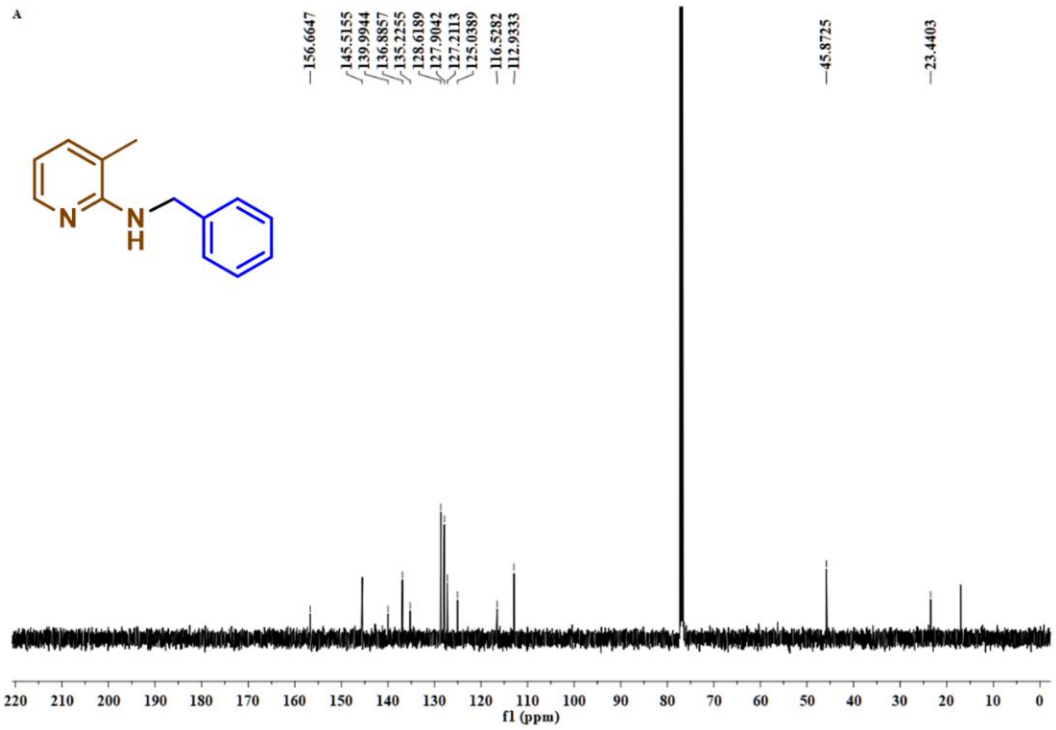

Figure S69: ^{13}C NMR spectrum of 3x in $CDCl_3$ at 126 MHz.

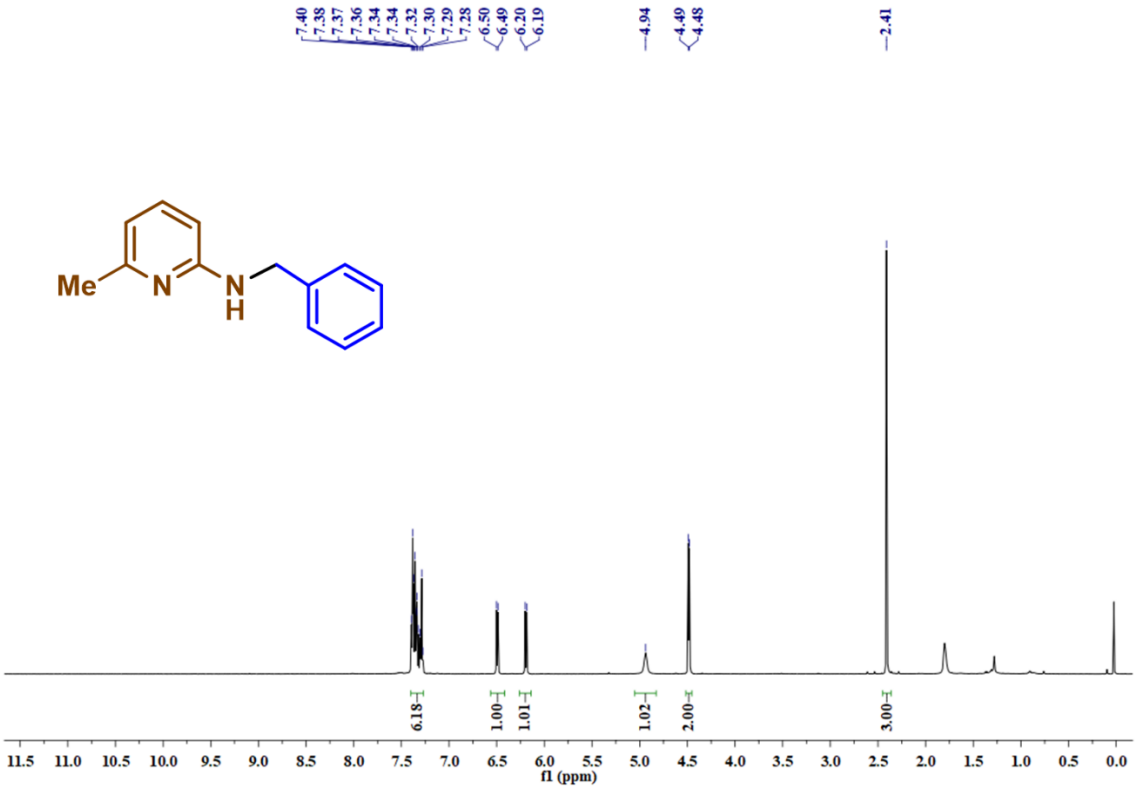

Figure S70: ^{1}H NMR spectrum of 3y in $CDCl_3$ at 500 MHz.

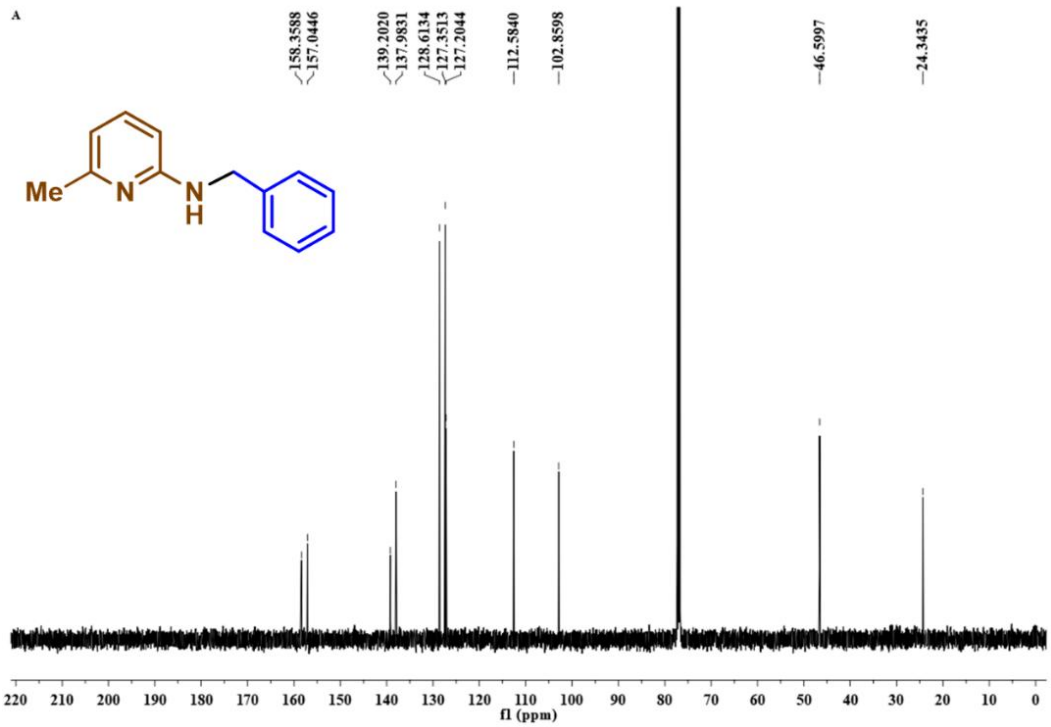

Figure S71: ^{13}C NMR spectrum of 3y in $CDCl_3$ at 126 MHz.

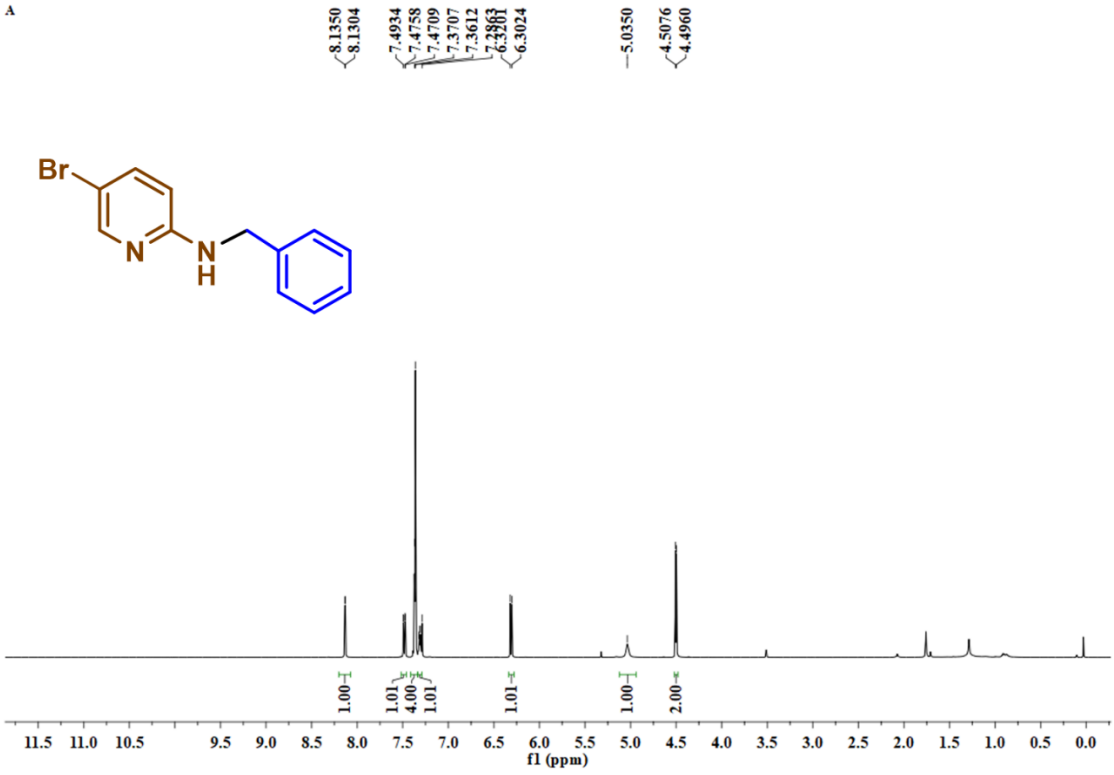

Figure S72: ^{1}H NMR spectrum of 3z in $CDCl_3$ at 500 MHz.

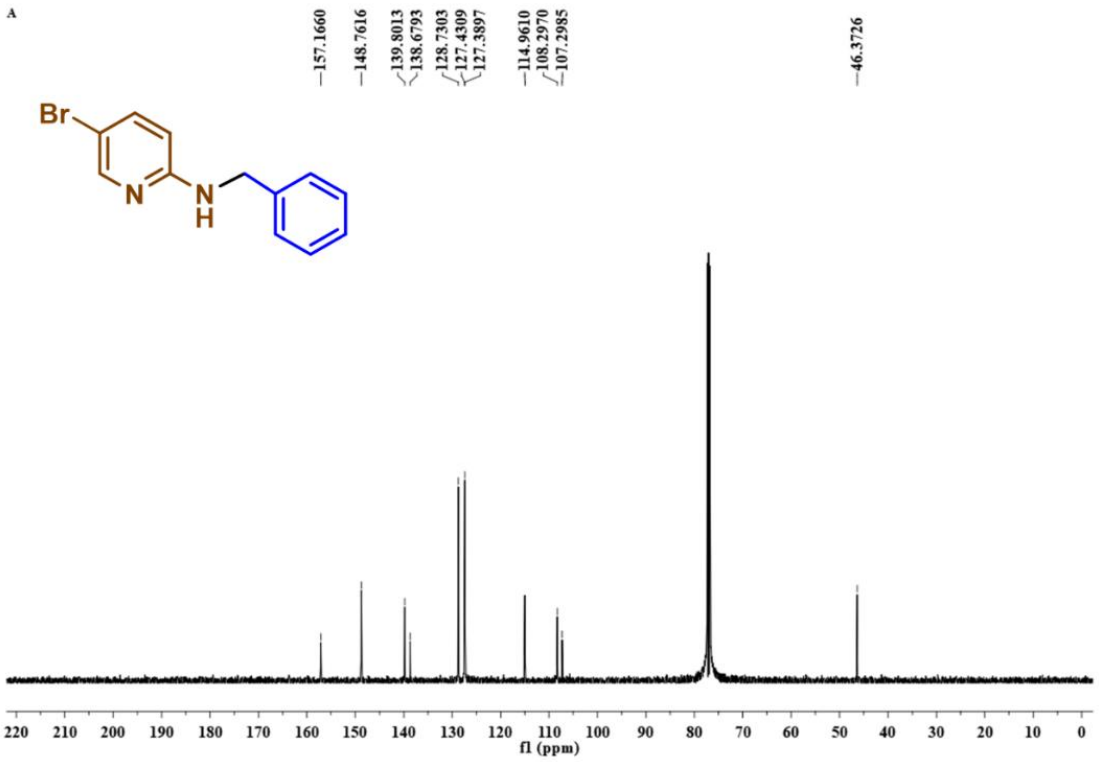

Figure S73: ^{13}C NMR spectrum of 3z in $CDCl_3$ at 126 MHz.

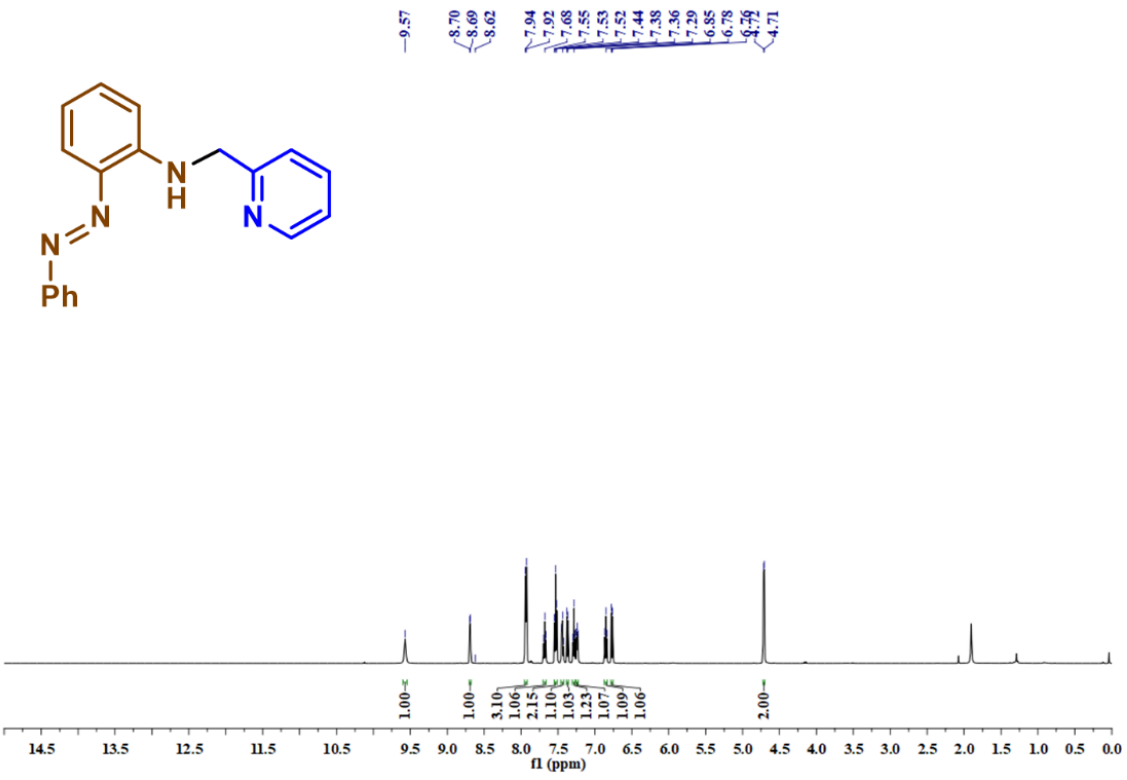

Figure S74: ^{1}H NMR spectrum of 3aa in $CDCl_3$ at 500 MHz.

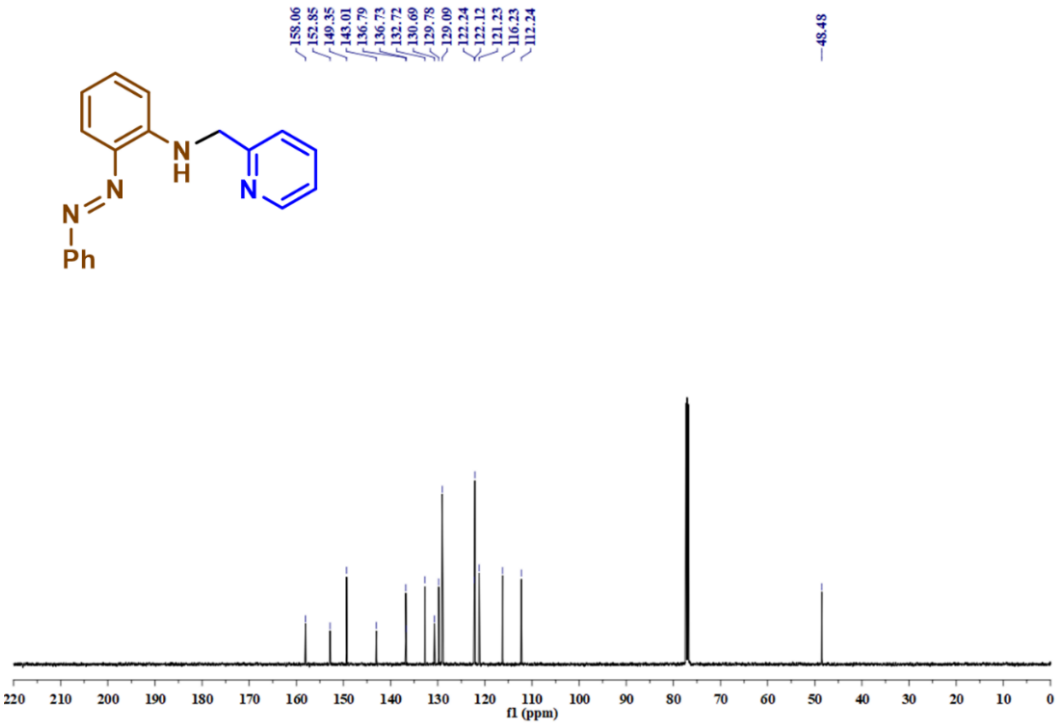

Figure S75: ^{13}C NMR spectrum of 3aa in $CDCl_3$ at 126 MHz.

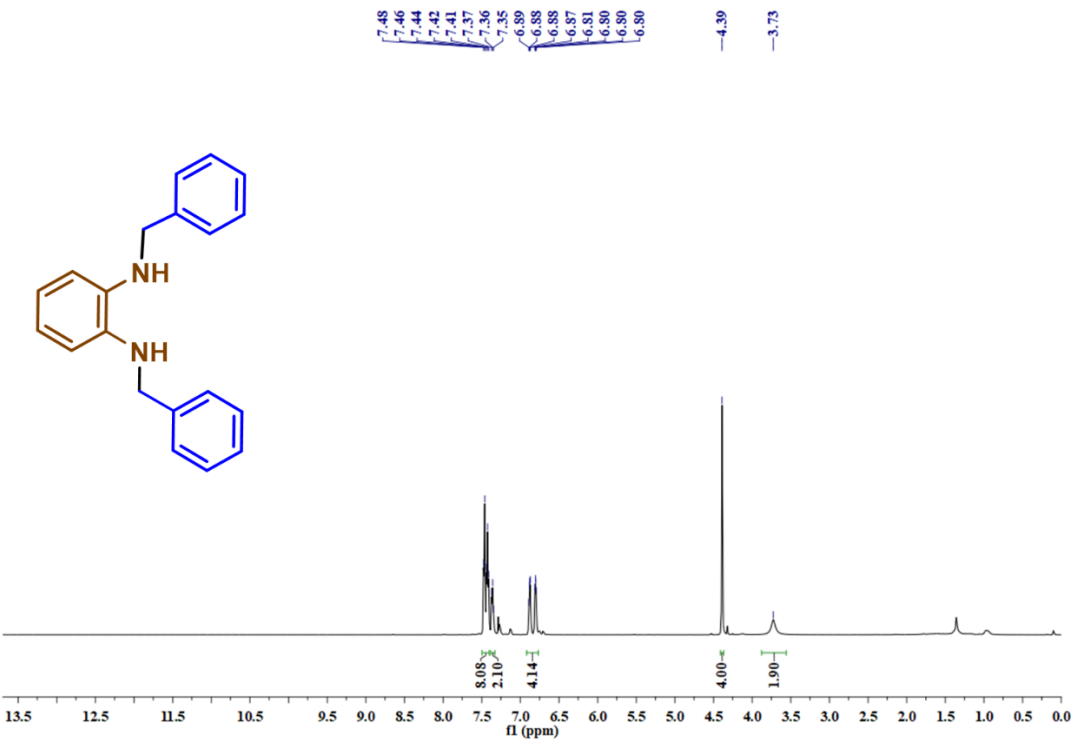

Figure S76: ^{1}H NMR spectrum of 3ab in $CDCl_3$ at 500 MHz.

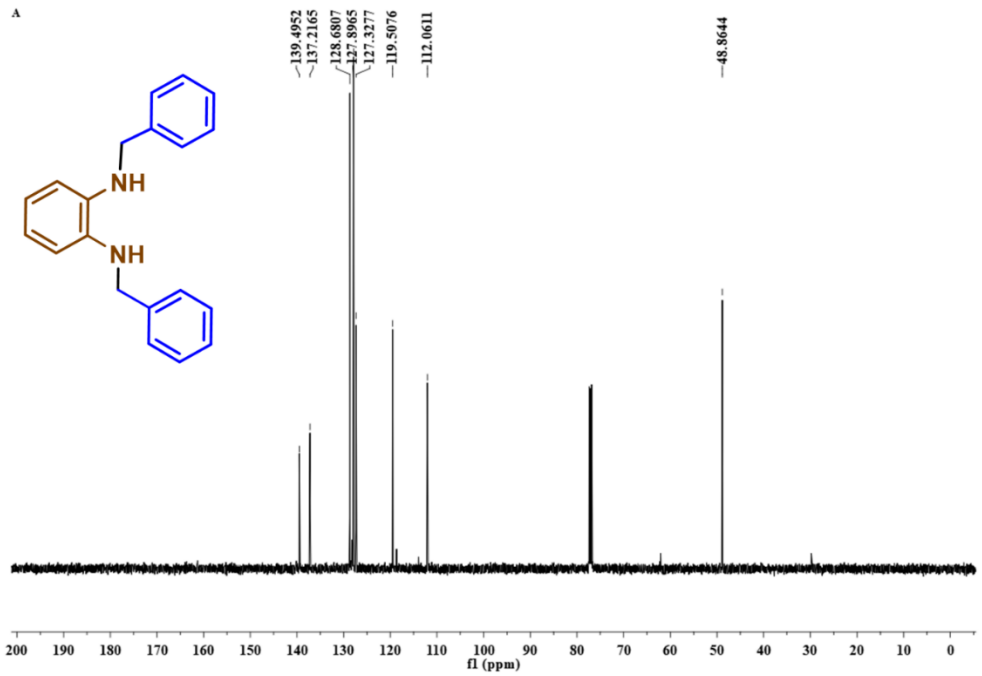

Figure S77: ^{13}C NMR spectrum of 3ab in $CDCl_3$ at 126 MHz.

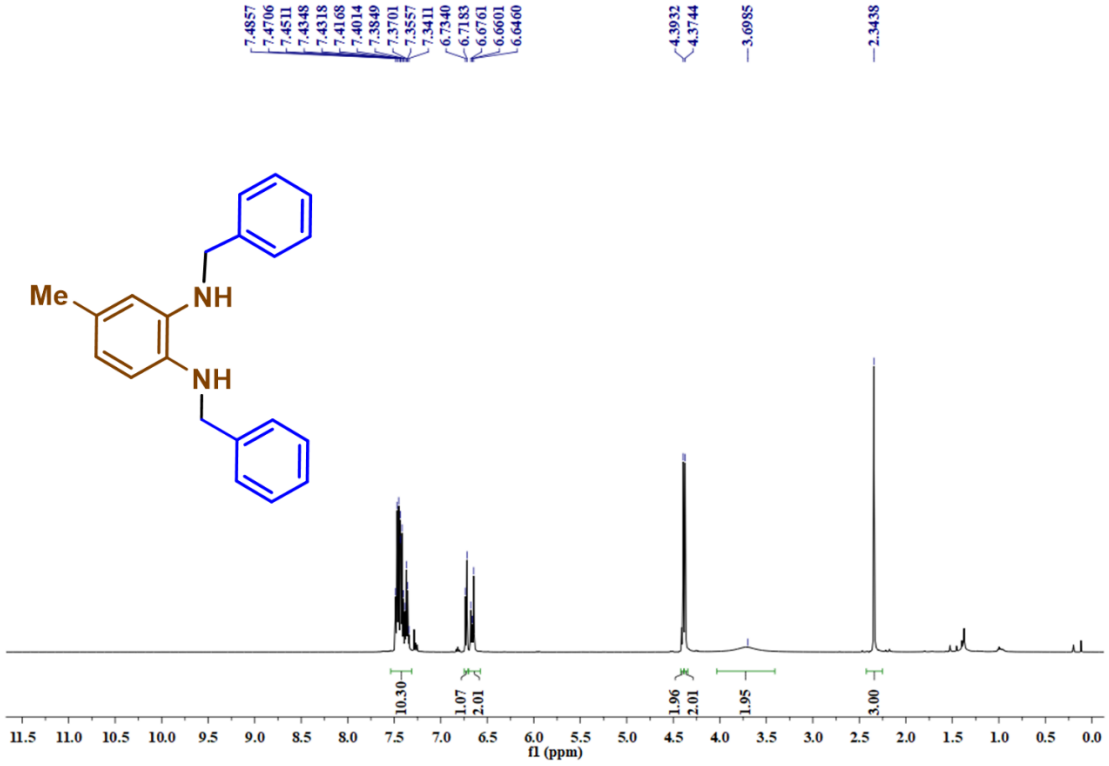

Figure S78: ^{1}H NMR spectrum of 3ac in $CDCl_3$ at 500 MHz.

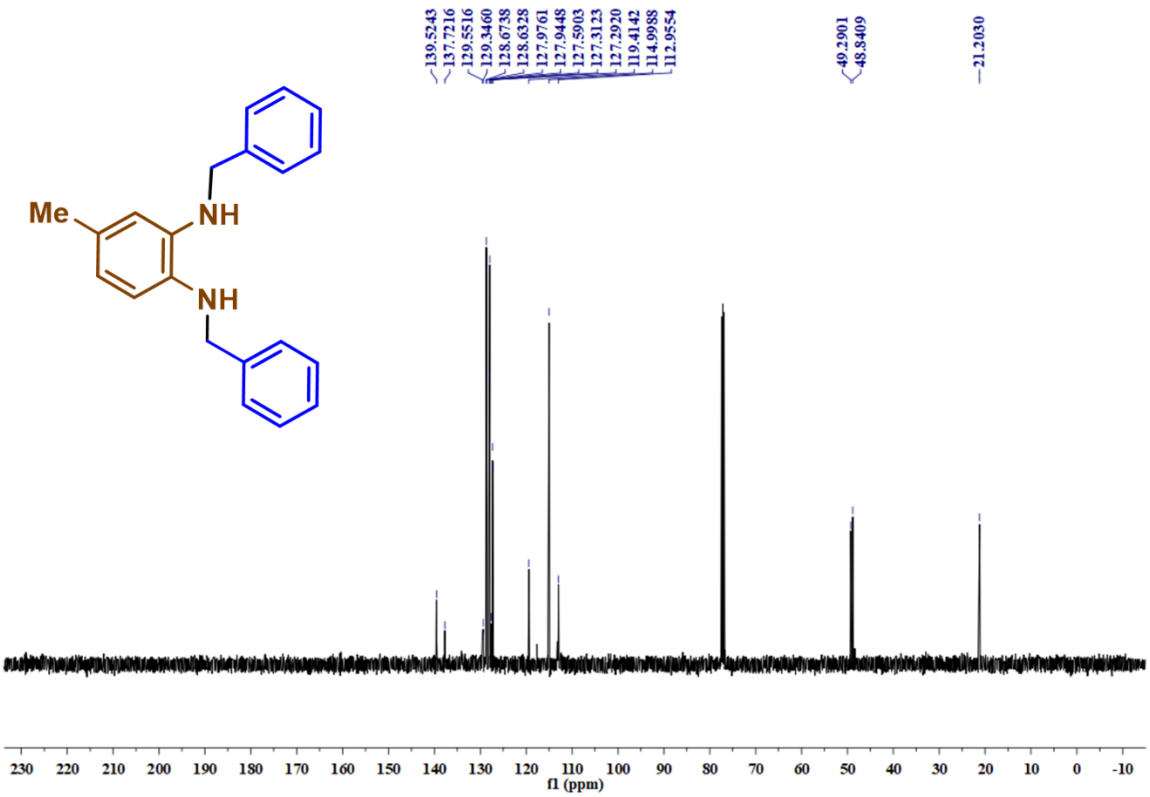

Figure S79: ^{13}C NMR spectrum of 3ac in $CDCl_3$ at 126 MHz.

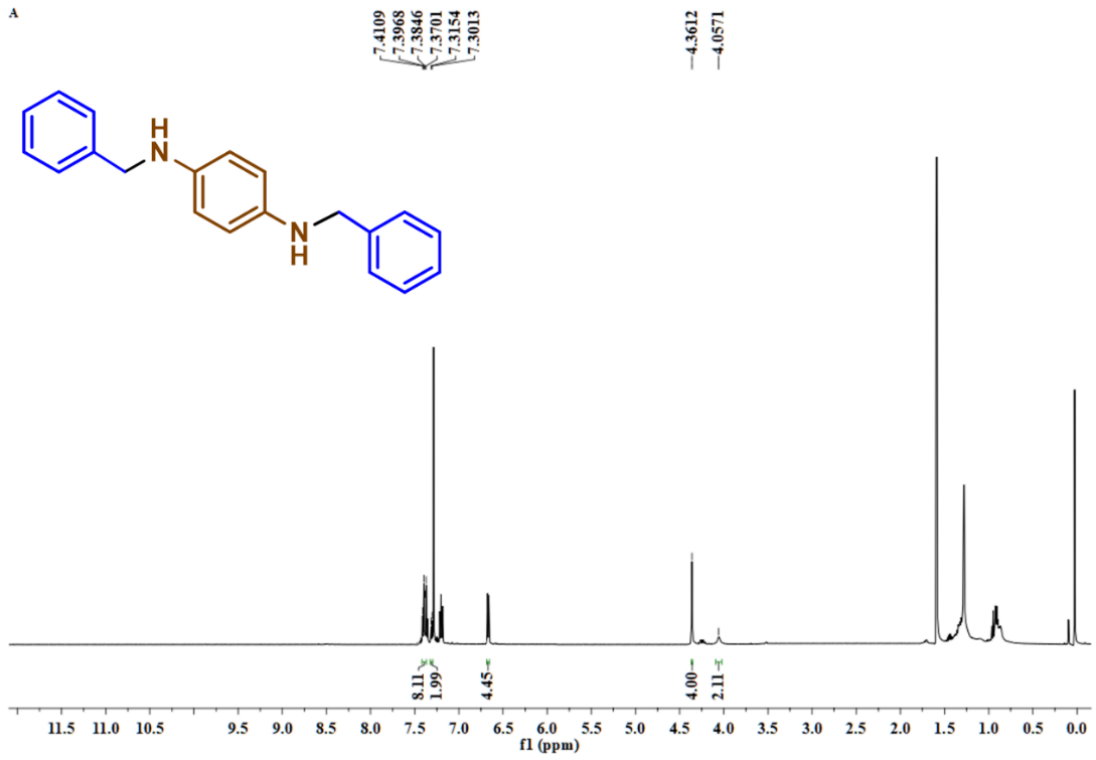

Figure S80: ^{1}H NMR spectrum of 3ad in $CDCl_3$ at 500 MHz.

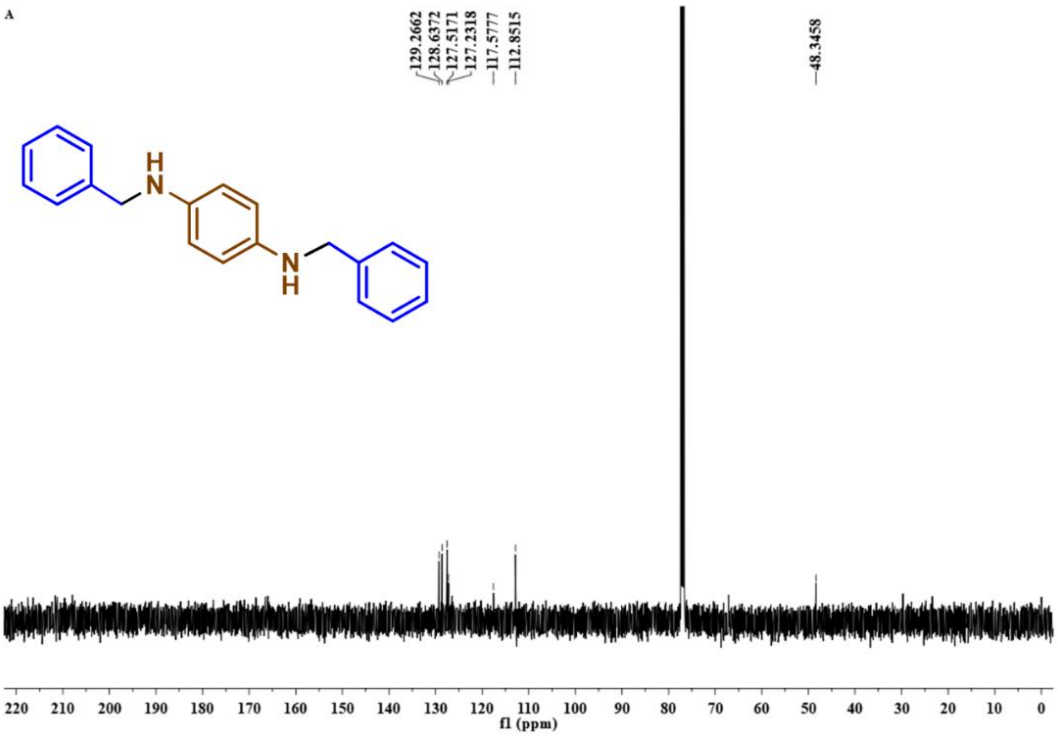

Figure S81: ^{13}C NMR spectrum of 3ad in $CDCl_3$ at 126 MHz.

11. Coordinates for optimized structures

11.1 Cartesian coordinates for C2A

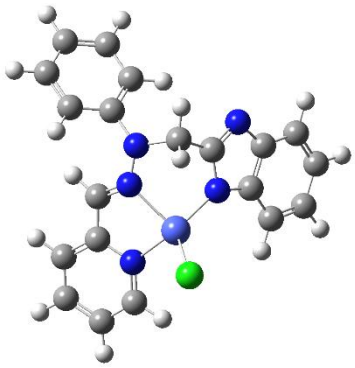

C2A Quartet G = -2887.898774, EZPE = -2887.845097

27	0.382559	7.665217	7.839371
17	-1.163020	8.312810	9.388852
7	0.150222	5.630273	7.807567
7	1.949572	8.751346	7.512191
7	3.090119	10.148164	6.080208
7	0.135854	7.364946	5.768172

7	0.324086	8.376076	4.893986
6	0.064842	4.805452	8.872754
1	0.186131	5.268739	9.843793
6	-0.180724	3.439689	8.730007
1	-0.237033	2.804693	9.605082
6	-0.353747	2.919444	7.440522
1	-0.546130	1.861809	7.297881
6	-0.288384	3.772766	6.338105
1	-0.433814	3.397057	5.331869
6	-0.040645	5.139055	6.541897
6	1.934873	9.548503	6.375630
6	3.954091	9.745845	7.112867
6	3.251975	8.881992	8.005419
6	0.042603	6.095494	5.449732
1	0.061623	5.741440	4.425413
6	0.587108	8.169585	3.495452
6	-0.409437	7.628445	2.667454
1	-1.380564	7.381648	3.083782
6	-0.151955	7.445071	1.305501
1	-0.923428	7.031879	0.664182
6	1.086634	7.815744	0.767106
1	1.280575	7.680039	-0.291649
6	2.069755	8.371608	1.594788
1	3.027488	8.666978	1.179777
6	1.831009	8.545942	2.961848
1	2.588967	8.977327	3.608753
6	0.690831	9.664444	5.553054
1	-0.165865	9.970908	6.165844
1	0.834526	10.405681	4.769324
6	5.299206	10.064868	7.338079
1	5.827067	10.724260	6.657669

6	5.923840	9.513986	8.457022
1	6.964925	9.745382	8.659760
6	5.223024	8.661049	9.341329
1	5.739200	8.257716	10.207246
6	3.882734	8.334190	9.129322
1	3.348318	7.690251	9.821257

11.2 Cartesian coordinates for C2B

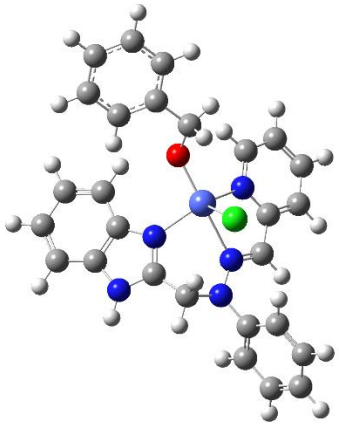

C2B Quartet G = -3234.492263, EZPE = -3234.424973

27	0.209214	-0.545726	0.049881
17	-0.479049	-1.171571	2.355456
7	-0.354456	-2.018157	-1.285572
7	0.129839	1.495354	-0.174416
7	-0.727873	3.553551	-0.059707
1	-1.360427	4.299029	0.184452
7	-2.077326	-0.299939	-0.257009
7	-2.818964	0.695668	0.297296
6	0.572778	-2.823773	-1.849525
1	1.599807	-2.560938	-1.631289
6	0.215835	-3.908201	-2.651421
1	0.983196	-4.536215	-3.086775
6	-1.144338	-4.165276	-2.871666
1	-1.451902	-5.004977	-3.485009
6	-2.103426	-3.329118	-2.297398

1	-3.162061	-3.500667	-2.455664
6	-1.682896	-2.248493	-1.507013
6	-0.886332	2.229394	0.278568
6	0.468911	3.682129	-0.771085
6	1.004802	2.373213	-0.837465
6	-2.604390	-1.306284	-0.897287
1	-3.675216	-1.454818	-1.000366
6	-4.205571	0.493150	0.657944
6	-4.529630	-0.385552	1.704497
1	-3.735662	-0.913369	2.224183
6	-5.870475	-0.561321	2.060916
1	-6.126858	-1.235694	2.871013
6	-6.878250	0.137027	1.381337
1	-7.916847	-0.000280	1.663845
6	-6.547519	1.011874	0.339108
1	-7.327526	1.550833	-0.188296
6	-5.208223	1.189042	-0.028651
1	-4.934690	1.856961	-0.838516
6	-2.029105	1.684545	1.071459
1	-1.639151	1.208268	1.981537
1	-2.713948	2.485380	1.354826
6	1.121295	4.778063	-1.345085
1	0.712826	5.781169	-1.294312
6	2.332647	4.518251	-1.988906
1	2.873021	5.339153	-2.448476
6	2.876984	3.213668	-2.050383
1	3.827869	3.063622	-2.550340
6	2.225667	2.122582	-1.475141
1	2.635211	1.118775	-1.472730
8	2.092785	-0.758958	-0.022391
6	2.887052	-1.668838	0.738575

1	2.415171	-1.853941	1.719536
1	2.954268	-2.657943	0.243842
6	4.305240	-1.170521	0.975461
6	4.608056	0.198471	0.929898
6	5.333328	-2.076543	1.288829
6	5.906313	0.652378	1.193865
1	3.814660	0.892402	0.680100
6	6.631300	-1.626943	1.556144
1	5.114361	-3.141681	1.321404
6	6.923340	-0.257258	1.509354
1	6.123981	1.716304	1.154103
1	7.413353	-2.342227	1.795275
1	7.930418	0.094484	1.713512

11.3 Cartesian coordinates for C2C

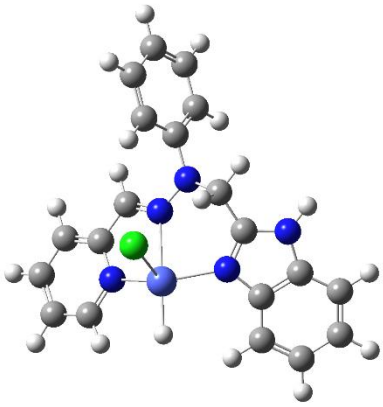

C2C Quartet G = -2889.040661, EZPE = -2888.984652

27	-0.774601	1.271878	0.836623
17	0.546442	0.768163	2.878547
7	0.343575	2.652593	-0.248854
7	-1.812896	-0.451026	0.313994
7	-2.159145	-2.627112	-0.060705
1	-1.973608	-3.616402	-0.110471

7	0.959188	0.071902	-0.190195
7	1.130930	-1.274868	-0.090127
6	-0.016851	3.953663	-0.272284
1	-0.951404	4.180331	0.225676
6	0.767167	4.928703	-0.890817
1	0.449136	5.963943	-0.884528
6	1.962729	4.539846	-1.508941
1	2.593858	5.274437	-1.996772
6	2.336892	3.195062	-1.490863
1	3.256366	2.863619	-1.959917
6	1.506413	2.262434	-0.850774
6	-1.262561	-1.665733	0.342208
6	-3.367435	-1.996260	-0.367752
6	-3.138737	-0.618630	-0.129938
6	1.823523	0.847670	-0.781396
1	2.755825	0.486995	-1.206085
6	2.436051	-1.883364	-0.233313
6	3.415606	-1.672496	0.750551
1	3.189712	-1.039401	1.602894
6	4.666193	-2.284029	0.616248
1	5.424939	-2.128210	1.375723
6	4.935793	-3.101273	-0.490276
1	5.906346	-3.576331	-0.588661
6	3.955100	-3.306057	-1.468703
1	4.164253	-3.936805	-2.326287
6	2.702381	-2.693231	-1.344284
1	1.932998	-2.836207	-2.095510
6	0.136620	-1.950651	0.776968
1	0.267209	-1.613734	1.814526
1	0.341675	-3.020707	0.721320
6	-4.599822	-2.479991	-0.817328

1	-4.770266	-3.535490	-0.997603
6	-5.606075	-1.534970	-1.023815
1	-6.578916	-1.864950	-1.372581
6	-5.388454	-0.158183	-0.784546
1	-6.201672	0.540171	-0.950637
6	-4.157777	0.318985	-0.334731
1	-3.978542	1.366521	-0.128632
1	-2.075318	2.283351	1.10734

Step	hartree	kcal/mol
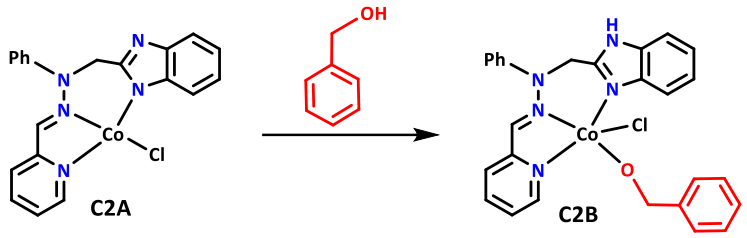	-0.00759	-4.76
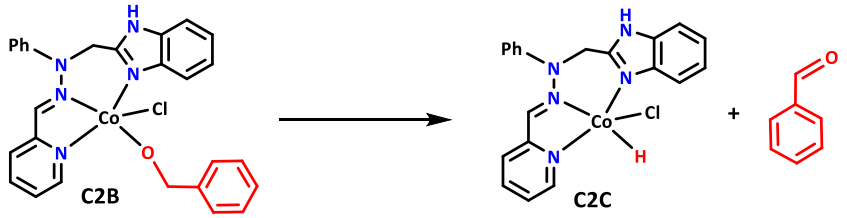	0.04419	27.73
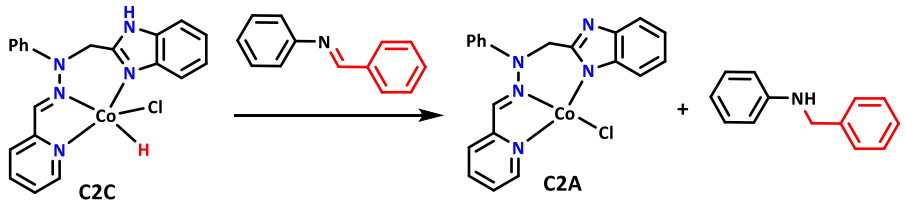	-0.05432	-34.09

12. Comparison between previous phosphene free NNN pincer Co(II) catalysts and present catalysts

methodology. We have compared the current methodology with previously reported cobalt(II) NNN pincer complexes by Balaraman & co-workers (**Catal. Sci. Technol., 2018, 8, 3469–3473**), Ghosh & co-workers (**Dalton Trans., 2021, 50, 8567–8587**), Gupta & co-workers (**Inorg. Chem. Front., 2021, 8, 1599–1609**) and Paul & co-workers (**Eur. J. Inorg. Chem. 2023, 26, e202300263**) as shown below. The catalytic methodology developed by Balaraman & co-workers utilized 5 mol% of catalyst, 1.1 equivalent of base, 150 °C temperature and 32 hours reaction time. Ghosh & coworkers utilized 4 mol% of catalyst, 0.5 equivalent of base, 110 °C temperature and 24 hours reaction time. Gupta & coworkers utilized 2 mol% of catalyst, 4.0 equivalent of base, 100 °C temperature and 8 hours reaction time. Paul & coworkers utilized 1 mol% of catalyst, 0.5 equivalent of base, 120 °C temperature and 12 hours reaction time. The previous methodologies developed by Ghosh & co-workers and Gupta & coworkers showed to explore only 12 and 10 examples. Balaraman and coworkers explore 24 examples but utilized higher temperature, catalyst mol%. Paul & co-workers explore 50 examples.

The current methodologies utilized 2 mol% catalyst, 0.5 equivalent base, 110 °C temperature and 12 hours reaction time. Using current protocol total 30 substrates were explored. On comparing current protocol with previous one it has been found out that current protocol provides higher catalytic yield of the respective N-alkylated substrates as shown below.

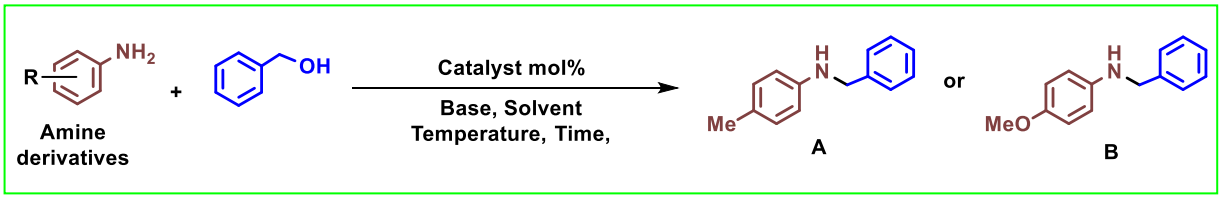

Catalyst	Catalyst mol%	Temp. (°C)	Time (hour)	Base (equivalent)	Yield (%)	Total number of substrates explored
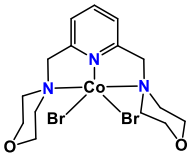 Balaraman (2018)	5 mol%	150	32	^{t}BuOK (1.1 eq.)	A = 76% B = 80%	24 examples
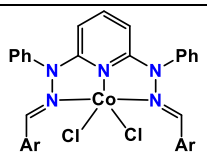 Ghosh (2021)	4 mol%	110	24	^{t}BuOK (0.5 eq.)	A = 83% B = not explored	12 examples
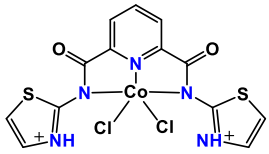 Gupta (2021)	2 mol%	100	8	KOH (4 eq.)	A = not explored B = 89%	10 examples
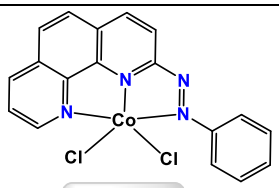 Paul (2023)	1 mol%	120	12	^{t}BuOK (0.5eq.)	A = 82 B = 84%	50 examples
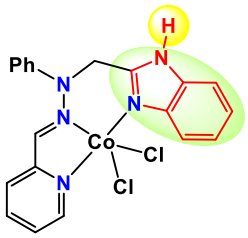	2 mol%	110	12	^{t}BuOK (0.5 eq.)	A = 88% B = 91%	30 examples

Table S7. Comparison with previous reported and present report

13. References

1 O. V. Dolomanov, L. J. Bourhis, R. J. Gildea, J. A. K. Howard and H. J. Puschmann, *J. Appl. Crystallogr.*, 2009, **42**, 339–341.

2 G. M. Sheldrick, *Acta Crystallogr.*, 2014, **A71**, 3–8.

3 C. F. Macrae, P. R. Edgington, P. McCabe, E. Pidcock, G. P. Shields, R. Taylor, M. Towler and J. van de Streek, *J. Appl. Crystallogr.*, 2006, **39**, 453–457.

4 Frisch, M. J.; Trucks, G. W.; Schlegel, H. B.; Scuseria, G. E.; Robb, M. A.; Cheeseman, J. R.; Scalmani, G.; Barone, V.; Mennucci, B.; Petersson, G. A.; et al. Gaussian 09; Gaussian, Inc.: Wallingford, CT, U.S., 2009.